Calibration of Rutile (U-Th)/He Thermochronology: assessing the thermal evolution of the KTB drill hole, Germany and adjacent Bohemian Massif

by

Melissa R. Wolfe
B.S., The University of Puget Sound, 2005

Submitted to the Department of Geology and the
Faculty of Graduate School of the University of Kansas
In partial fulfillment of the requirements for the
Degree of Master of Science

Advisory Committee

_____
Daniel F. Stockli (Chairman)

_____
J. Douglas Walker

_____
David A. Fowle

_____
Gwen L. Macpherson

Date Defended: May 11, 2009

The Thesis Committee for Melissa Wolfe certifies that
this is the approved version of the following Thesis

Calibration of Rutile (U-Th)/He Thermochronology: assessing the thermal evolution of the KTB drill hole, Germany and adjacent Bohemian Massif

Advisory Committee

_____
Daniel F. Stockli (Chairman)

_____
J. Douglas Walker

_____
David A. Fowle

_____
Gwen L. Macpherson

Date Approved: May 12, 2009

ABSTRACT

Calibration of Rutile (U-Th)/He Thermochronology: assessing the thermal evolution of the KTB drill hole, Germany and adjacent Bohemian Massif

By

Melissa R. Wolfe, M.S.
Department of Geology, May 2009
University of Kansas

This study empirically calibrates zircon and rutile (U-Th)/He dating by evaluating the experimentally-derived He diffusion kinetics and their extrapolation over geological time by (U-Th)/He dating a suite of borehole samples with a well-defined thermal history. Age dating is coupled with cycled step-heating diffusion experiments and thermal modeling of zircon and rutile. The German Continental Deep Drilling Project (KTB) is ideally suited for this approach given its depth and zircon- and rutile-bearing metamorphic rocks. Results from zircon (U-Th)/He analyses display a helium partial retention zone between ~140-210°C which agrees well with laboratory-derived He diffusion kinetics. While regional rutile (U-Th)/He age data confirm the feasibility of rutile (U-Th)/He thermochronometry ($T_c \approx 220°C$) in eclogites and granulites, anomalous rutile (U-Th)/He ages from the KTB drill hole illustrate the implications of retrograde rutile breakdown to titanite and the importance of petrographic characterization of rutile for obtaining reliable and meaningful thermochronometric data.

DEDICATION

I would like to dedicate this work to my parents, Steven and Debbie Wolfe, you have instilled in me a devotion to education and the pursuit of knowledge. I know that without your love and support I would not be here (case in point that the telescope still is not finished). Thank you for always allowing me to follow after my dreams and for sacrificing your very selves for my betterment. More than this education or any success in life, thank you for instilling in me Truth that is built on the firm foundation (1Cor 3:11).

ACKNOWLEDGEMENTS

Funding for this project was provided through a NSF grant awarded to Daniel Stockli and J.D. Walker EAR 0439824. Additional funding was provided through a DOSECC Internship, a GSA Student Scholarship, a AWG Osage Chapter Scholarship, and University of Kansas Department of Geology graduate summer research support.

To Gwen Macpherson, thank you for your thorough help in my trace element geochemistry of rutile, I am grateful for standard solutions, help reducing data, and your time. To Doug Walker thank you for your wise and enjoyable counsel in the lab; Roman Kislitsyn for your macro-making skills- we all appreciate it. To Andreas Moller thank you for being so willing to help with my endless questions on petrology. Lisa Stockli, thank you for your assistance with my time on the SEM and review of my work. Heather Shingole at MAI for always being ready to help me while on the SEM. Wayne Dickerson, thank you for your help with my polished thick sections on short notice.

I would like to thank my lab mates for discussions on myriads of topics, assistance in labwork, and eating my experiments on Monday mornings. Chris Hager for his dedication to MATLAB and help with my 'rims' and your willingness to always answer questions. To Markella Hoffman for her friendship and support- I have enjoyed these last three years! To Eugene Szymanski who has endured my presence in the office for three years (enough said), and to recent additions Travis

Glauser and Evan Bargnesi thank for your patience with my coffee grinding and balsamic.

I would like to thank my committee members for their time and constructive reviews of my work. I am grateful to Danny Stockli, my advisor, for continually pushing me to be a better scientist and for the opportunities that this degree has provided in traveling, meetings and conferences, and watered-down beer. Your ever-continuous patience with my breaking machines and 'drama' is appreciated.

I would like to thank JeMiMe&Co. Without you these last three years would have been very different and I am so very grateful for the depth of these friendships, Sunday evening dinners and your unconditional care for my soul. Finally, to Christ, you are my only hope in life and death- may my life better reflect what you have accomplished on my behalf. Jehovah Jireh, you did provide as promised.

TABLE OF CONTENTS

PAGE

TITLE PAGE **i**

ACCEPTANCE PAGE **ii**

ABSTRACT **iii**

DEDICATION **iv**

ACKNOWLEDGEMENTS **v**

TABLE OF CONTENTS **vii**

LIST OF TABLES AND FIGURES **xi**

CHAPTER 1: INTRODUCTION **12**

CHAPTER 1: REFERENCES **17**

CHAPTER 2: Zircon (U-Th)/He thermochronometry in the KTB drill hole, Germany, and its implications for He diffusion in zircon **20**

ABSTRACT **20**

INTRODUCTION **21**

Zircon (U-Th)/He thermochronology *24*

Regional Geologic Setting: KTB drill hole **28**

Thermal evolution of KTB drill hole *29*

Zircon thermochronometry of KTB drill hole *32*

ANALYTICAL METHODLOGY **33**

Zircon (U-Th)/He analysis *33*

Cycled step-heating experiments *34*

RESULTS **35**

Cycled step-heating experiment results *36*

IMPLICATIONS **37**

KTB zircon (U-Th)/He ages *37*

Thermal modeling *38*

CONCLUSIONS **44**

CHAPTER 2: REFERENCES **47**

CHAPTER 3: Rutile (U-Th)/He thermochronometry on poly-metamorphic rocks from the KTB drill hole, Germany **80**

ABSTRACT **80**

INTRODUCTION **81**

Empirical He diffusion calibration *84*

RUTILE **85**

Rutile mineralogy and petrology *85*

Rutile thermochronometry *86*

GERMAN CONTINENTAL DEEP DRILLING PROJECT (KTB) **88**

Regional geology *88*

Geology of the KTB drill hole *89*

Metamorphic evolution of KTB *90*

Post-Variscan thermal evolution *91*

Previous thermochronometric studies of KTB *94*

ANALYTICAL METHODOLOGY **94**

(U-Th)/He thermochronology *94*

Rutile alpha ejection correction *97*

Cycled step-heating diffusion experiment *98*

Trace element geochemistry *99*

RESULTS **100**

KTB Rutile (U-Th)/He results *100*

Cycled step-heating diffusion experiment results *101*

Rutile trace element geochemistry *102*

Petrography of rutile in the KTB drill hole *106*

DISCUSSION **110**

Interpretation of rutile (U-Th)/He results *110*

Comparison of rutile (U-Th)/He results *111*

Potential causes of inaccurate rutile (U-Th)/He results *113*

Effect of titanite overgrowth on rutile (U-Th)/He results *116*

Effect of titanite rims on alpha ejection correction *119*

Corrected rutile (U-Th)/He data from KTB drill hole *122*

Regional rutile (U-Th)/He results *127*

Implications for rutile (U-Th)/He thermochronometry *129*

CONCLUSION **131**

CHAPTER 3: REFERENCES CITED **134**

LIST OF TABLES AND FIGURES

PAGE

CHAPTER 2: FIGURES

Figure 1. Down-hole lithologic profile of KTB drill hole 56

Figure 2. Simplified regional geologic map of KTB region 58

Figure 3. Age vs. depth previous thermochronometers 60

Figure 4. time-Temperature history from the KTB drill hole 62

Figure 5. Arrhenius plot zircon diffusion experiments 64

Figure 6. Age vs. depth plot of zircon (U-Th)/He results 66

Figure 7. Comparison of thermal modeling with zircon (U-Th)/He results 73

Figure 8. Comparison of anisotropic diffusion with zircon (U-Th)/He results 75

Figure 9. Effective uranium concentration [eU] of zircon (U-Th)/He results 77

CHAPTER 2: TABLES

Table 1. Average zircon (U-Th)/He age 68

Table 2. Results from cycled step heating diffusion experiments 71

CHAPTER 3: FIGURES

Figure 1. Regional geologic map of KTB region 146

Figure 2. Down-hole lithologic profile of the KTB drill hole 148

Figure 3. Metamorphic history of ZEV 150

Figure 4. Arrhenius plot rutile diffusion experiment 152

Figure 5. Down hole rutile (U-Th)/He results KTB drill hole 156

Figure 6. Nb, Ta, Zr, Hf concentrations in rutile 163

Figure 7. Nb vs. Cr concentrations in rutile 165

Figure 8. Calculated peak metamorphic temperatures 167

Figure 9. BSEM images from KTB1239 169

Figure 10. BSEM images from KTB1252 171

Figure 11. BSEM images from KTB1464 173

Figure 12. BSEM images from 3575 and 3595 m 175

Figure 13. BSEM images from grain mounts 1230-4070 m 177

Figure 14. BSEM images from grain mounts 4668-9000 m 179

Figure 15. Comparison RHe, zircon (U-Th)/He and thermal modeling results 181

Figure 16. Titanite rim scenario 183

Figure 17. Age bias enriched rim 185

Figure 18. Age bias plot rim removal 187

Figure 19. Contour plot corrected RHe ages RKTB1516 189

Figure 20. Contour plot corrected RHe ages RKTB4172 191

Figure 21. Contour plot corrected RHe ages RKTB5720 193

CHAPTER 3: TABLES

Table 1. Column chemistry procedure 154

Table 2. Average rutile (U-Th)/He ages from KTB drill hole 158

Table 3. Selected trace element geochemistry results 160

Table 4. Regional rutile (U-Th)/He ages 195

CHAPTER 1: INTRODUCTION

The research presented here utilizes down-hole sampling of the German Continental Deep Drilling Project (KTB) to assess *in-situ* He diffusion kinetics over geologic time scales and temperatures in zircon, a well-established thermochronometer (Chapter 2), and rutile (Chapter 3), a developing thermochronometer. This project was initially funded under an NSF grant awarded to Daniel Stockli and J.D. Walker on the Development and Calibration of Rutile (U-Th)/He Geo- and Thermochronometry. Additional funding, awarded to Melissa Wolfe was provided through a DOSECC Internship, a GSA Student Scholarship, a AWG Osage Chapter Scholarship, and University of Kansas Department of Geology graduate summer research support. This work represents part of a larger efforts of the development, calibration, and applications of rutile (U-Th)/He dating and builds on initial calibration and development of rutile (U-Th)/He geo- and thermochronometry at the University of Kansas undertaken by Terry Blackburn (Blackburn, 2006).

Empirical calibration studies of a (U-Th)/He thermochronometer evaluates whether laboratory-derived diffusion kinetics can be accurately extrapolated to temperatures and timescales pertinent in nature. Such studies are best completed on samples from either exhumed crustal sections (e.g., Stockli, 2005) or on drill holes that have a well-characterized thermal history and temperature profile (e.g., House et al., 1999; Stockli and Farley, 2004). The KTB drill hole offers a unique opportunity to study the diffusive behavior of He in a thermochronometer in nature. The well-

studied KTB drill hole, Germany, samples a series of alternating fault-bound Variscan metamorphic blocks and reaches a final depth of 9100 m with a bottom hole temperature of ~260°C (Emmerman and Lauterjung, 1997; Clauser et al., 1997; Coyle et al., 1997; Hejl et al., 1997; Wagner et al., 1997; Stockli and Farley, 2004). We have utilized down-hole sampling to assess the He diffusion in zircon and rutile. In addition to down-hole (U-Th)/He analysis, we have performed step-heating diffusion experiments on zircon and rutile samples from the KTB drill hole. Thermal modeling of laboratory diffusion kinetics measured at the University of Kansas and those widely used in the (U-Th)/He community, with the thermal history of the KTB drill hole provides a direct test if laboratory diffusion kinetics accurately reflect the down-hole (U-Th)/He age distribution.

The second chapter of this thesis is titled *Zircon (U-Th)/He thermochronometry in the KTB drill hole, Germany, and its implications for He diffusion in zircon.* Zircon, a well established (U-Th)/He thermochronometer, is routinely utilized to characterize thermal histories in igneous, volcanic, and sedimentary basins with an estimated closure temperature (T_c, Dodson, 1973) between 175-210°C (10°C/m.y.) (e.g., Reiners, 2005). However, recent investigations and mechanistic modeling of He diffusion in zircon indicated that He diffusion in a perfect zircon lattice should be strongly anisotropic along the c-axis and affected by structural defects within zircon lattice (Reich et al., 2007; Saadoune et al., 2009). Utilizing the well-constrained setting of the KTB drill hole, down-hole zircon (U-Th)/He analysis will assess He diffusion of zircon in nature.

KTB Down-hole zircon (U-Th)/He results from this study display consistent and systematic ages which largely agree with titanite (U-Th)/He results from the KTB drill-hole (Stockli and Farley, 2004). Zircon ages steadily decrease in age over the temperature range ~130-200°C, which we define as the helium partial retention zone (HePRZ). This study confirms projection of laboratory diffusion data to accurately reflect zircon (U-Th)/He results to geologic timescales and temperatures. This thesis chapter is as a journal manuscript to be submitted to Earth and Planetary Science Letters with Daniel Stockli as co-author.

The third and final chapter, entitled *Rutile (U-Th)/He thermochronometry on poly-metamorphic rocks from the KTB drill hole, Germany,* furthers the development of rutile (U-Th)/He thermochronometry. Rutile is a common U-bearing accessory mineral that occurs in a wide range of geologic settings and can be found as a metamorphic, hydrothermal, and detrital mineral phase. It is extremely resistant to chemical and mechanical weathering. Rutile presents a unique opportunity to understand the intermediate temperature history of high pressure (HP) and high temperature (HT) metamorphic rocks, particularly blueschists, eclogites and granulites. This study presents down-hole (U-Th)/He analysis and He diffusion experiments on rutile from the KTB drill hole to evaluate the diffusivity of He in rutile over geologic timescales and temperature ranges, particularly by comparison of thermal modeling of rutile He-diffusion kinetics to down-hole RHe results. Trace element geochemical analysis and petrographic characterization performed on rutile from the KTB drill hole studies the effects of metamorphic breakdown. Application

of rutile (U-Th)/He analysis to regional high-grade metamorphic rocks assesses the influence of metamorphic assemblage and metamorphic grade and suggests high grade metamorphic rocks that have not undergone extensive retrograde metamorphism can provide information on the timing of exhumation of such terranes. The third chapter is a journal manuscript that will be submitted to *Earth and Planetary Science Letters* and the co-authors are Daniel Stockli and Chris Hager.

All zircon and rutile (U-Th)/He analysis and cycled step-heating diffusion experiments were performed at the University of Kansas Isotope Geochemistry Laboratory (KU-IGL). Thermal modeling and alpha ejection code was written by Chris Hager in MATLAB® (MATHWORKS, The, 2008b) following equations from Ketcham (2005). KTB samples were obtained from Dr. Grauert's collection from the University of Muenster (provided by Dr. Mezger) and the Bavarian Geological Survey (in collaboration with Dr. Ulrich Harms, Dr. J. Rohrmueller, Dr. Josef Schwarzmeier). Samples from the Bavarian Geological Survey were collected by Wolfe and Stockli during a trip to the KTB drill site and core repository in the fall 2007. Regional rutile samples were collected by Wolfe and Stockli in the Erzgebirge, Germany, and the Bohemian Massif (Czech Republic) or provided by Dr. Luvizotto and Dr. Zack (Univ. Heidelberg).

Rutile trace element geochemistry analyses were conducted by solution inductively coupled plasma mass spectrometry (ICP-MS) with input in methodology by Dr. Gwen Macpherson. Detailed petrographic investigations using BSE-SEM imaging and EDAX were conducted on LEO Field scanning electron microscope at

the University of Kansas Microscopy and Imaging Laboratory in the Chemistry Department. Procedures for anion exchange columns utilized for rutile (U-Th)/He thermochronometry were developed by J.D. Walker and T. Blackburn (Blackburn, 2006) and rutile alpha stopping distance calculations by Daniel Stockli.

CHAPTER 1: REFERENCES

Blackburn, T., 2006, Development of new applications in volcanic (U-Th)/He geochronology, M.S. Thesis Kansas University.

Clauser, C., Giese, P., Huenges, E., Kohl, T., Lehmann, H., Ryback, L., Safanda, J., Wilhelm, H., Windloff, K., Zoth, G., 1997. The thermal regime of the crystalline continental crust: implications from the KTB. Journal of Geophysical Research, v. 102, p. 18417-18441.

Coyle, D.A., Wagner, G.A., Hejl, E., Brown, R., and Van den Haute, P., 1997, The Cretaceous and younger thermal history of the KTB site (Germany). apatite fission-track data from the Vorbohrung. Geol. Rundschau, v.86, p. 203-209.

Crowhurst, P., Farley, K., Ryan, C., Duddy, I., and Blacklock, K., 2002, Potential of rutile as a U-Th-He thermochronometer. Geochimica et Cosmochimica Acta, v. 66, p. A-158.

Dodson, M.H., 1973, Closure temperature in cooling geochronological and petrological systems, Contributions to Mineralogy and Petrology, v. 40, p. 259-274.

Emmerman, R., and Lauterjung, J., 1997, The German Continental Deep Drilling Program KTB: Overview and major results. JGR, v. 102, p. 18,179-18,201.

Hejl, E., Coyle, D., Nand Lal, P., Van den Haute, P., and Wagner, G.A., 1997, Fission-track dating of the western border of the Bohemian massif: thermochronology and tectonic implications. Geol. Rundschau, v. 86, p. 210-219.

House, M., Farley, K., Kohn, B., 1999, An empirical test of helium diffusion in apatite: borehole deata from the Otway basin, Australia, Earth and Planetary Science Letters, v. 170, p. 463-474.

MathWorks, The, 2008b. MATLAB®, Natick, MA

O'Brien, P.J., Duyster, J., Grauert, B., Chreyer, W., Stockhert, B., and Weber, K., 1997, Crustal evolution of the KTB drill site: From oldest relics to the late Hercynian granites. Journal of Geophysical Research, v. 102, p. 18203-18220.

Reich, M., Ewing, R., Ehlers, T, Becker, U., 2007, Low-temperature anisotropic diffusion of heliumin izronc: implications for zircon (U-TH)/He thermochronometry. Geochimica Et Cosmochimica Acta. v. 71 pg. 2119-3130.

Reiners, P.W., Farley, K.A., and Hickes, H.J., 2002, He diffusion and (U-Th)/He thermochronometry of zircon: Initial results from Fish Canyon Tuff and Gold Butte, Nevada, Tectonophysics, v. 349, p. 297-308.

Reiners, P., 2005, Zircon (U-Th)/He Thermochronometry, in Reiners, P. W. and Elhers, T. A., Low Temperature Thermochronology: Techniques, Interpretations and Applications, Reviews in Mineralogy and Geochemistry, v. 58, p. 151-179.

Saadoune, I., Purton, J.A., Leeuw, N.H., 2009, He incorporation and diffusion pathways in pure and defective $ZrSiO_4$: A density functional theory study. Chemical Geology, v. 258, p. 182-196.

Stockli, D. and Farley, K., 2004, Empirical constraints on the titanite (U-Th)/He partial retention zone from the KTB drill hole: Chemical Geology, v. 207, p. 223-236.

Stockli, D., Wolfe, M., Blackburn, T., Zack, T., Walker, J.D., Luvizotto, G., 2007, He diffusion and (U-Th)/He thermochronometry of rutile. Abstract. Programs AGU Fall 2007.

Wagner, C., Coyle, D., Duyster, J., Henjes-Kunst, F., Peterek, A., Schroder, B., Stockhert, B., Wemmer, K., Zulauf, G., Ahrendt, H., Bischoff, R., Hejl, E., Jacobs, J., Menzel, D., Ll, N., Van den haute, P., Vercoutere, C., Welzel, B., 1997. Post-Variscan thermal and tectonic evolution of the KTB site and its surroundings. Journal of Geophysical Research, v. 102, p. 18221-18232.

Wolf, R. A., Farley, K. A., and Kass, F. M., 1998, Modeling of the temperature sensitivity of the apatite (U-Th)/He thermochronometer. Chemical Geology, v. 148, p. 105-114.

Zack, T., Kronz, A., Foley, S., Rivers, T., 2002, Trace element abundances in rutiles from eclogites and associated garnet mica schists. v. 184, p. 97-122.

CHAPTER 2: Zircon (U-Th)/He thermochronometry in the KTB drill hole, Germany, and its implications for He diffusion in zircon

ABSTRACT

We present down-hole zircon (U-Th)/He ages, laboratory derived diffusion kinetics, and thermal modeling on zircon from the Continental Deep Drilling Project (KTB), Germany as an *in situ* investigation of the diffusion kinetics controlling He diffusion in zircon in nature over geologic timescales. Single grain laser (U-Th)/He ages, corrected by standard alpha-ejection correction, display a decrease in ages from ~112-<1 Ma with reproducibility of ±8%. Down-hole results display consistent ages of ~85±10 Ma in the upper 4700 m, which largely agree with previous studies from the KTB drill hole. Beginning at 5000 m zircon ages begin a steady decrease in age until they are nearly reset (<1 Ma) at 7200 m. The manner and temperature range (~130-200°C) in which zircon (U-Th)/He ages systematically decrease resembles the helium partial retention zone (HePRZ). We also present cycled-step heating experiments on two zircon samples from the KTB drill hole. Results from ZKTB4050-DE diffusion kinetics indicate E_a 160 kJ/mol and D_0 0.03 s^{-1}/cm^2 with an estimated closure temperature (T_c) of 181°C, which agree with published diffusion kinetics for zircon. Diffusion kinetics for ZKTB1516-DE indicate E_a 82.5 kJ/mol and D_0 0.55 s^{-1}/cm^2, with a T_c 215°C, which is higher than previous studies. To compare the ZrHe results and bulk diffusion kinetics, we modeled diffusion parameters with an established thermal history of the KTB drill hole. The predicted zircon HePRZ based on thermal modeling is consistent with down-hole zircon (U-Th)/He ages and laboratory-derived diffusion kinetics from ZKTB4050-DE on zircon from the KTB

drill hole. Diffusion kinetic results from sample ZKTB1516-DE are more retentive than down-hole ZrHe results, which suggests that in general bulk diffusion kinetics correspond to diffusivity of He in zircon in nature, but can vary from sample to sample. Recent computational studies on a perfect zircon lattice indicate He diffusion is strongly anisotropic, preferring to diffuse parallel to the c-axis (Farley et al., 2007; Reich et al., 2007; Saadoune et al., 2009). Results from ZrHe analysis from the KTB drill hole may suggest that He diffusion of zircon in nature is not dominantly controlled by anisotropic diffusion but instead coincides with laboratory-derived diffusion kinetics.

INTRODUCTION

Zircon ($ZrSiO_4$) occurs as a common accessory mineral in a variety of sedimentary, igneous and metamorphic rock types and geologic environments. It is widely used in the geological sciences for geochemical and isotopic studies because of its affinity to retain minor and trace elements including actinides, lanthinides and radiogenic elements (Finch and Hanchar, 2003). Zircon's incorporation of U and Th in combination with its highly refractory nature, often surviving multiple geologic cycles, has made zircon the primary mineral utilized in U-Pb dating (Finch and Hanchar, 2003). Geochronologic investigations of zircon bearing rock types are diverse and include crystallization (Solar et al., 1998); provenance studies (Watson and Harrison, 2005; Fedo et al., 2003 [References therein]); timing of metamorphic events (e.g., Gibson and Ireland, 1995); and refining the stratigraphic record (e.g.,

Bowring et al., 1998). As a result of the decay of U to Pb zircon is also a carrier of radiogenic He, and more recently it has been established as a (U-Th)/He thermochronometer (Farley, 2002; Reiners et al., 2004, Tagami et al., 2003; Reiners, 2005).

With practical development of its analytical technique and ubiquitous presence in multiple rock types, zircon (U-Th)/He (ZrHe) thermochronology has become a routine procedure applied in the geosciences (Reiners et al., 2002; 2004). It has been employed on quickly cooled volcanic samples as a chronometer (e.g., Tagami et al., 2000; Tincher and Stockli, in press), to establish thermal histories for a temperature window between 150-210°C (Reiners et al., 2002; Stockli, 2005) and in combination with *in situ* U-Pb dating in sedimentary provenance studies (e.g., Campbell et al., 2005; Reiners et al., 2005; Rahl et al., 2003). Laboratory diffusion experiments (Reiners et al., 2002; 2004) and empirical studies on exhumed fault blocks (Reiners et al., 2002; Tagami et al., 2003; Stockli, 2005) have estimated a closure temperature (T_c, Dodson, 1973) between 175-210°C (with cooling rate of 10°C/my). Many aspects of ZrHe thermochronometry are well studied: the effect of grain size on diffusivity (Reiners et al., 2004), U/Th zonation (Hourigan et al., 2005; Dobson et al., 2008) and radiation damage or metamictization (e.g., Nasdala et al., 2004; Reiners et al., 2004). Consequently ZrHe thermochronometry is widely applied to zircon-bearing lithologies as a source of thermal information.

Although ZrHe thermochronometry is commonly implemented, aspects of He diffusion in zircon are not fully understood, particularly laboratory diffusion

experiments that display non-Arrhenius behavior in the early pro-grade steps (Reiners et al., 2002; 2004). Fundamentally, laboratory diffusion experiments extrapolate diffusive behavior at high temperatures and short time steps to geologically pertinent temperatures (<250°C) and timescales (millions of years). Due to the magnitude of extrapolation, potential errors are large and can be problematic in understanding diffusion in (U-Th)/He thermochronometry (Farley et al., 1999).

In this study we utilize natural zircon from the Continental Deep Drilling Project (KTB) in Germany to assess the *in situ* diffusivity of He in zircon. The KTB drill hole has a well-characterized thermal regime, petrologic, geochemical, and tectonic history and offers a unique opportunity to study the effect of temperature on a thermochronometer over geologic time scales (e.g., Coyle and Wagner, 1998, Coyle et al., 1997; Warnock et al., 1997; Stockli and Farley, 2004). With down-hole ZrHe analyses from a temperature range of ~7-265°C we seek to expand on previously published work that empirically calibrates ZrHe thermochronometry in exhumed fault blocks, further constrain the intermediate thermal history of the KTB drill hole, and determine if in fact anisotropic diffusion and structural defects significantly impact ZrHe thermochronometry over geologic time scales and temperatures.

Zircon (U-Th)/He Thermochronology

(U-Th)/He thermochronometry is based on the accumulation of radiogenic ^{4}He produced by the decay of ^{238}U, ^{235}U, ^{232}Th, and ^{149}Sm. (The contribution of Sm in zircon is minor in comparison to U and Th). It is now a well-established

thermochronometric technique for apatite, titanite, and zircon dating (e.g. Reiners and Farley, 1999; Farley, 2000; Reiners et al., 2002; Stockli and Farley, 2004) and has filled in the thermochronometric gap between apatite fission track closure temperature, T_c ~110°C and ^{40}Ar-^{39}Ar, T_c >150°C (e.g., Wagner et al., 1997; Harrison, 1985; Harrison, 2005 [References therein]). Since its recent resurgence (Zeigler et al., 1987; Farley, 1996), (U-Th)/He thermochronology has been applied to an extensive range of geologic, tectonic, and geomorphologic processes (House et al., 1999; Farley, 2000; Reiners et al., 2000, 2007; Stockli, 2005; Mitchell & Reiners, 2003).

Specifically, ZrHe thermochronology is appealing because of its high U and Th concentrations, which are typically an order(s) of magnitude higher than established thermochronometers apatite and titanite, and its presence in a diverse range of lithologies. High U and Th concentrations make it conducive for application to young earth processes, and even Quaternary geochronology using disequilibrium corrected ZrHe ages (Farley et al., 2002; Schmidtt et al., 2006). The resistance of zircon to chemical and physical weathering makes ZrHe dating applicable on silisiclastic sedimentary rocks to investigate the thermal history of orogenic source terranes in which apatite and titanite are not found (Rahl et al., 2003; Reiners et al., 2005; Campbell et al., 2005). The understanding and application of ZrHe studies is based primarily on results from step heating experiments that determine He diffusion in zircon. Established laboratory-derived diffusion kinetics for zircon range in activation energies (E_a) from 163-173 kJ/mol (30-41 kcal/mol) and diffusivity at

infinite temperature (D_o) from 0.09-1.5 cm^2/s (Reiners et al., 2002; 2004, 2005). These studies yield a closure temperature between 175-193°C (average 183°C) for grains 40-100 μm in width. It was also noted that diffusivity scales with grain size (Reiners et al., 2002; 2005). ZrHe analysis of old, highly radiogenic zircons also determined that large doses of radiation damage lowers He diffusivity in zircon. The approximate threshold of damage that affects zircon diffusivity typically occurs at alpha levels >2-4x10^8 α/g (Nasdala et al., 2004; Reiners, 2005). He diffusion experiments in zircon have displayed anomalously high diffusivities in the prograde heating steps; for these experiments well-behaved Arrhenius diffusivity typically begins at temperature steps between 425-520°C (Reiners, et al., 2004). The cause of erratic behavior is unknown, but proposed causes include zones of radiation damage, crystallographically anisotropic diffusive behavior, or unevenly distributed He (Reiners et al., 2004, 2005). Ultimately, the implications of this behavior on application to ZrHe analysis are not fully known.

Recent studies have sought to address the potential cause of non-Arrhenius behavior in early steps of diffusion experiments on zircon, through computational studies at the atomic level. Reich and others (2007) studied anisotropic diffusion in zircon along the c-axis while Saadoune and others (2009) investigated the affect of structural defects on He diffusivity. Results found He diffusivity in a perfect zircon lattice is strongly anisotropic and a tracer He atom preferentially diffuses along the c-axis [001] (Reich et al., 2007). They also note that diffusion in zircon did not behave isotropically until temperatures >580°C, well above the published closure

temperature. In order to approximate the influence of anisotropic diffusion, they use the difference between the two most energetically favorable diffusion pathways [001] and [100] (~31% or 31 kJ/mol) as the uncertainty of bulk diffusion measurements (Reich et al., 2007). On the lower end, corrected E_a for anisotropic diffusion is 138 kJ/mol, which is significantly lower than bulk diffusivities that estimate E_a 169 kJ/mol (Table 4- Reich et al., 2007; Reiners et al., 2004; Reiners, 2005). The implication of anisotropic diffusivity could produce a range of closure temperatures between 54-323°C. If true, any thermal history, exhumation rate or magnitude of exhumation based on bulk diffusion kinetics (T_c of ~180°C) could be significantly miscalculated (Reich et al., 2007). Another study examined the effect of point defects in a zircon crystal structure on He diffusivity (Saadoune et al., 2009). They calculated an effective E_a of 40 kJ/mol in a perfect zircon lattice, but found the presence of point defects along the c-axis produced 'He traps,' which effectively doubled the E_a of the dominant He c-axis pathways. To quantitatively understand the large error produced by extrapolation of laboratory-derived diffusion kinetics to geologic timescales and temperatures, both of these studies modeled the diffusion behavior in zircon at the atomic level, demonstrating that He diffusivity in zircon is anisotropic, preferentially diffusing out of the c-axis, and largely affected by structural defects in the zircon lattice. To accurately understand and apply ZrHe thermochronometry, constraining the rate and timing of geologic processes, it is essential to have accurate and precise understanding of He diffusivity at temperatures and timescales that apply to geologic events.

Laboratory derived diffusion kinetics are determined by in-vacuum experiments that utilize high temperatures (>400°C) and consequently shorter time steps to assess how ^{4}He moves through, and eventually escapes, the mineral grain. Such experiments are a necessity since diffusivity under natural conditions occurs on time scales far too slow for laboratory studies. Once determined, diffusion kinetics are extrapolated to lower, geologically pertinent temperatures by assuming simple thermally activated Arrhenius behavior. Uncertainty depends on the accuracy and precision of the laboratory diffusion data and assumes the behavior seen at higher temperatures also occurs at the lower extrapolated temperatures (House et al., 1999). The goal of empirically calibrating a (U-Th)/He thermochronometer is to validate if experimentally determined diffusion kinetics are consistent in nature. Preservation of diffusion kinetics is displayed in the helium partial retention zone (HePRZ), a mineral specific temperature range in which helium is partially (<10%) to completely (>90%) retained (Wolf et al., 1998). Empirical calibration is best completed on samples from drill holes that have a well-known thermal history and temperature profile and the down-hole age variation (defining the HePRZ) should coincide with modeled diffusion kinetics (House et al., 1999; Stockli and Farley, 2004).

Previous empirical calibration studies on zircon (U-Th)/He dating have utilized exhumed fault blocks in the Basin and Range (Reiners et al., 2002; Tagami et al., 2003; Stockli, 2005). Zircon (U-Th)/He analysis along the exhumed fault block in Gold Butte, Nevada identified the lower inflection point of the ZrHePRZ at an estimated paleodepth of 10 km, in the temperature range of 180-250°C (Reiners et al.,

2002). A similar study from the Wassuk Range, Nevada displayed a lower inflection point at reconstructed paleodepth of 6.5 km and paleotemperature of ~180°C (Tagami et al., 2003; Stockli, 2005). These studies agree well with the established T_c for zircon which is based on laboratory-derived diffusion kinetics. This study utilizes sampling at a closer interval of the well-constrained thermal regime and tectonic history of the KTB drill hole to improve our understanding of the *in situ* He diffusivity of zircon in nature over geologic timescales

REGIONAL GEOLOGIC SETTING: KTB drill hole

In Europe the Variscan Orogen is exposed as a series of east-west trending massifs, the easternmost being the Bohemian Massif (BM). The BM, located in eastern Germany, western Czech Republic and portions of Austria and Poland is composed of Variscan fault-bounded metamorphic terranes, each with a distinct tectonic and metamorphic history (Hirschmann et al., 1997). The Zone of Ebendorf-Vohenstrauss (ZEV) sits on the western border of the BM and is a small distinct gneiss-metabasic complex unit (O'Brien et al., 1997). The ZEV is a series of alternating metapelite paragneiss, metabasic, and amphibolite metamorphic blocks that are bound by zones of reverse faulting (O'Brien et al., 1997) (Figure 1). The KTB borehole is located on the western margin of the ZEV and drilled to a depth of ~9.1 kilometers. The South German Sedimentary Basin lies west of the KTB borehole and is separated from the BM by the Franconian Lineament (SE1/FL). The FL is a major reverse fault that dips ~45-50º to the NW and intersects the KTB drill

hole at a depth of ~7000 m (Wagner et al., 1997) (Figure 1 and Figure 2). Two other major fault zones were identified in the KTB drill hole, the Nottersdorf Fault Zone (NFZ) between 500-1600 m and SE2 between 3200-4000 m. Since the Cretaceous, the KTB region has been largely quiescent and the most recent tectonic activity produced late Tertiary Eger graben and basaltic volcanism, approximately 30 km to the northwest (Figure 2) (Schroder, 1997). The thermal regime of the KTB drill hole has been well studied with an undisturbed equilibrated geothermal gradient of ~27.5°C/km (Clauser et al., 1997).

Thermal Evolution of KTB drill hole

The KTB drill hole, having been well-characterized in its thermal regime, petrologic, geochemical, and tectonic context, has provided a unique opportunity to study the *in situ* behavior of various thermochronometers over geologic time scales and temperatures. Previous thermochronometric studies include apatite (AFT- Wagner et al., 1997) and titanite fission track (TFT- Coyle and Wagner, 1998), and titanite (U-Th)/He (THe- Stockli and Farley, 2004) (Figure 3). AFT results confirmed the apatite partial annealing zone (PAZ) between 60-110°C, exhibited by a systematic decrease in ages from 50-6.2 Ma from 2000 m down to 4000 m. Analysis of titanite fission track interpreted a paleo-PAZ between 265-310 ± 5-10°C, but no present day PAZ was documented in the TFT data (Coyle and Wagner, 1998). TiHe results record the HePRZ between ~115-195°C by a systematic decrease in ages from ~80-5 Ma beginning at 4500 m down to 7000 m (Stockli and Farley, 2004).

These studies also assessed the tectonic history of the KTB drill hole. The combination of thermochronometric results and depositional history of the South German Sedimentary Basin (Schroder et al., 1997), adjacent to the ZEV and offset by the FL (Figure 2), records two major periods of rapid cooling. The earliest cooling episode is recorded in the Triassic by K-feldspar ^{40}Ar-^{39}Ar cooling age of ~225 Ma at 7762 m depth (Warnock and Zeitler, 1997) and the invariant down-hole TFT ages from 0-4000 m of ~245 Ma (Coyle and Wagner, 1998). Although TFT annealing kinetics are not well constrained denudation between 225-245 Ma is confirmed by coincident alluvial fan deposits in the South German Sedimentary Basin (Schroder et al., 1997). The second cooling episode is recorded in the Late Cretaceous by all the thermochronometric studies. ^{40}Ar-^{39}Ar results from samples at 0 m and 3203 m were quickly cooled between 125-95 Ma and again at 70-60 Ma (Warnock and Zeitler, 1998). TiHe results record invariant down-hole ages from ~75-85 Ma in the upper four kilometers (Stockli and Farley, 2004). AFT results (Coyle et al., 1997) document cooling between ~58-70 Ma from 120°C to ~45°C by ~25 Ma. Surface AFT data near the KTB drill site range from 70-60 Ma (Wagner et al., 1989). TiHe data suggest the upper portion cooled rapidly in the late Cretaceous from ~180-210°C to >110°C (Stockli and Farley, 2004). This event is also recorded in the depositional history of the South German Sedimentary Basin with ~500 m of Cretaceous alluvial fan deposits. Down-hole muscovite and amphibole K-Ar ages exhibit invariant ages between 300-350 Ma for the entire KTB drill hole (Wemmer, 1993).

Thermo-tectonic reconstructions of the KTB drill hole divide the KTB into four metamorphic blocks (A-D), which are bound by zones of reverse faulting (Wagner et al., 1997) (Figure 3). All four blocks were a single ~2000 km thick crustal layer, which slowly cooled through the Permian, evidenced by the invariant K-Ar muscovite ages. Down-hole thermochronometric studies from the KTB record the subsequent faulting of the crustal layers into a ~ 9000 m thick antiformal stack. Movement on the SE2 fault zone (3200-4000 m) in the Triassic separated blocks A and B from C and D. The FL was active during the early Cretaceous separating blocks C and D and continued through the Eocene, which is largely recorded in AFT and THe ages (Coyle et al., 1997; Stockli and Farley, 2004). The Nottersdorf Fault Zone (NFZ) became active in the Eocene, thickening blocks A and B, recorded in AFT results (Coyle et al., 1997). This South German Sedimentary Basin records these events by deposition of more than 15 km of exhumed rock since the end of the Permian (Schroder et al., 1997). Early studies attributed this rapid cooling and subsequent deposition in the Cretaceous to onset of the Alpine orogeny (Warnock and Zeitler, 1998; Coyle et al., 1997). More recent assessments attribute Late Cretaceous shortening in Central Europe to the onset of Africa-Iberia-Europe convergence and postpone the coupling of the Alps and Europe to the Cenozoic (Kley and Voight, 2008; Bosworth et al., 2008s).

Zircon (U-Th)/He Thermochronometry in the KTB drill hole

Building on previous empirical calibration studies (Reiners et al., 2002; Tagami et al., 2003; Stockli, 2005; Stockli and Farely, 2004), this research seeks to understand if laboratory derived diffusion kinetics are representative of He diffusivity in nature. In contrast to previous work, we sample at a more closely spaced interval with accurate *in situ* temperature-depth knowledge, along side a well-documented tectonic history to provide a more quantitative comparison of published zircon diffusion kinetics to a known geologic history. Recent studies raise caution in ZrHe thermochronometry by investigating interactions of He in the zircon lattice at the atomic level with computer simulations (Reich et al., 2007; Saadoune et al., 2009), but similar to laboratory derived diffusion kinetics, modeling does not accurately reflect natural geologic conditions. Down-hole ZrHe analysis from the KTB drill hole, in contrast, provides a natural setting to measure zircon He diffusion kinetics.

Zircon is present as an accessory mineral in amphibolite, metagabbro and paragneiss units throughout the KTB borehole. The KTB is uniquely suited for *in situ* calibration of zircon diffusion kinetics because the total depth of 9.1 km and bottom hole temperature reaches ~265°C (Clauser et al., 1997). At bottom hole temperatures (~265°C) zircon (T_c ~180°C) should not retain He and therefore down hole (U-Th)/He analysis should document a complete zircon HePRZ. In addition, ZrHe results will provide further data on the intermediate temperature evolution of the KTB drill hole, and can be directly compared to titanite (U-Th)/He and $^{40}Ar/^{39}Ar$ thermochronometric studies.

ANALYTICAL METHODOLOGY

Zircon (U-Th)/He Analysis

All ZrHe analysis was performed in the Isotope Geochemistry Laboratory at the University of Kansas. After routine mineral separation zircon, grains were hand selected based on similarity in morphology, clarity and size (between ~65-120 μm in width). Morphometric analysis of each grain measured length and width to calculate the alpha ejection correction factor (F_T, Farley et al., 1996; Farley, 2000).

Helium was extracted by a Nd:YAG laser heated to ~1290°C for ten minutes and reheated to ensure complete degassing of the sample (>99%). The liberated gas was spiked with ^{3}He and cryogenically purified. The $^{4}He/^{3}He$ ratio was measured by isotope dilution on a quadrapole noble gas mass spectrometer that is calibrated against a manometerically-determined ^{4}He standard. After He extraction, zircon grains were unwrapped from Pt tubing and dissolved by pressure vessel dissolution procedures (e.g., Stockli et al., 2000). Samples were spiked with an enriched ^{230}Th, ^{235}U, ^{149}Sm and REE tracer and subsequently dissolved using an HF-HNO_3 mixture heated for 72 hours at 225°C in the dissolution vessel. This was followed by dry down and resdissolution in 6N HCl for 12 hours at 200°C to remove Th-F salts. In preparation for ICP-MS, the HCl was dried down and the dissolved zircon was brought up in concentrated HNO_3 and diluted with 1000 μL of water. All parent nuclide concentrations were measured by isotope dilution on VG PQII quadrapole ICP-MS. Comparing the spike against a gravimetric 1 ppb U-Th-Sm-REE normal solution. (U-Th)/He ages were calculated using standard F_T corrections (Farley et al.,

1996). Estimated analytical uncertainty of ~8% (2σ) is based on replicate analysis and all ZrHe ages are reported as such unless otherwise noted.

Cycled Step-Heating Experiments

Two cycled step-heating experiments were completed on zircon from the KTB drill hole, samples ZKTB1516 and ZKTB4050. Experiments were completed at the University of Kansas, Isotope Geochemistry Laboratory and ran on a fully automated diffusion experiment apparatus as described by Farley (1999). Multiple zircon grains (2-4), based on grain size, morphology and clarity, were packaged in a Pt jacket and Cu-foil envelope. The packaged sample was wrapped around the thermocouple, to assure that the thermocouple was in direct contact with the sample. The package was suspended in a vacuum chamber and heated by a 350W light bulb through a sapphire window. The estimated accuracy of the thermocouple temperature reading was ± 5°C per step with stability of ± 1-2°C per step. The diffusion experiment begins with a set of isothermal steps at 400°C followed by a cycle of prograde, retrograde, and prograde steps. Each temperature stepped up or down in 10°C increments and each cycle finished with a blank (0°C) measurement. The first prograde sequence increased in temperature from 420-590°C, followed by a retrograde sequence from 575-485°C. The final prograde sequence increased in temperature from 492-640°C (see Appendix A for complete data set). After each step, the ^{4}He liberated from the sample was measured by isotope dilution of ^{3}He on a quadrapole mass spectrometer. Calculation of bulk diffusion kinetics required subsequent complete degassing of the

sample to determine total grain gas in order to compare the cumulative fraction of gas released in each step. A Nd:YAG laser heated the sample to ~1285°C for 10 minutes repeatedly to attain the total gas fraction (>99%).

RESULTS

KTB Zircon (U-Th)/He Results

ZrHe ages (N =120) were obtained from 37 samples from the KTB borehole. Six samples, between the depths of 1230 and 1740, are from the pilot hole (VB), and the final 31 are from the main hole (HB). Zircon separates are mostly from amphibolites and garnet amphibolites, but a handful are from paragneiss units (from depths 52-525, 1575-1740, 2020-3268, 7790-8380). Down-hole ZrHe data display a spread in ages from 112-0.8 Ma (Table 1, Figure 5). In the upper portion of the KTB drill hole (0-4668 m depth), there is a range of ZrHe ages from 71.2 ± 5.7 Ma (ZKTB1575) to 111.7 ± 8.1 Ma (ZKTB1230). There are three groups of ages in upper ~4700 m that vary in ZrHe age 71-76 Ma, 81-87 Ma and 93-96 Ma. This spread in ages produces an average age interval of 85 ± 15 Ma (MSWD). Sample ZKTB1230 is anomalously, but reproducibly, old with an average age of 111.7 ± 8.1 Ma. There is a marked decrease beginning at 5008 m (ZKTB5008 57.5 ± 4.6 Ma) and the younging trend continues with depth. By 7200 m, zircon no longer retains He and ZrHe ages are near zero (ZKTB7200 0.9 ± 0.1 Ma). Reset ages continue with depth except for an outlier ZKTB7553 at 17.7 ± 1.4 Ma. Based on a uniform geothermal

gradient of ~27°C/km and a mean annual surface temperature of ~7°C, the marked slope of decreasing ZrHe ages occurs over the temperature range ~130 - 210°C.

Cycled step-heating experiment results

Two step heating experiments on zircon from different amphibolite units (ZKTB1516-DE and ZKTB4050-DE) yielded well-defined Arrhenius behavior and excellent linear correlations (Figure 5; Table 2). Calculated diffusion kinetics for sample ZKTB1516-DE E_a = 43.6 kcal/mol (182.5 kJ/mol) and $\log(D/a^2)$ = 4.21 s^{-1}/cm^2 and ZKTB4050-DE E_a = 38.2 kcal/mol (159 kJ/mol) and $\log(D/a^2)$ = 2.99 s^{-1}/cm^2. Data from ZKTB1516 do not display anomalously high diffusivities or erratic behavior in the first prograde series as noted in previously published zircon diffusion data (Reiners et al., 2002; 2004). The calculated closure temperature for ZKTB1516 is 215°C, based on 10°C/m.y. cooling rate. Results from diffusion experiment ZKTB4050 display higher diffusivities in the first prograde steps from 400-520°C (not displayed in Figure 5, see Appendix B). Bulk diffusion kinetics calculations are based on steps after 520°C. From measured kinetics the estimated T_c is ~181°C based on a cooling rate of 10°C/m.y. Diffusion kinetics and closure temperature for ZKTB4050 agree well with published ranges for bulk diffusion kinetics, while results from ZKTB1516 are distinctly higher than the range of published T_c for zircon (171-193°C; Reiners et al., 2002, 2004). The average equivalent sphere radius of 3 grains for diffusion experiments ZKTB1516-DE and ZKTB4050-DE is 59.1 μm and 51.1 μm respectively. In summary, the zircon diffusion experiments from the KTB

borehole display varying results. ZKTB1516 is extremely well behaved but calculates a T_c of 215°C, which is higher than expected for zircon by 20°C. ZKTB4050-DE on the other hand displays a T_c of ~181°C, which is in excellent agreement with previously published bulk diffusion kinetics.

IMPLICATIONS

KTB Zircon (U-Th)/He Ages

In general, ZrHe results from the KTB drill hole decrease in age with increasing depth and temperature from ~112 to <1 Ma. Although there is notable scatter in ZrHe ages (72 - 112 Ma) from 0-4700 m, ZrHe results document a mean down-hole age of 85 ± 15 Ma (stdev) for this depth range. Beginning at 5000 m ZrHe results display a controlled and uniform decrease in ages through a depth of 7200 m, from ~58 - <1 Ma. The temperature range of this decrease in ages occurs between ~130°C and ~210°C (Figure 5). We suggest the straightforward explanation for the distinctive shape and corresponding temperature range is the zircon HePRZ. A zircon HePRZ between 130-210°C is in agreement with previous studies that have sought to document zircon diffusion kinetics in nature. These studies sampled along exhumed fault blocks in the Basin and Range region of Nevada (Reiners et al., 2002; Tagami, 2003; Stockli, 2005). In these studies, zircon data display the characteristic shape of the lower half of a HePRZ with an inflection point at paleotemperatures predicted between 180-210°C. ZrHe results from the KTB drill hole not only confirm these results but provide a more comprehensive study of zircon diffusion kinetics by

sampling with greater resolution and because depth-temperature values of KTB samples are known with certainty. Additionally, ZrHe results agree with previous thermochronometric studies on the KTB drill hole, particularly TiHe results. TiHe results display invariant ages of ~85 Ma through the first 4 km and the titanite HePRZ between ~115-195°C, which agrees with a T_c of 200 ±10°C (Reiners and Farley, 1999; Stockli and Farley, 2004). Bulk laboratory-derived diffusion kinetics for zircon estimate a T_c between ~170-195°C. ZrHe data from the KTB drill hole display similar results, but push He diffusivities toward the higher T_c > ~200°C for zircon in the KTB drill hole. A precursory comparison of ZrHe results from the KTB drill hole to previous empirical calibration studies of ZrHe thermochronometry, THe results from the KTB drill hole, and laboratory derived diffusion kinetics confirm that a T_c > ~200°C is consistent over geologic timescales and temperatures for the studied samples. These results support extrapolation of the well-behaved Arrhenius behavior measured in bulk laboratory diffusion kinetics, which is often disputed because of the difference in timescale and temperature from laboratory to nature.

Thermal Modeling

Because the shape and slope of the HePRZ is a function of both diffusion kinetics and the thermal history, we compare model predictions to ZrHe results from the KTB drill hole. This exercise provides a more comprehensive test if bulk laboratory diffusion kinetics control ZrHe ages from the KTB drill hole and if ZrHe results are congruent with established thermal histories. Forward modeling results are

based on published thermal histories of four metamorphic fault blocks (A-D), which have been established with previous thermochronometric studies of the KTB drill hole (Wagner et al., 1997; Stockli and Farley, 2004) and a geothermal gradient of 27°C/km (Clauser et al., 1997). To assess the effects of diffusivity on down-hole ZrHe results, we modeled a range of published diffusion parameters that encompass the least to the most retentive results (Reiners et al., 2004; 2005) and the measured diffusion kinetics from cycled step heating experiments from the KTB drill hole (Table 2). Forward modeling results were produced with a MATLAB® (2008b, The MathWorks, Natick, MA) code developed at KU following equations outlined by Ketcham (2005). Comparison of results from HeFTY (Ketcham, 2005) in comparison to results from code developed at KU agree within ± 2%.

Figure 8 compares the thermal history of four coherent fault blocks modeled with the range of published diffusion kinetics (hatched envelope), and diffusion parameters from zircon KTB diffusion experiments (square ZKTB1516-DE and circle ZKTB4050-DE) with ZrHe results. Not including the scatter seen in the first 4 km of ZrHe data (71-112 Ma), the ZrHe results fall within the envelope of published diffusion parameters through the HePRZ (130-210°C). ZrHe results sit low in the hatched envelope indicating that higher diffusivities control the bulk of ZrHe ages from the KTB drill hole. Diffusion kinetics from ZKTB4050-DE, T_c ~180°C, delineate the top edge of ZrHe results within the HePRZ, while diffusion kinetics from ZKTB1516-DE, T_c 215°C, sit well below the hatched envelope. The difference in diffusivity and consequent T_c between the two diffusion experiments is not

understood but may demonstrate natural variation within zircon. Interestingly, the high diffusion kinetics from ZKTB1516-DE can account for anomalously old ages in ZrHe data, for example ZKTB7553 and ZKTB4668, which are outside the predicted results. With a higher T_c, modeled results for ZKTB1516-DE also produce a 'tail' of older ages in the first ~1000 m of Block A and Block B as He is retained prior to the rapid uplift at ~85 Ma (Figure 8). This tail or more accurately, higher diffusion kinetics, could account for the group of ZrHe ages between 93-96 Ma for samples in the upper 4700 m (ZKTBQ, ZKTB52, ZKTB125, ZKTB1358, ZKTB1516 - see Table 1). Thus modeling predictions can account for two groups within the ZrHe ages which vary between ~85-94 Ma. The five paragneiss samples that group together with ZrHe ages between 71-76 Ma (ZKTB525, ZKTB1575, ZKTB3059, ZKTB3269, ZKTB3575) are not predicted by the modeled results. Although all of these samples are from paragneiss units except ZKTB3575, other paragneiss samples do not display similarly young ages (e.g., ZKTB525 77.2 ± 6.2 Ma and ZKTB125 93.2 ± 7.5 Ma). To produce a (U-Th)/He age of ~75 Ma, diffusion kinetics would reflect a T_c near ~150°C, which seems unlikely for zircon. Zoning was not considered for zircon from the KTB, and it has been shown that a U-, Th-enriched rim will produce a young ZrHe age due to an inaccurate α-ejection correction (Hourigan et al., 2005, Dobson et al., 2008).

ZrHe data agree well with modeled results from a fault block tectonic history as noted in Stockli and Farley (2004). The range of diffusion kinetics that best match the ZrHe ages have a lower PRZ inflection point at ~200-210°C. The diffusion

experiments ran on zircon from the KTB drill hole may indicate that a wide range of diffusion kinetics can influence samples from the KTB drill hole. Experiment ZKTB4050-DE, with a measured T_c of 180°C, outlined the youngest ZrHe ages from the KTB drill hole. Experiment ZKTB1516-DE, with a measured T_c of 215°C, sat well below the hatched envelope of published bulk diffusion kinetics (Reiners et al., 2004), but did predict anomalously old ZrHe ages, which were more retentive than modeled results from bulk diffusion kinetics (e.g., ZKTB7553, ZKTB4668). Higher diffusivities may also account for ~93 Ma ZrHe ages in Block A and B. In summary, the bulk of ZrHe data can be accounted for by variations in sample-by-sample diffusion kinetics. The hatched envelope of Figure 8, represents the range of published diffusion parameters (Reiners et al., 2004; 2005) utilized in ZrHe thermochronometry to deduce cooling ages and geologic rates in ZrHe studies.

Modeling results (Figure 7) also display an offset in predicted ages near the three main fault zones, which delineate fault blocks A-D. ZrHe ages from the upper 4700 m of the KTB borehole do not appear to be controlled by faulting. Samples within the NFZ display the largest scatter in ZrHe data with a range from 72 Ma to 112 Ma (Figure 7). The unusually old ages seen at 1230 m depth (five aliquots yield an average age of 112 ± 9 Ma) could be associated with faulting in the NFZ and sampling of a faulted sliver. Rutile (U-Th)/He ages (see Chapter 3) display a similarly old age from the same sample (RKT1230 ~118 ± 46 Ma). There is no evidence of older ages in Block A from AFT (Coyle et al., 1997) or TiHe KTB results (Stockli and Farley, 2004), however these studies did not sample within 45 m of 1230

m. Tectonic activity in the early Cretaceous is recorded in down-hole TFT results, which display invariant ages between 97-112 Ma from 5500 to 6500 m (Coyle and Wagner, 1998). Similarly, ^{40}Ar-^{39}Ar results document a cooling event between ~95-125 Ma on microcline from 0 m and 3203 m depth (Warnock and Zeitler, 1998). Although we cannot fully account for early Cretaceous ZrHe ages at 1230 m, we do not interpret them as irrelevant nor erroneous, the ages are reproducible and not unrelated to other thermochronometric results from the KTB drill hole.

Recent studies that employed computational studies at the atomic level reported that diffusion of He in zircon is anisotropic, and controlled by diffusion along the c-axis at geologically pertinent temperatures (Reich et al., 2007). They suggested that anisotropic diffusion could alter bulk diffusion kinetics by ~30% or ± 31 kJ/mol. Figure 8 also compares results from this study to the calculated diffusion kinetics which are proposed to "evaluate the potential effect of anisotropy on the bulk experimental E_a and D_0" (Reich et al., 2007- Table 4). The high and low estimates of anisotropic diffusivities are far too retentive (T_c 272°C) and conversely not sufficiently retentive (T_c 104°C) to reflect ZrHe results from the KTB drill hole. Saadoune and others (2009) reported that the presence of point defects along the c-axis effectively doubled diffusivity in zircon by producing 'He traps' in their computer simulated zircon lattice. Down-hole ZrHe results from the KTB drill hole suggest that anisotropic diffusion in natural zircon is negated by the presence of defects along the c-axis to the extent in which diffusivity reflects a T_c of ~200°C.

It has also been suggested that the magnitude of anisotropic He diffusion in zircon will be influenced by the extent of radiation damage in the mineral (Reich et al., 2007). ZrHe data do not display a major correlation between the effective uranium concentration (e[U] = [^{238}U] + 0.235*[^{232}Th]) and ZrHe age (Figure 9). Effective uranium concentration has recently been utilized as a proxy to measure radiation damage for apatite (U-Th)/He thermochronometry (e.g., Shuster et al., 2006; Flowers et al., 2008). Figure 9a displays the effective uranium concentration of ZrHe ages from the upper 5000 m, and no correlation is seen with age and eU concentration. Particularly older than expected ZrHe ages do no correlate with increased eU concentration (e.g., ZKTB1230 112 ± 9 Ma larger squares). Figure 9b displays the eU concentration of ZrHe ages from the lower portion of the KTB drill hole. Within these data, sample ZKTB7553 displays anomalously old ZrHe ages (17.7 ± 7 Ma) at temperatures of ~215°C. This is the only sample that displays a possible correlation for radiation damage to produce these old ZrHe ages. No other samples appear to show a positive correlation with eU concentration. Similarly, measured bulk diffusion kinetics from laboratory step-heating experiments from the KTB drill hole are not controlled by eU concentration. Based on zircon analyzed for ZrHe analysis, the more retentive ZKTB1516-DE, with a T_c 215°C, has an average eU concentration of 30 ± 20 ppm (stdev n = 4). ZKTB4050-DE, with a T_c of 180°C, has a higher eU concentration of 300 ± 200 ppm (stdev n = 3). As far as we know, there is no study that positively correlates diffusivity to scale with radiation damage/effective uranium concentration for zircon. Previous studies on the subject

suggest radiation damage in zircon is a complex relationship between He retention, fractional crystallinity and radiation damage (Nasdala et al., 2004; Reiners, 2005).

From ZrHe results we interpret a zircon HePRZ between ~130-210°C, this temperature range agrees with previous empirical calibrations on exhumed fault blocks. The shape and slope of the zircon HePRZ can be accurately predicted by published thermal histories and laboratory derived diffusion kinetics measured from zircon within the KTB drill hole and published bulk diffusivities. Approximated diffusivities based on anisotropic diffusion in zircon were compared against ZrHe data from the KTB and results suggest that anisotropic diffusion does not control He diffusion of zircon in this setting. Instead bulk laboratory-derived diffusion kinetics more accurately reflects the thermal sensitivity of ZrHe results from the KTB drill hole.

CONCLUSION

Recently the application of utilizing bulk laboratory-derived diffusion kinetics to determine geologic time scales and temperatures has been under investigation. This comes from a need to better understand atomic level interactions between He and the crystal lattice and possibly explain non-Arrhenius behavior often seen in laboratory-derived diffusion data. In this study we present down-hole ZrHe results from the KTB drill hole, which provide significant information on the diffusion kinetics that control He diffusion in the natural zircon studied. ZrHe results from 37 samples display ages from ~112 to <1 Ma from down-hole analysis of the 9-km deep KTB

drill hole. There is a marked decrease in ages beginning at ~130°C that continues through 210°C where ages are nearly reset. We define this temperature range as the zircon HePRZ. The base inflection point of the HePRZ corresponds well with laboratory measured diffusivities that measure higher diffusivities, ~T_c 190°C. This study complements previous attempts to identify the zircon HePRZ from exhumed fault blocks, which predict a lower inflection point between 180-210°C (e.g., Reiners et al., 2002; Tagami et al., 2003; Stockli, 2005). Concurrently, ZrHe results strengthen our knowledge of the laboratory derived diffusion kinetics that operate in nature, by removing uncertainty of projecting paleodepths and paleotemperatures and replaces uncertainty with well constrained temperatures and depths of each sample in the KTB drill hole. ZrHe results also help confirm and refine the well-established thermal history of the KTB drill hole, recording rapid movement on the FL in the Cretaceous followed by protracted cooling, as seen in THe results (Stockli and Farley, 2004).

This study confirms that projection of laboratory diffusion data (e.g., diffusion experiment ZKTB4050-DE E_a 159.9 kJ/mol, D_0 0.03 s^{-1}, T_c 181°C) accurately reflects down-hole ZrHe ages, and ZrHe ages in turn reflect conditions over geologic timescales and temperatures. But this study also displays the degree of variation that is possible within laboratory bulk diffusion results (ZKTB1516-DE E_a 182.5 kJ/mol, D_0 0.55 s^{-1}, T_c 215°C). Although ideal, it is not reasonable to perform weeklong cycled step-heating experiments for every ZrHe analysis. But we suggest it should be considered, particularly in studies when estimating the rate and magnitude of

exhumation, when laboratory derived diffusion kinetics are directly used in predictions. Although we believe this study confirms bulk diffusion kinetics apply to geologic timescales and temperatures, it does not attempt to specify why the effects of anisotropic diffusion (i.e. lower diffusivities) are not seen in natural zircon. It seems likely that structural defects and radiation damage produces a sufficient number of 'He traps' to constipate the preferred diffusion pathways [001], which has been suggested by Saadoune and others (2009). Further research is needed to systematically analyze the effect of radiation damage and its influence on anisotropic diffusion. Additional ZrHe studies on well-constrained drill holes with bottom hole temperatures greater than ~210°C in combination with intra-sample laboratory diffusion experiments, possibly on more samples than conducted here, will provide further evidence if published diffusion kinetics can be accurately applied to constrain thermal histories.

Chapter 2: REFERENCES

Bowring S.A., Erwin D.H., Jin Y.G., Martin M.W., Davidek K., Wang W., 1998, U/Pb zircon geochronology and tempo of the end-Permian mass extinction. Science v. 280, p. 1039-1045.

Campbell, I, Reiners, P., Allen, C., Nicolescu, S., Upbahydyay, R., 2005, He-Pb double-dating of detrital zircons from the Ganges and Indus rivers: Implication for quantifying sediment recycling, exhumation rates and provenance studies. Earth and Planetary Sciences. v. 237. p. 402-432.

Clauser, C., Giese, P., Huenges, E., Kohl, T., Lehmann, H., Ryback, L., Safanda, J., Wilhelm, H., Windloff, K., Zoth, G., 1997. The thermal regime of the crystalline continental crust: implications from the KTB. Journal of Geophysical Research, v. 102, p. 18417-18441.

Coyle, D.A., Wagner, G.A., Hejl, E., Brown, R., and Van den Haute, P., 1997, The Cretaceous and younger thermal history of the KTB site (Germany). apatite fission-track data from the Vorbohrung. Geol. Rundschau, v.86, p. 203-209.

Dobson, K., Stuart, F., Dempster, T., EIMF, 2008, U and Th zonation in Fish Canyon Tuff zircons: Implications for a zircon (U-Th)/He standard. Geochimica et Cosmochimica Acta, v. 72, p. 4745-4755.

Dodson, M.H., 1973, Closure temperature in cooling geochronological and petrological systems, Contributions to Mineralogy and Petrology, v. 40, p. 259-274.

Ehlers, T.A. and Farley, K.A., 2003, Apatite (U-Th)/He thermochronometry: methods and applications to problems in tectonic and surface processes. Earth and Planetary Science Letters, v. 206, p. 1-14.

Emmerman, R., and Lauterjung, J., 1997, The German Continental Deep Drilling Program KTB: Overview and major results. JGR, v. 102, p. 18,179-18,201.

Farley, K., 2007, He diffusion systematic in minerals: evidence from synthetic monzite and zircon structure phosphates. Geochimica et Cosmochimica Acta. v. 71, p. 4015-4024

Farley, K.A. and Stockli, D.F., 2002, (U-Th)/He Dating of Phosphates: Apatite, Monazite, and Xenotime. In: Kohn, M., Rakovan, J., and Hughes, J. M. (eds), Phosphates. Review of Mineralogy, v. 47, p. 559-578.

Farley, K.A., 2002, (U-Th)/He dating: Techniques, calibrations, and applications in: Noble Gases in Geochemistry and Cosmochemistry, Reviews in Mineralogy and Geochemistry, v. 47, p. 819-844.

Farley, K.A., 2000, Helium diffusion from apatite: General behavior as illustrated by Durango fluorapatite, Journal of Geophysical Research, v. 105, p. 2903-2914.

Farley, K.A., Reiners, P.W., and Nenow, V., 1999, An apparatus for high-precision helium diffusion measurements from minerals. Analytical Chemistry, v. 71, p. 2059-2061.

Farley, K.A., Wolf, R., and Silver, L., 1996, The effects of long alpha-stopping distances on (U-Th)/He ages, Geochimica et Cosmochimica Acta, v. 60, p. 4223-4229.

Fedo, C., Sircombe, K., Rainbird, R., 2003, Zircon Analysis of the Sedimentary Record. Rev. Mineral. Geochem. v. 53, p. 278-303.

Finch R.J., and Hanchar J.M., 2003, Structure and chemistry of zircon and zircon-group minerals, Zircon. Rev. Mineral. Geochem. v. 53, p. 1–25.

Gibson GM, Ireland TR (1995) Granulite formation during continental extension in Fiordland, New Zealand. Nature v. 375, p. 479-482.

Harrison, T.M., and Zeitler, P.K., 2005, Fundamentals in Noble Gas Thermochronometry, in Reiners, P.W. and Ehlers, T.A., Low Temperature Thermochronology: Techniques, Interpretations and Applications, Reviews in Mineralogy and Geochemistry, v. 58, p. 123-149.

Hejl, E., Coyle, D., Nand Lal, P., Van den Haute, P., and Wagner, G.A., 1997, Fission-track dating of the western border of the Bohemian massif: thermochronology and tectonic implications. Geol. Rundschau, v. 86, p. 210-219.

Hirschmann, G., Duyster, J., Harms, U., Kontny, A., Lapp, M., de Wall, H. & Zulauf, G., 1997, The KTB superdeep borehole: petrography and structure of a 9-km-deep crustal section. Geol. Rundsch , v. 86, p. 3-15.

Hourigan J.K., Reiners, P.W., and Brandon, M.T., 2005, U-Th zonation-dependent alpha-ejection in (U-Th)/He chronometry. Geochimica et Cosmochimica Acta., v. 69, p. 3349-3365.

House, M.,A., Farley, K. A., and Stockli, D.F., 2000, Helium chronometry of apatite and titanite using Nd-YAG laser heating. Earth and Planetary Science Letters, 183, 365-368.

House, M.A., Farley, K.A., Kohn, B., 1999, An empirical test of helium diffusion in apatite: borehole data from the Otway basin, Australia, Earth and Planetary Science Letters, v. 170, p. 463-474.

Ketcham, R.A., 2005, Forward and inverse modeling of low-temperature thermochronometry data, in Low-Temperature Thermochronology: Techniques, Interpretations, and Applications, Rev. Mineral. Geochem., v. 58, pp. 275 – 314.

MathWorks, The, 2008b. MATLAB®, Natick, MA.

Mingram, B., Kroner, A., Hegner, E., Krentz, O., 2004, Zircon ages, geochemistry, and Nd isotopic systematics of pre-Variscan orthogeneisses from the Erzgebirge, Saxony (Germany) and geodynamic interpretation. Geol Rundschau, v. 93, p. 706-727.

Mingram B., 1998, The Erzgebirge, Germany, a subducted part of northern Gondwana: geochemical evidence for repetition of early Palaeozoic metasedimentary sequences in metamorphic thrust units. Geological Magazine v. 135 p. 785–801.

Mitchell S.G., Reiners P.W., 2003, Influence of wildfires on apatite and zircon (U-Th)/He ages. Geology v. 31 p. 1025-1028.

Nasdala, L., Hanchar, J.M., Kronz, A., Whitehouse, M.J., 2005. Long-term stability of alpha particle damage in natural zircon. Chemical Geology v. 220 p. 83–103.

Nasdala L., Wenzel M., Vavra G., Irmer G., Wenzel T., Kober B., 2001, Metamictisation of natural zircon: accumulation versus thermal annealing of radioactivity-induced damage. Contribution to Mineralogy Petrology v. 141 p. 125–144.

O'Brien, P.J., Duyster, J., Grauert, B., Chreyer, W., Stockhert, B., and Weber, K., 1997, Crustal evolution of the KTB drill site: From oldest relics to the late Hercynian granites. Journal of Geophysical Research, v. 102, p. 18203-18220.

O'Brien, P.J., and Carswell., D.A., 1993, Tectonometamorphic evolution of the Bohemian Massif: evidence from high pressure metamorphic rocks. Geol. Rundsch, v. 82, p. 531-555.

Quadt., A. von, U-Pb zircon and Sr-Nd-Pb whole–rock investigations from the continental deep drilling (KTB). Geol. Rundsch. v. 86, p

Rahl J., Reiners P.W., Campbell I., Nicolescu S., Allen C.M., 2003, Combined single-grain (U-Th)/He and U/Pb dating of detrital zircons from the Navajo Sandstone, Utah. Geology v. 31, p. 761-764.

Reich, M., Ewing, R., Ehlers, T, Becker, U., 2007, Low-temperature anisotropic diffusion of heliumin izronc: implications for zircon (U-TH)/He thermochronometry. Geochimica Et Cosmochimica Acta. v. 71 pg. 2119-3130.

Reiners, P. and Farley, K., 1999, He diffusion and (U-Th)/He thermochronometry of titanite, Geochimica et Cosmochimica Acta, v. 62, p. 3845-3859.

Reiners, P., Farley, K., and Hickes, H., 2002, He diffusion and (U-Th)/He thermochronometry of zircon: Initial results from Fish Canyon Tuff and Gold Butte, Nevada, Tectonophysics, v. 349, p. 297-308.

Reiners, P., Spell, T., Nicolescu, S., Zanetti, K., 2004, Zircon (U-Th)/He thermochronometry: He diffusion and comparisons with Ar-40/Ar-39 dating. Geochimica Et Cosmochimica Acta v. 68. Ph. 1857-1887

Reiners, P., 2005, Zircon (U-Th)/He Thermochronometry, in Reiners, P. W. and Elhers, T. A., Low Temperature Thermochronology: Techniques, Interpretations and Applications, Reviews in Mineralogy and Geochemistry, v. 58, p. 151-179.

Saadoune, I., Purton, J.A., Leeuw, N.H., 2009, He incorporation and diffusion pathways in pure and defective $ZrSiO_4$: A density functional theory study. Chemical Geology, v. 258, p. 182-196.

Schmitt, A.K, Stockli, D.F., and Hausback, B.P., 2006, Magma evolution and eruption age of Tres Vírgenes (Baja California) constrained by combined $^{230}Th/^{238}U$ and (U, Th)/He dating of zircon. Journal of Volcanology and Geothermal Research, v. 158, p. 281–295.

Schroder, B., Ahrendt, H., Peterek, A., Wemmer, K., 1997, Post-Variscan sedimentary record of the SW margin of the Bohemian massif: a review. Geol Rundsch, v. 86, p. 178-184.

Solar, G., Pressley, R., Brown, M., Tucker, R., 1998, Granite ascent in convergent orogenic belts: Testing a model. Geology. v. 26, p. 711-714.

Stockli, D.,2005, Application of low-temperature thermochronometry to extensional tectonic settings. Review in Mineralogy and Geochemistry. v 58 p. 411-448. in Reiners, P.W. and Ehlers, T.A., Low Temperature Thermochronology: Techniques, Interpretations and Applications, Reviews in Mineralogy and Geochemistry, v. 58, p. 123-149.

Stockli, D. and Farley, K. A., 2004, Empirical constraints on the titanite (U-Th)/He partial retention zone from the KTB drill hole: Chemical Geology, v. 207, p. 223-236.

Stockli, D.F., Farley, K.A., and Dumitru, T.A., 2000, Calibration of the apatite (U-Th)/He thermochronometer on an exhumed fault block, White Mountains, California: Geology, v. 28, p. 983-986.

Tagami T., Farley K.A., and Stockli D.F., 2003, (U-Th)/He geochronology of zircon using Nd-YAG laser heating. Earth and Planetary Science Letters v. 207, p. 57-67.

Thomson, S.N., and Zeh, A., 2000, Fission-track thermochronology of the Ruhla Crystalline Complex: new constraints on the post-Variscan thermal evolution of the NW Saxo-Bohemian Massif. Tectonophysics, v. 324, p. 17-35.

Tincher, C.R. and Stockli, D.F., 2008, Cenozoic volcanism and tectonics in the Queen Valley area, Esmeralda County, western Nevada, GSA Bulletin Special Paper 445, p. 225-274.

Wagner, G., Michalski, I., and Zaun, P., 1989, Apatite fission track dating of the Central European Basement. Post-Variscan thermo-tectonic evolution, in The

German Continental Deep Drilling Program (KTB), edited by Emmermann, R. and Wohlenberg, p. 481-500, Springer-Verlag, Berlin.

Wagner, C.A., Coyle, D.A., Duyster, J., Henjes-Kunst, F., Peterek, A.,Schroder, B., Stockhert, B., Wemmer, K., Zulauf, G., Ahrendt, H., Bischoff, R., Hejl, E., Jacobs, J., Menzel, D., Ll, N., Van den haute, P., Vercoutere, C., Welzel, B., 1997. Post-Variscan thermal and tectonic evolution of the KTB site and its surroundings. Journal of Geophysical Research, v. 102, p. 18221-18232.

Warnock, A.C., Zeitler, P.K., Wolf, R.A., and Bergman, S.C., 1997, An evaluation of low temperature apatite U-Th/He thermochronometry. Geochimica et Cosmochimica Acta, v. 61, p. 5371-5377.

Watson E.B., and Harrison T.M., 2005, Zircon thermometer reveals minimum melting conditions on earliest Earth. Science. v. 308, p. 841–844.

Wemmer, K., 1991, K/Ar-Altersdatienrungsmoglickkeiten fur retrograde Deformationsprozesse im sproden und duktilen Bereich- Beispiele aus der KTB VB (Oberfalz) und dem Bereich der Insubrischen Linie. Gottinger Arb. Geol. Palantol, v. 51, p. 1-61.

Wolf, R.A., Farley, K.A. and Silver, L.T., 1996, Helium diffusion and low-temperature thermochronometry of apatite, Geochimica et Cosmochimica Acta, v. 60, p. 4231-4240.

Wolf, R.A., Farley, K.A., and Kass, F.M., 1998, Modeling of the temperature sensitivity of the apatite (U-Th)/He thermochronometer. Chemical Geology, v. 148, p. 105-114.

Zeitler, P.K., Herczeg, A.L., McDougall, I. and Honda, M., 1987, U-Th-He dating of apatite: A potential thermochronometer: Geochimica et Cosmochimica Acta, v. 51, p. 2865-2868.

Zulauf, G., Palm, S., Petschick, R., Spies, O., 1999, Element mobility and volumetric strain in brittle and brittle-viscous shear zones of the superdeep well KTB (Germany). Chemical Geology, v. 156, p. 135-149.

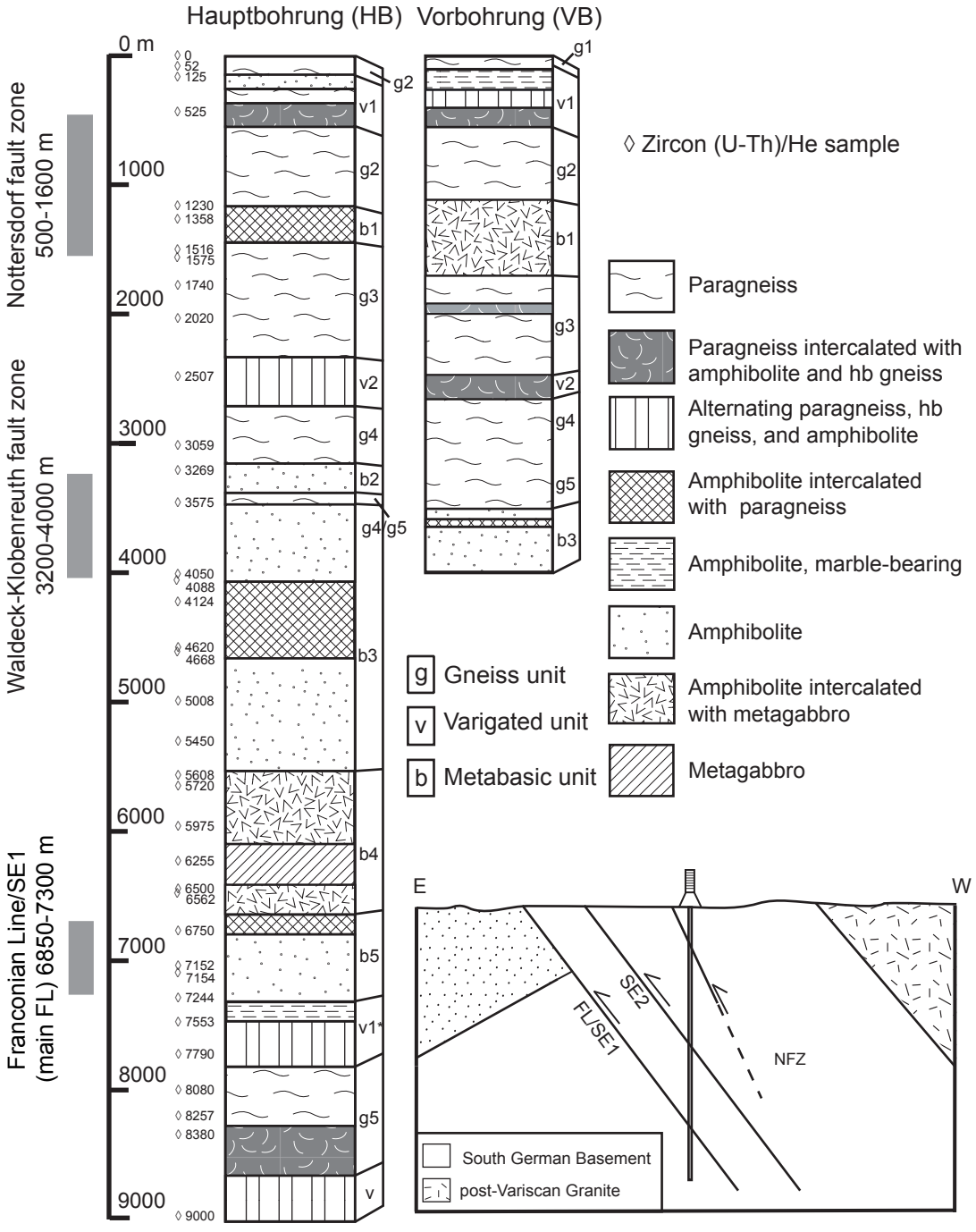
Hauptbohrung (HB)
Vorbohrung (VB)
0 m
1000
2000
3000
4000
5000
6000
7000
8000
9000
Nottersdorf fault zone
500-1600 m
Waldeck-Klobenreuth fault zone
3200-4000 m
Franconian Line/SE1
(main FL) 6850-7300 m
◊ Zircon (U-Th)/He sample
Paragneiss
Paragneiss intercalated with amphibolite and hb gneiss
Alternating paragneiss, hb gneiss, and amphibolite
Amphibolite intercalated with paragneiss
Amphibolite, marble-bearing
Amphibolite
Amphibolite intercalated with metagabbro
Metagabbro
g Gneiss unit
v Varigated unit
b Metabasic unit
E
W
SE2
FUSE1
NFZ
South German Basement
post-Variscan Granite

Figure 1. Down-hole profile of KTB drill hole, including the pilot hole, vorbohrung (VB) and main drill hole, hauptbohrung (HB). Simplified lithologic columns (after Hirschmann et al., 1997), displays repetition of gneissic (g), variegated (v) and metabasic (b) units. Major fault zones, noted on the far left identify boundaries which produce the stacked and repeated metamorphic blocks. Depth of sampled zircon (U-Th)/He analysis is noted to left of HB column, with ◊ and sampled depth.

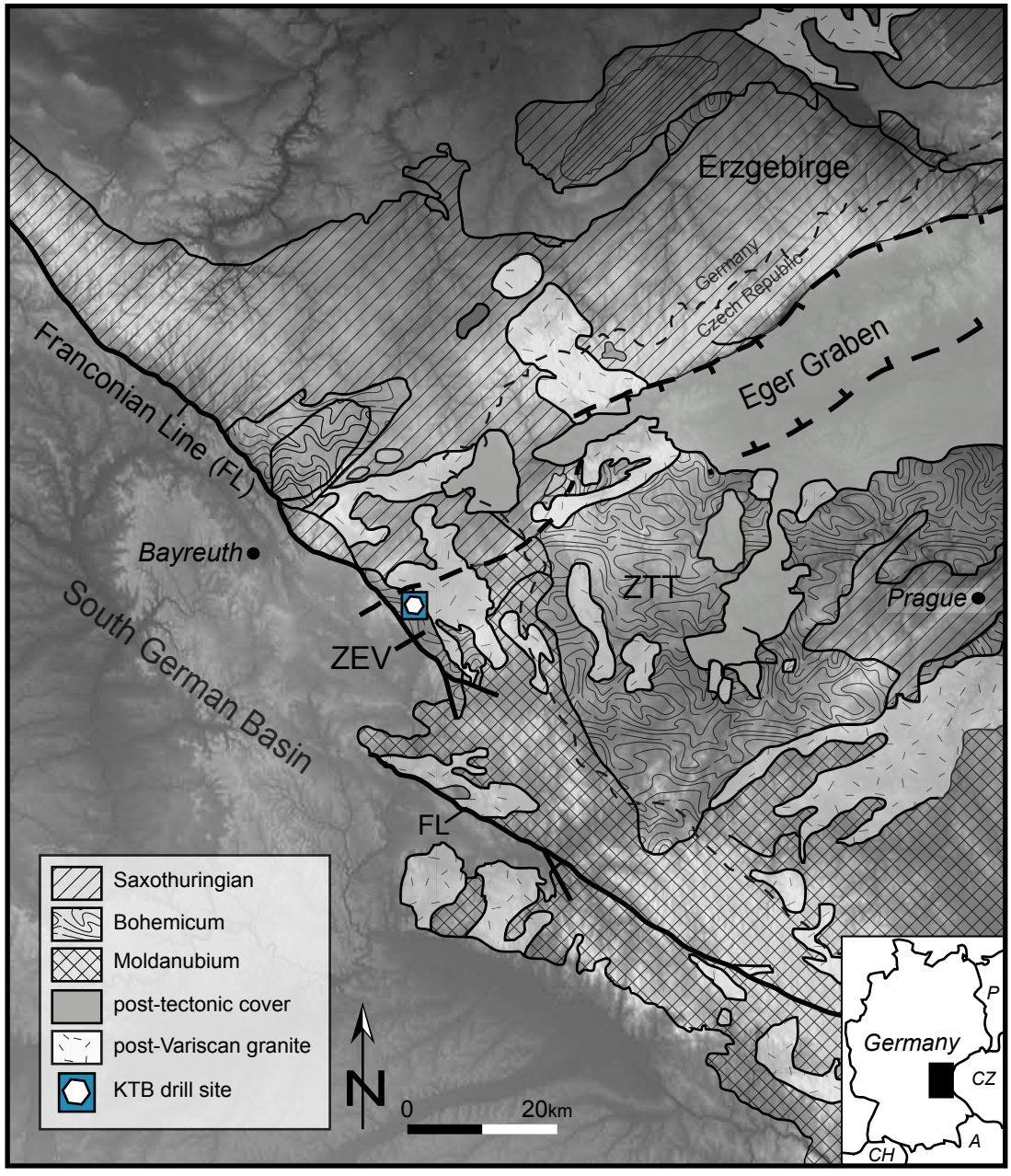
Erzgebirge
Germany
Czech Republic
Eger Graben
Franconian Line (FL)
Bayreuth
South German Basin
ZTT
Prague
ZEV
FL
Saxothuringian
Bohemicum
Moldanubium
post-tectonic cover
post-Variscan granite
KTB drill site
N
0
20km
Germany
P
CZ
A
CH

Figure 2. Simplified regional geologic map of KTB region and surrounding BM (modified from Franke, 1989). The Franconian Line (FL) delineates the western border of the BM with the South German sedimentary Basin to the west.
.

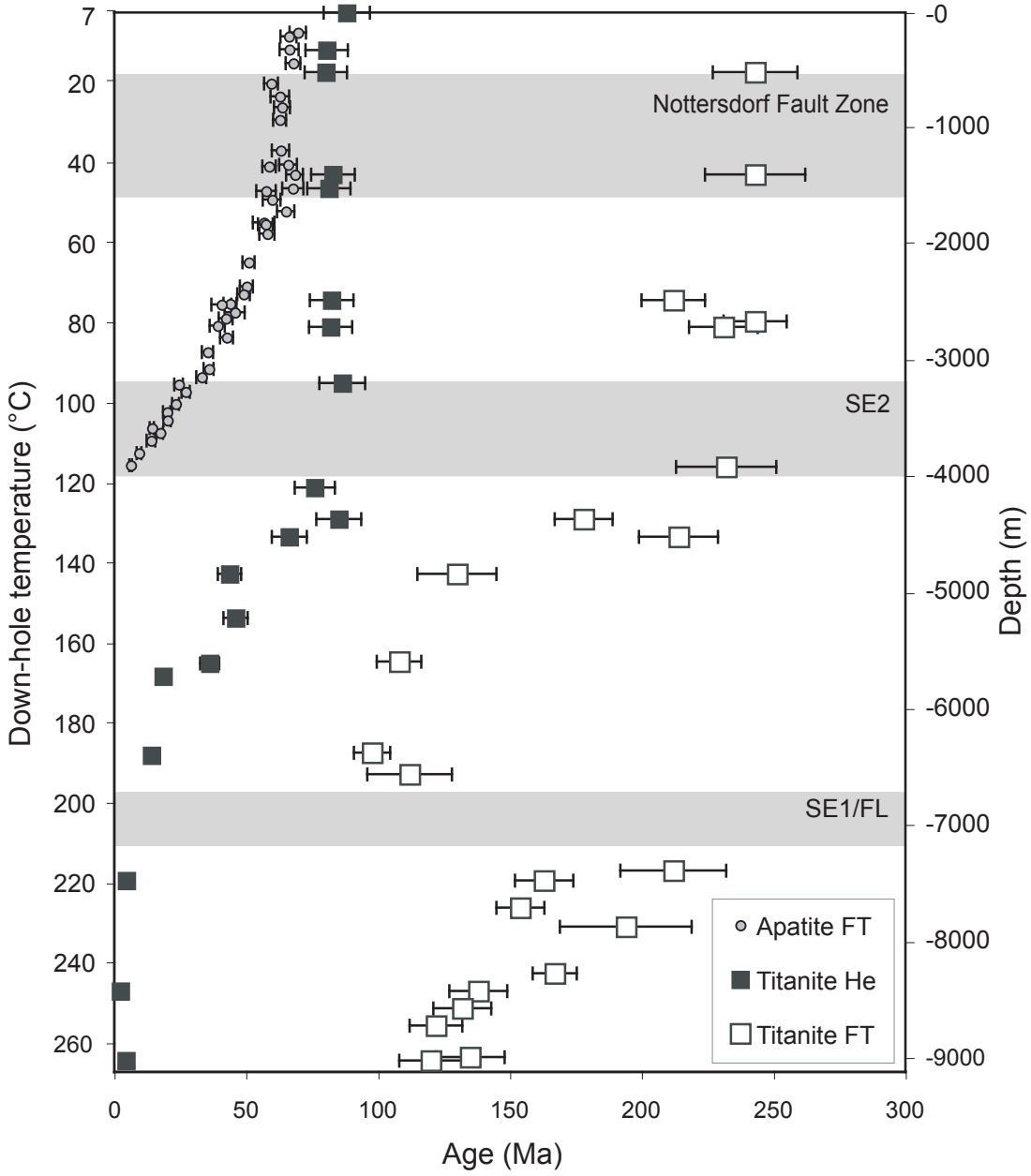
Down-hole temperature (°C)
Depth (m)
Age (Ma)
Nottersdorf Fault Zone
SE2
SE1/FL
Apatite FT
Titanite He
Titanite FT
7
20
40
60
80
100
120
140
160
180
200
220
240
260
-0
-1000
-2000
-3000
-4000
-5000
-6000
-7000
-8000
-9000
0
50
100
150
200
250
300

Figure 3. Depth array of age data collected for various thermochronometers in previous studies apatite FT (Coyle et al., 1997), titanite FT (Coyle and Wagner, 1998), titanite (U-Th)/He (Stockli and Farley, 2004) that reveal partial annealing/retention zone of each low temperature thermochronometer. Large grey boxes define reverse fault zones encountered during down-hole drilling. Offset due to faulting, is seen in apatite FT data by repetition in the Nottersdorf Fault Zone, while faulting along the FL is seen in titanite FT data.

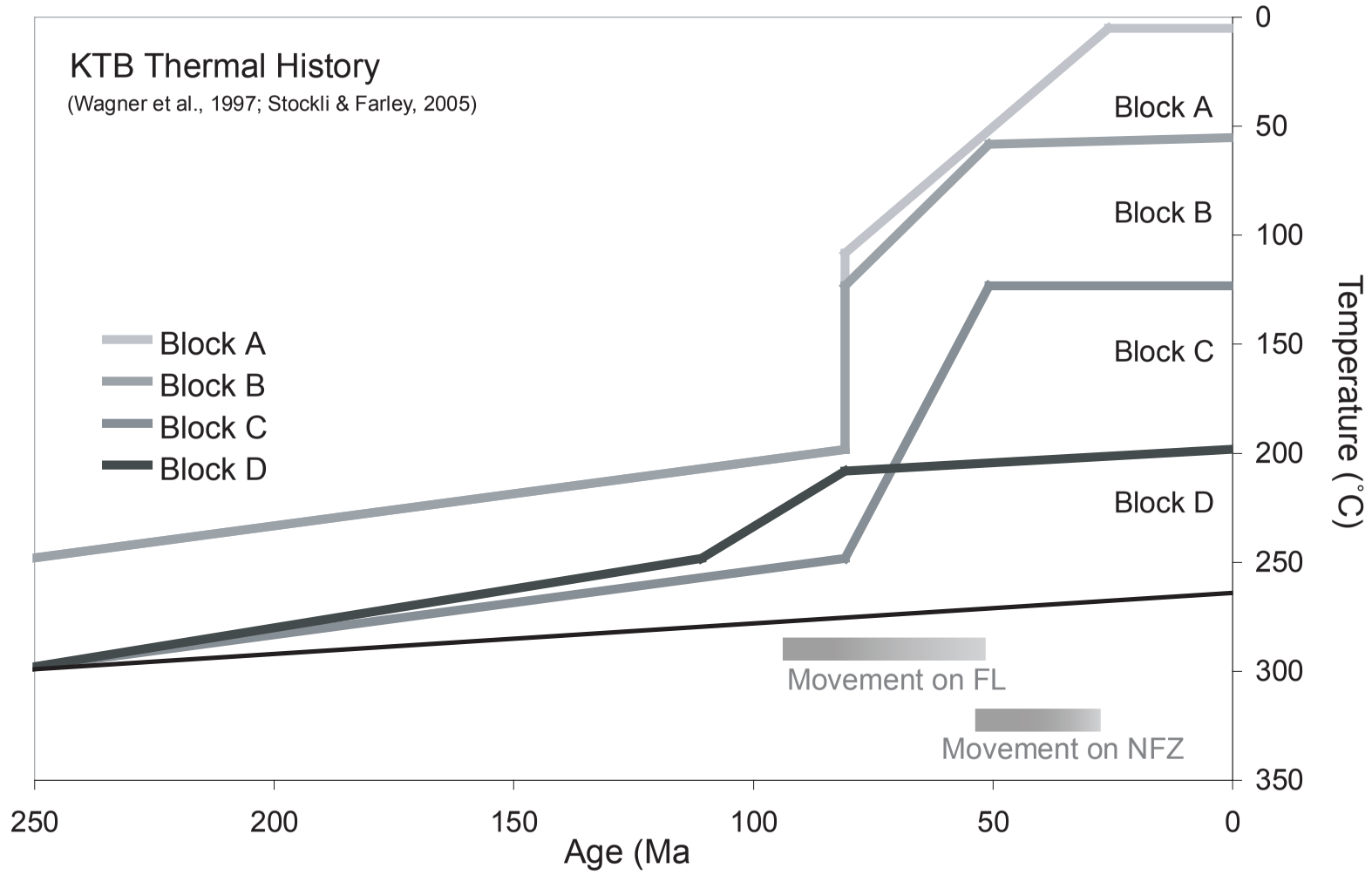
KTB Thermal History
(Wagner et al., 1997; Stockli & Farley, 2005)
Block A
Block B
Block C
Block D
Block A
Block B
Block C
Block D
Movement on FL
Movement on NFZ
0
50
100
150
200
250
300
350
Temperature (°C)
250
200
150
100
50
0
Age (Ma

Figure 4. Plot of the thermal history of the four fault blocks from the KTB drill hole for the past 250 Ma, as proposed by Wagner et al., (1998) and later modified by Stockli and Farley (2004) with down-hole titanite (U-Th)/He analysis. Thermal history utilized in modeling of laboratory derived diffusion kinetics of hatched envelope in Figure 7.

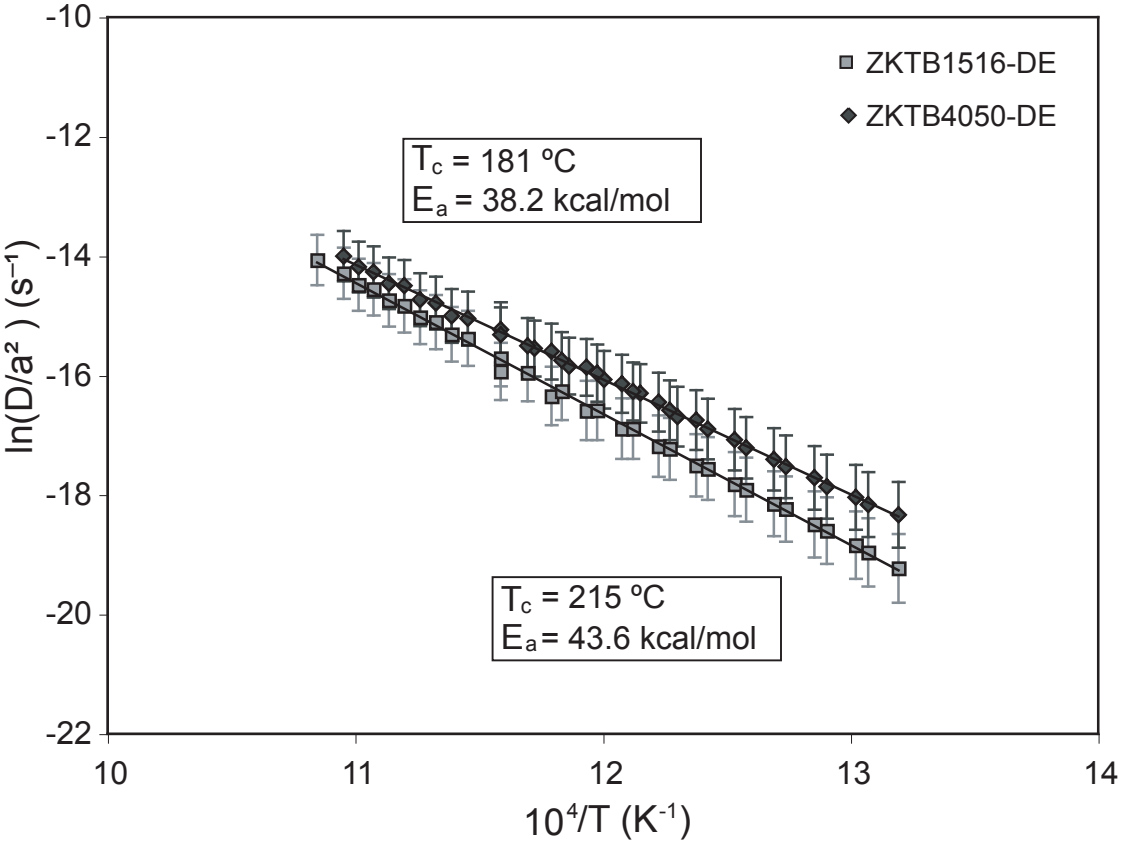
ZKTB1516-DE
ZKTB4050-DE
T_c = 181 ºC
E_a = 38.2 kcal/mol
T_c = 215 ºC
E_a = 43.6 kcal/mol
ln(D/a²) (s⁻¹)
10^4/T (K^{-1})
-10
-12
-14
-16
-18
-20
-22
10
11
12
13
14

Figure 5. Arrhenius plot of post-high temperature steps of cycled step-heating diffusion experiments from two zircon samples from KTB drill hole, ZKTB1516-DE and ZKTB4050-DE. Plot does not display initial prograde steps between 400-520°. Both samples come from amphibolite units and analyze three grains to ensure sufficient gas yields. ZHe results for ZKTB1516 and ZKTB4050 are 94.9 ± 7.6 Ma and 81.4 ± 1.4 Ma, respectively. Diffusion kinetics for ZKTB1516-DE indicate E_a 182.5 kJ/mol (43.6 kcal/mol) and D_0 0.55 cm^2/s and ZKTB4050-DE indicate E_a 159.9 kJ/mol (38.2 kcal/mol) and D_0 0.03 cm^2/s. For an effective grain radius of 60 μm and a cooling rate of 10°C/m.y., the T_c is 215°C and 181°C. ZKTB4050-DE (T_c 180°C) results agree with previously published laboratory-derived diffusion experiments on zircon, which range in T_c from 171-196°C (Reiners et al., 2004; Reiners, 2005), but ZKTB1516-DE with T_c of 215°C is much higher.

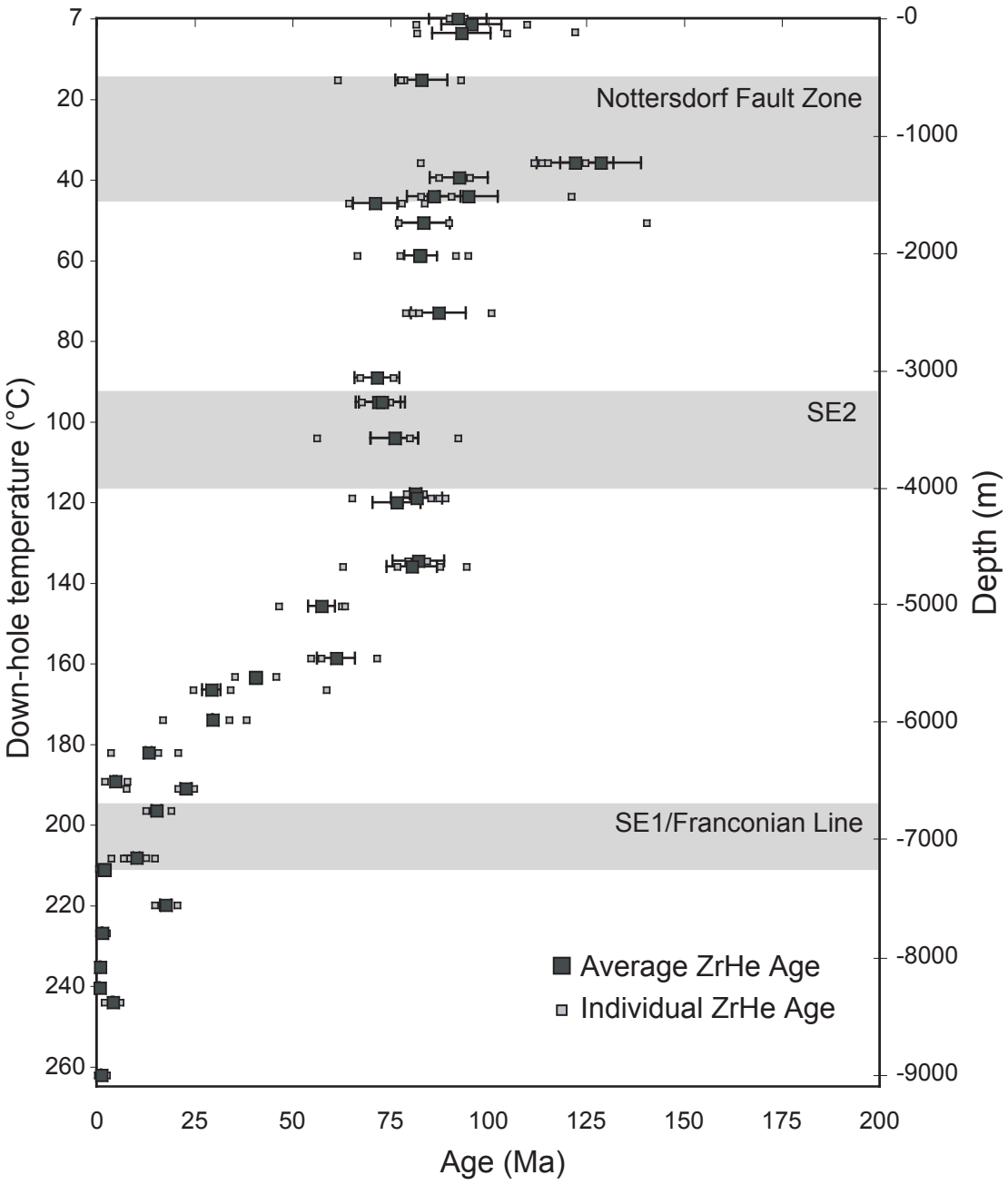
Nottersdorf Fault Zone
SE2
SE1/Franconian Line
Average ZrHe Age
Individual ZrHe Age
Down-hole temperature (°C)
Depth (m)
Age (Ma)
7
20
40
60
80
100
120
140
160
180
200
220
240
260
-0
-1000
-2000
-3000
-4000
-5000
-6000
-7000
-8000
-9000
0
25
50
75
100
125
150
175
200

Figure 6. Diagram displaying both individual (open square) and average (filled square) zircon (U-Th)/He age plotted with depth and down-hole temperature, assuming an equilibrated geothermal gradient of ~27.5°C (Clauser et al., 1997). Large grey boxes define reverse fault zones encountered during down-hole drilling. Zircon data define a well-constrained helium partial retention zone (HePRZ) beginning at ~130°C with a systematic decrease in ages until ~210°C, when ages are reset. Analytical errors displayed are 8% error.

Sample	Age [Ma]	± (8%) [Ma]	U [ppm]	Th [ppm]	Th/U	eU [ppm]	He [nmol/mg]	Mass [mg]	F_T	stddev	n	~ Temp * (°C)	Depth [m]
ZKTBQ	92.3	7.4	745.8	270.8	0.33	808.2	300.8	3.8	0.73	2.0	3	7	0
ZKTB 52[PG]	95.7	7.7	257.9	28.6	0.12	264.5	2010.0	1.6	0.67	20.0	2	8.5	-52
ZKTB 125[PG]	93.2	7.5	37.4	13.6	1.2	40.6	14.7	2.8	0.7	16.3	3	10.6	-125
ZKTB 525[PG]	77.7	6.2	131.5	43.2	0.9	181.9	0.3	47.6	0.7	8.7	4	22	-525
ZKTB 1230	111.7	8.9	83.2	38.1	13.0	92.0	943.7	11.2	0.8	16.9	5	42	-1230
ZKTB 1358	92.6	7.4	69.9	3.5	0.06	70.7	25.8	3.4	0.73	4.5	3	45.7	-1358
ZKTB 1516	94.9	7.6	28.5	5.8	0.2	29.8	7.7	4.5	0.8	17.8	4	50.2	-1516
ZKTB 1575[PG]	71.2	5.7	75.5	1.2	0.01	75.8	461.1	4.7	0.75	9.5	3	51.9	-1575
ZKTB 1740[PG]	83.5	6.7	117.8	16.8	0.1	121.7	41.59	3.5	0.74	9.1	4	56.6	-1740
ZKTB 2020[PG]	82.6	6.6	235.5	20.0	1.0	198.4	85.2	3.4	0.7	13.1	3	64.6	-2020
ZKTB 2507	87.3	7.0	26.4	1.6	0.8	26.7	9.4	4.0	0.7	11.8	3	78.4	-2507
Z747 A1[PG]	71.7	5.7	346.5	31.4	0.10	353.7	2079.1	3.0	0.72	4.3	3	94.2	-3059
Z798A1g2[PG]	72.0	5.8	193.1	74.3	0.40	210.2	1340.4	2.6	0.70	3.8	3	100.2	-3269
ZKTB 3575	76.1	6.1	123.4	50.6	0.36	342.5	39.58	3.2	0.72	18.4	3	108.9	-3575
ZKTB 4050	81.4	1.4	321.3	59.6	0.23	135.0	116.1	9.2	0.80	2.2	3	122.4	-4050
ZKTB 4088	81.7	6.5	383.7	142.6	0.42	335.0	3059.8	5.4	0.7	11.1	4	123.6	-4088
ZKTB 4124	76.7	6.1	221.7	50.7	0.19	416.5	74.5	5.1	0.76	0.6	3	124.5	-4124
ZKTB 4620	82.2	6.6	115.3	71.20	1.37	233.4	41.97	3.03	0.71	2.4	3	138.7	-4620
ZKTB 4668	80.5	6.4	81.1	26.2	0.7	131.7	5.3	0.8	0.8	11.9	5	124.0	-4668
ZKTB 5008	57.5	4.6	113.7	30.6	0.8	87.1	30.2	7.6	0.8	9.5	3	129.7	-5008
ZKTB 5450	61.2	4.9	101.5	14.5	0.6	120.7	28.6	8.2	0.8	9.1	3	162.3	-5450
ZKTB 5608	40.7	3.3	136.9	0.7	0.0	104.9	23.6	6.0	0.8	5.3	3	166.8	-5608
ZKTB 5720	29.3	2.3	65.1	44.6	2.7	75.3	8.4	2.0	0.7	6.7	3	170.0	-5720
ZKTB 5975	29.6	0.1	49.9	29.9	0.56	56.8	7.4	10.0	0.79	11.2	3	177.3	-5975
ZKTB 6255	13.3	1.1	100.3	0.9	0.4	100.5	7.2	7.2	0.8	8.8	3	185.3	-6255
ZKTB 6500	4.8	0.4	10.3	3.0	3.6	11.0	0.2	3.4	0.7	2.91	3	192.3	-6500
ZKTB 6562	22.8	1.4	117.1	46.1	0.40	127.8	10.0	5.4	0.76	9.1	3	194	-6562
ZKTB 6750	15.3	1.2	186.0	15.3	1.2	189.6	11.1	4.3	0.7	3.3	3	199.4	-6750

Sample	Age [Ma]	± (8%) [Ma]	U [ppm]	Th [ppm]	Th/U	eU [ppm]	He [nmol/mg]	Mass [mg]	F_T	stddev	n	~ Temp * (°C)	Depth [m]
ZKTB 7152	10.2	0.8	162.0	38.6	1.3	170.9	7.2	5.3	0.8	2.5	3	210.8	-7152
ZKTB 7154	8.4	0.7	111.3	1.5	0.2	111.7	4.6	6.0	0.8	5.8	3	210.9	-7154
ZKTB 7244	0.9	0.1	40.5	1.1	0.1	40.7	0.1	4.3	0.8	0.4	3	213.3	-7244
ZKTB 7553	17.7	1.4	702.5	365.1	0.51	786.6	1214.4	2.7	0.71	4.0	2	222.6	-7553
ZKTB 7790 [PG]	1.4	0.1	150.3	11.1	0.3	152.8	1.0	5.3	0.8	1.0	3	229.0	-7790
ZH034 [PG]	1.0	0.1	252.6	8.5	0.03	254.5	22.8	4.7	0.75	0.4	3	237.3	-8080
ZKTB 8257 [PG]	0.8	0.1	91.8	2.7	1.0	92.4	0.3	3.3	0.7	0.6	3	242.3	-8257
ZKTB 8380	4.2	0.3	209.6	34.9	0.4	217.6	4.2	5.8	0.8	2.0	3	245.3	-8380
ZKTB 9000	1.2	0.1	215.5	19.1	0.9	219.9	1.4	5.4	0.8	1.2	3	263.5	-9000

[PG] Zircon separate derived from paragneiss units, all other zircon from amphibolite or garnet amphibolite units

* Temperatures calculated on uniform geothermal gradient of 27°C/km with a mean annual surface temperature of 7°C (Clauser et al., 1997)

Table 1. Average zircon (U-Th)/He age from down-hole analysis of KTB drill hole. Single grain laser heating, mineral dissolution and parent analysis completed at the Isotope Geochemistry Laboratory at the University of Kansas (For more detailed methodology see text).

Sample	Rock Type	E_a (kcal/mol)	D_0 (s^{-1})	T_c (°C)	R^2	$T_{initial}$ (°C)[1]	a (μm)[2]	ZHe Age ± stdev (Ma)	e[U] ± stdev (ppm)	# grains
ZKTB1516	Grnt Amph (VB)	43.6	0.55	215	0.999	N/A	57.9	94.9 ± 17.8	29.8 ± 18.1	3
ZKTB4050	Amph (HB)	38.2	0.03	181	0.998	520	51.9	81.4 ± 2.2	335 ± 228.5	3
Published diffusion kinetics[3]		39-41	0.09-1.5	171-196		425-520				

[1] Nominal closure temperature based on 10°C/m.y. cooling (Dodson, 1972)
[2] The initial temperature from heating steps that used in E_a and D_0 calculations, due to anomalously high diffusivities in early steps
[3] Average equivalent sphere radius
[4] Values from Reiners et al., 2004, Reiners, 2005
[5] Values from Reich et al., 2007 (Table 4) given to approximate anisotropic diffusion along c-axis in natural zircon (established E_a 169 kJ/mol from Reiners et al., 2004 ± 31 kJ/mol

Table 2. Results from cycled step heating diffusion experiments on zircon from the KTB drill hole run in the Isotope Geochemistry Laboratory at the University of Kansas and pertinent information which could control diffusivity, grain size, eU concentration and the effect of diffusivity of the ZHe age. Both of these samples, based on modeling results, suggest that ZHe age should be ~85 Ma. The more diffusive ZKTB1516, results in ZHe age of ~95 Ma, which we assume is a product of high diffusivities. Also listed are published bulk laboratory derived diffusion kinetics from Reiners et al., 2004 and Reiners, 2005, which are modeled with thermal history of KTB drill hole (Wagner et al., 1997; Stockli and Farley, 2004). Also the published range of E_a corrected for the effect of anisotropic diffusion, which are modeled within the thermal history of the KTB drill hole in order to compare results to measured results (Reich et al., 2007).

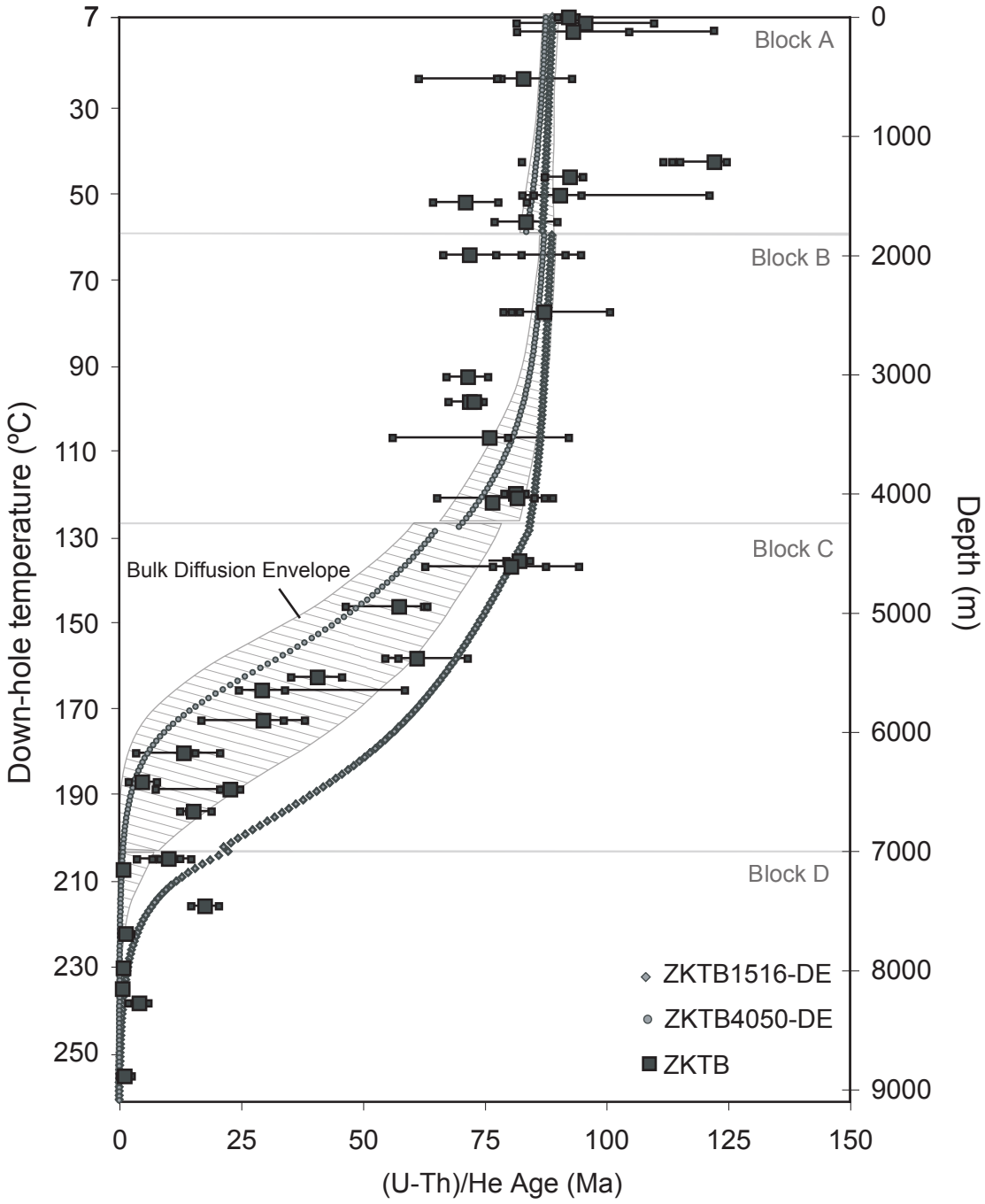
Block A
Block B
Block C
Block D
Bulk Diffusion Envelope
ZKTB1516-DE
ZKTB4050-DE
ZKTB
Down-hole temperature (°C)
Depth (m)
(U-Th)/He Age (Ma)
7
30
50
70
90
110
130
150
170
190
210
230
250
0
1000
2000
3000
4000
5000
6000
7000
8000
9000
0
25
50
75
100
125
150

Figure 7. Displays predicted down-hole zircon ages from modeling the thermal history seen in Figure 4 (based on Wagner et al., 1997; Stockli and Farley, 2004) in comparison to ZrHe results from KTB drill hole from this study. ZrHe ages are plotted as individual ages (small grey square) and average ages (large grey square) with maximum age spread plotted as error. Hatched envelope models zircon bulk laboratory derived diffusion kinetics in a range from E_a 165-171 kJ/mol and D_0 0.09-0.46 cm^2/s (Reiners et al., 2004; Reiners, 2005). White shapes (circle and square) reflect modeled results from laboratory derived diffusion kinetics from cycled step heating experiments on zircon from KTB drill hole. ZKTB4050-DE with T_c of ~181°C fits well with ZrHe ages, while ZKTB1516-DE with T_c of 215°C sits well below ZHe ages but can account for anomalously old ZrHe ages that sit outside of bulk diffusion envelope. ZKTB4050-DE appears to cap the ZrHe results within the HePRZ.

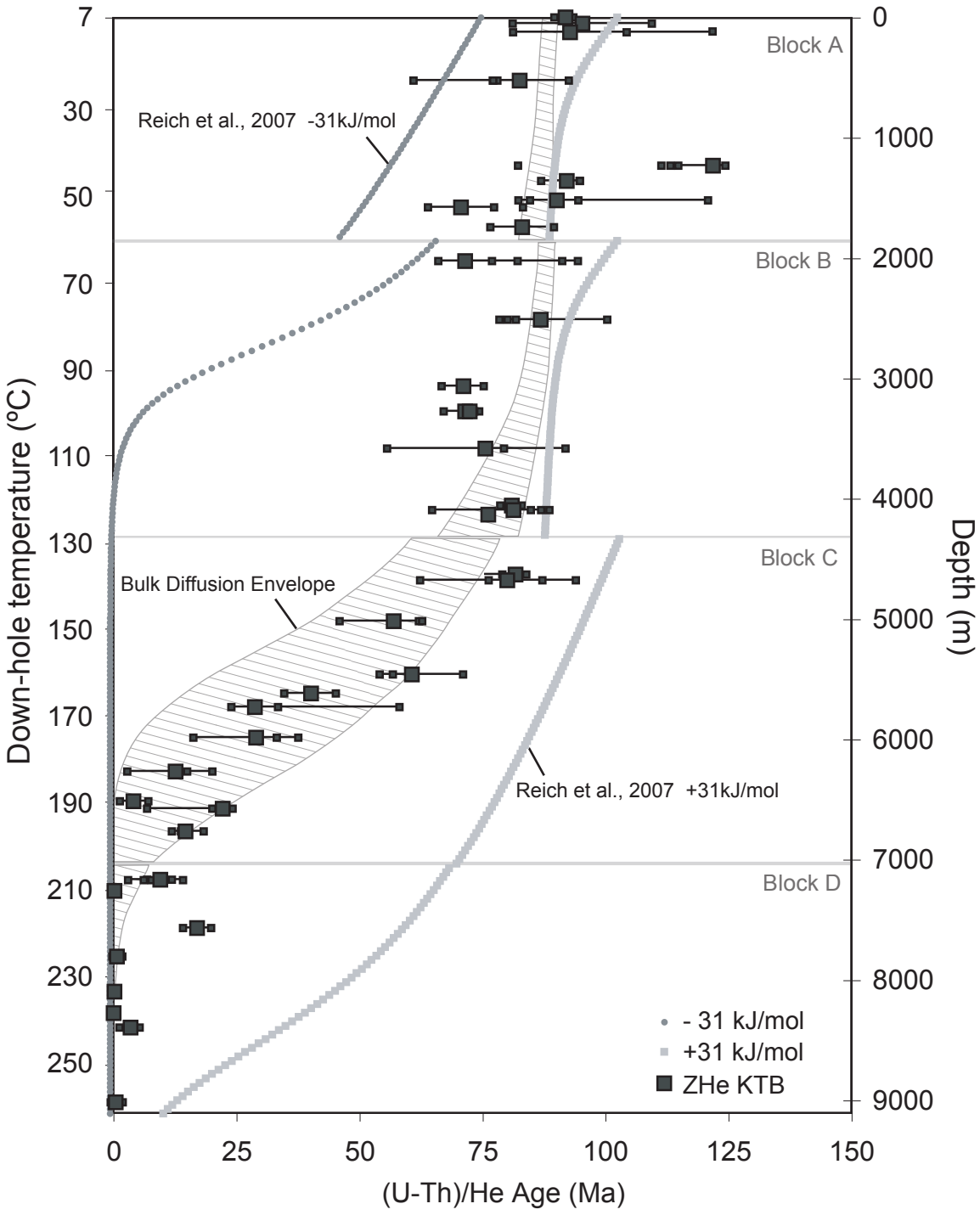
Block A
Block B
Block C
Block D
Reich et al., 2007 -31kJ/mol
Bulk Diffusion Envelope
Reich et al., 2007 +31kJ/mol
- 31 kJ/mol
+31 kJ/mol
ZHe KTB
Down-hole temperature (ºC)
Depth (m)
(U-Th)/He Age (Ma)
7
30
50
70
90
110
130
150
170
190
210
230
250
0
1000
2000
3000
4000
5000
6000
7000
8000
9000
0
25
50
75
100
125
150

Figure 8. Displays predicted down-hole zircon ages from modeling the thermal history seen in Figure 4 (based on Wagner et al., 1997; Stockli and Farley, 2004) in comparison to ZrHe results from KTB drill hole from this study. ZrHe ages are plotted as individual ages (small grey square) and average ages (large grey square) with maximum age spread plotted as error. Hatched envelope models zircon bulk laboratory derived diffusion kinetics in a range from E_a 165-171 kJ/mol and D_0 0.09-0.46 cm^2/s (Reiners et al., 2004; Reiners, 2005). Grey circle and square represent modeled results of E_a published by Reich and others (2007) as an approximation of anisotropic diffusion in natural zircon using 169 kJ/mol as the established E_a of zircon +31 kJ/mol and -31 kJ/mol. Comparing the effect of anisotropic diffusion on zircon by ~30% (-31 kJ/mol) to ZrHe results from KTB drill hole clearly shows that such a degree of anisotropic diffusion is not affecting ZrHe ages. Instead ZrHe ages sit low is bulk diffusion envelope, as more retentive diffusion parameters control ZrHe ages from KTB.

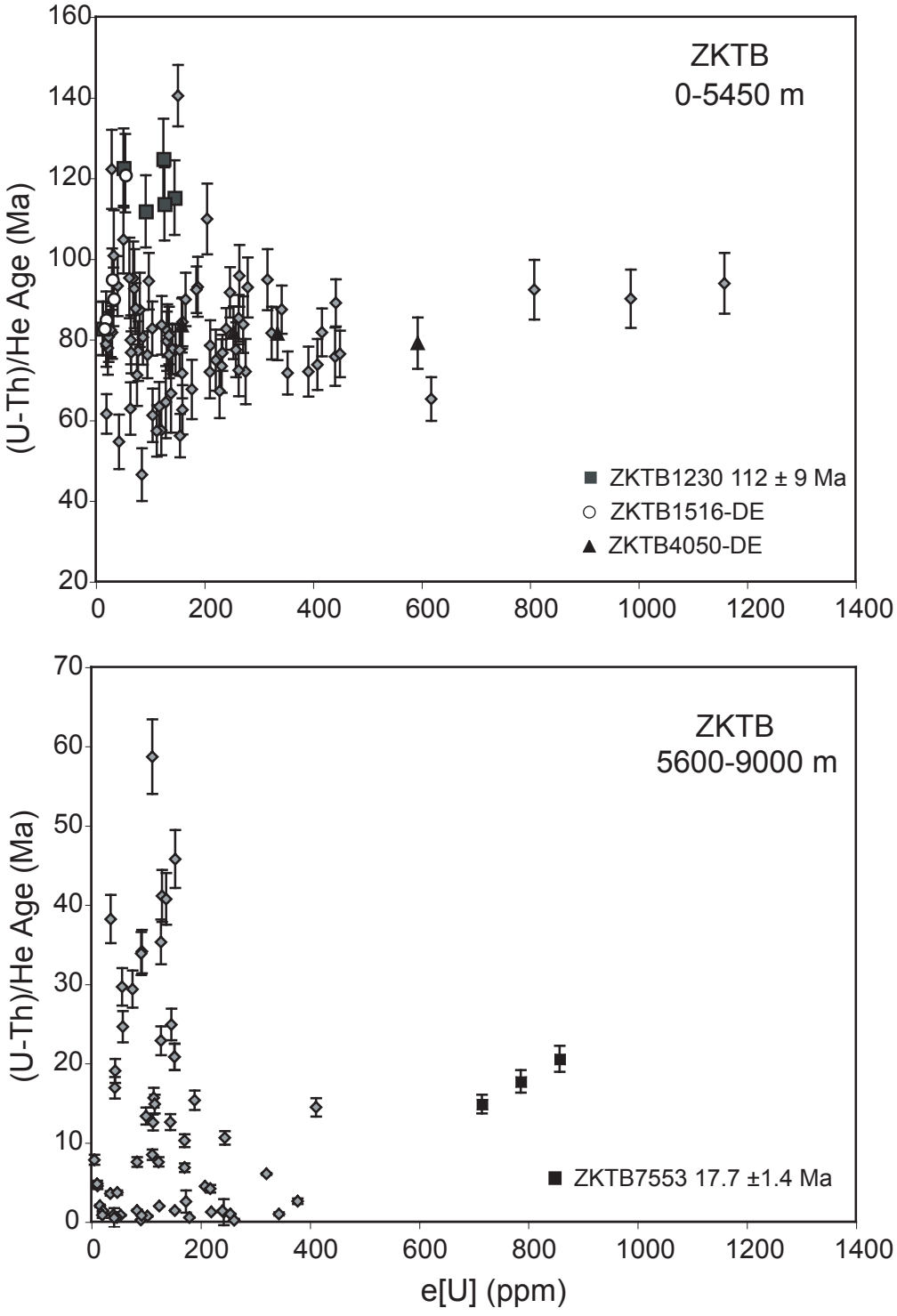
ZKTB
0-5450 m
(U-Th)/He Age (Ma)
ZKTB1230 112 ± 9 Ma
ZKTB1516-DE
ZKTB4050-DE
ZKTB
5600-9000 m
(U-Th)/He Age (Ma)
ZKTB7553 17.7 ±1.4 Ma
e[U] (ppm)

Figure 9. Zircon samples (gray diamond) from the KTB drill hole plotted as effective uranium concentration [eU] (U + 0.235*Th) by ZrHe age broken up into the upper ~5450 m (20a) and lower portion of KTB drill hole data (10b). There is no major correlation between eU concentration and age, suggesting radiation damage did not influence ZrHe ages, except for a single sample. One sample ZKTB7553, should be reset due to an approximate down-hole temperature of 230°C. In contrast, it displays a precise age of 18 ± 1.4 Ma, at eU concentrations which may lead to speculate radiation damage influencing the unexpectedly old ZrHe age. But no other sample, including ZKTB1230 (black square), which is anomalously old, ZrHe 112 ± 9 Ma, have no correlation with eU concentration. Similarly eU concentration does not directly influence diffusion kinetics, as ZKTB1516-DE (white circle), with T_c 215°C, has the lower eU concentration, compared to ZKTB4050-DE (black triangle) with T_c 181°C.

Page left intentionally blank

CHAPTER 3: Rutile (U-Th)/He thermochronometry on poly-metamorphic rocks from the KTB drill hole, Germany

ABSTRACT

This study presents rutile (U-Th)/He (RtHe) results from a suite of poly-metamorphic rocks in their geochemical and petrographic context from the German Continental Deep Drilling Project (KTB). Down-hole RtHe ages and a He diffusion experiment on KTB rutile were carried out as part of an effort to develop rutile (U-Th)/He thermochronometry and to investigate He diffusion kinetics in rutile. RtHe ages in the KTB generally decrease in age with increasing depth from ~120 Ma to <10 Ma over a depth range of 1230-9000 m, but are characterized by significant age scatter and low degrees of aliquot reproducibility. Lower portions of the KTB exhibit more reproducible RtHe ages that are anomalously young compared to corresponding zircon and titanite (U-Th)/He ages and numerical models of expected down-hole RtHe age variations, based on new laboratory-derived He diffusion kinetics. Age scatter and anomalous RtHe ages do not appear to be the result of low-temperature alteration or recrystallization, as trace element geochemical analysis suggest rutile is in its primary state. Detailed petrographic analysis of KTB rutile, however, documents progressive rutile breakdown to ilmenite and titanite, resulting in a ubiquitous thin titanite overgrowth on rutile. High U and Th reaction rims of titanite on rutile is problematic for (U-Th)/He analysis as it invalidates the homogeneous U and Th distribution assumption applied by the standard α-ejection correction. Application of an α-ejection correction that accounts for a U- and Th- enriched rim,

based on observed rim widths and estimates of titanite rim U and Th concentrations, yields more accurate RtHe ages for most KTB rutile that are younger than expected. In contrast to KTB rutile, regional RtHe ages from high-grade metamorphic rocks in the Erzgebirge (250-270 Ma) and Bohemian Massif (~200 Ma) yield RtHe ages that are consistent with the thermal evolution of these regions. We attribute this to the metamorphic grade and lack of widespread retrograde metamorphism influencing the stability of rutile. While regional RtHe results and KTB rutile He diffusion data are consistent with a He closure temperature of ~200-220ºC and illustrates the potential of RtHe thermochronometry of high-grade metamorphic rocks, results from the KTB drill hole illustrates the importance of detailed petrographic and geochemical characterization in order to obtain meaningful and reliable age data.

INTRODUCTION

(U-Th)/He thermochronometry is based on the accumulation of radiogenic ^{4}He produced by the decay of ^{238}U, ^{235}U, ^{232}Th, and ^{149}Sm and is a well-established technique on apatite, titanite, and zircon (e.g. Reiners and Farley, 1999; Farley, 2000; Reiners et al., 2002; Stockli and Farley, 2004). It is commonly used to reconstruct the time-temperature histories to an extensive range of geologic, tectonic, and geomorphic events (House et al., 1999; Farley, 2000; Reiners et al., 2000; Stockli, 2005; Mitchell & Reiners, 2003; Reiners et al., 2007). Other U- and Th-bearing phosphate, silicate, and oxide minerals such as monazite, xenotime, fluorite, magnetite, and goethite have been investigated as potential geo- and

thermochronometers (e.g., Farley and Stockli, 2002; Boyce et al., 2006; Blackburn et al., 2007; Shuster et al., 2005). The addition of a new (U-Th)/He chronometer, characterized by distinct He diffusion kinetics and closure temperatures, offers the capability to constrain different portions of a rock's low-temperature thermal history, often coupled with the potential to date alternate lithologies and geologic processes. For example, the recent development of magnetite as a (U-Th)/He geochronometer, can be utilized on intermediate to mafic volcanic rocks with the potential to date processes of the oceanic and continental crust (Blackburn et al., 2007).

In this study we present new developments of rutile as a (U-Th)/He thermochronometer. Rutile is an appealing candidate as a thermochronometer as it is a widely occurring oxide with U and Th contents similar to apatite with a documented range of 3-130 ppm of U (Mezger et al., 1989). Rutile can be found in a variety of geologic settings including alkali-rich plutonic rocks and as ore-deposits. Similar to zircon, it is extremely resistant to weathering and is a common detrital mineral in sedimentary rocks. Rutile is also found as a primary mineral in high-grade metamorphic rocks such as blueschists, eclogites and granulites (Deer et al., 1966; Mezger et al., 1989; Zack et al., 2002). The main attraction of calibrating rutile as a (U-Th)/He thermochronometer is its presence in these rocks, with the objective to reconstruct the rates and timing of metamorphic terrain exhumation. Initial studies have presented preliminary He diffusion data for rutile and its ability to accurately date quickly cooled rutile-bearing xenoliths and minettes (Crowhurst et al., 2002;

Stockli et al., 2005; 2007). These results strongly suggest the feasibility of rutile (U-Th)/He dating.

This study presents down-hole rutile (U-Th)/He (RtHe) analysis and results from a cycled step-heating experiment from amphibolites from the Continental Deep Drilling Project (KTB), Germany. Down-hole RtHe analysis provides an *in situ* measurement of He diffusivity in rutile over geologic timescales and temperatures. Modeling of laboratory-derived diffusion kinetics to the well-established thermal history of the KTB drill hole (Wagner et al., 1997; Stockli and Farley, 2004) in combination with down-hole titanite and zircon (U-Th)/He analysis (Stockli and Farley, 2004; Chapter 2, respectively) provides a direct reference to compare RtHe results. As a consequence of rutile being a primary mineral in metamorphic rocks, and not an accessory phase like zircon and apatite, this study also investigates the effect of metamorphic breakdown reactions on RtHe thermochronometry through trace element geochemistry and petrographic investigations of rutile in the KTB drill hole. Additionally, we present RtHe ages of regional surface samples from high-grade metamorphic rocks from Erzgebirge, Germany, and the Blanksy les Granulite Massif, Czech Republic in order to compare RtHe analysis to rocks of varying protolith and metamorphic grade. This study expands on previous RtHe thermochronometric studies with down-hole (U-Th)/He analysis to assess *in situ* diffusion kinetics, the application of RtHe to the slowly cooled high-grade metamorphic rocks, and draws attention to the crucial need for thorough petrographic context when analyzing primary minerals by (U-Th)/He thermochronometry.

Empirical He Diffusion Calibration

Development of a thermochronometer requires accurate knowledge of He diffusion kinetics and mineral-specific physical or chemical parameters that may affect diffusivity (e.g., Farley et al., 1998, Reiners and Farley, 1999; House et al., Wolf et al., Reiners et al., 2004); successful geochronometric application to quickly cooled volcanic samples of a known age to demonstrate reliability as a chronometer and refine analytical technique (e.g., Farley et al., 199-; Tagami et al., 2003; Blackburn et al., 2007); and empirical calibration to validate experimentally-determined diffusion kinetics and their extrapolation to geologic temperatures and time scales (>10^6 years) (e.g., House et al., 1999; Reiners et al., 2002; Stockli and Farley, 2004; Stockli, 2005).

Laboratory diffusion kinetics are determined by in-vacuum experiments that utilize high temperatures (>400 °C) and consequently shorter time steps to assess how He moves through, and eventually leaves, the mineral grain. Such experiments are a necessity as diffusivity under natural conditions occurs on time scales far too slow for laboratory studies (House et al., 1999). Once calculated, diffusion kinetics are extrapolated to lower, geologically pertinent temperatures by assuming simple, thermally activated ArRtHenius behavior. Uncertainty depends on the accuracy and precision of the laboratory diffusion data and presumes the behavior seen at higher temperatures occurs at lower geologically pertinent temperatures (House et al., 1999). Empirical calibration of a (U-Th)/He thermochronometer hypothetically tests if

laboratory-measured diffusion kinetics behave similarly in nature. Ideal results document the helium partial retention zone (HePRZ), which is the temperature range in which helium is partially (<10%) to entirely (>90%) retained (Wolf et al., 1998). Therefore an empirical calibration study is best completed on samples from drill holes that have a well-known thermal history and temperature profile. If assumptions from laboratory results are valid the down-hole age variation (defining the HePRZ) should coincide with modeled diffusion kinetics (House et al., 1999).

RUTILE

Rutile Mineralogy and Petrology

Rutile (TiO_2) is one of the major Ti-phases and occurs as a polymorph with the anatase and brookite. Of the polymorphs, it is the densest and most common natural form (Deer et al., 1966). The rutile (TiO_2) structure is based on the hexagonal closest packing arrangement with significant distortion, which produces tetragonal symmetry. The Ti in rutile exists in six-fold coordination with O (Waychunas, 1991). Rutile is known to be a carrier of high-field-strength elements (HFSE) because of the charge and size of Ti (4+ and ~0.6 Å). Elements such as Nb, Ta, V, Fe, Cr, Sb and W are readily substituted into the crystal lattice and can be common up to the percent level (Deer et al., 1992; Zack et al., 2002). Other elements with an ionic charge of 4+, including U and minimally Th, can also substitute in for Ti. Concentrations of U in rutile can very between ~0.1 and 100 ppm which has made it accessible to U-Pb dating (Mezger et al., 1989; Zack et al., 2002).

Rutile is common in many rock types including alkali-rich plutonic rocks, hydrothermal ore deposits, detrital mineral suite in sedimentary rocks and in metamorphic rocks. As a primary mineral in high-grade metamorphic rocks, particularly in blueschists, eclogites and granulites, it typically can be the main carrier of Ti and Nb in the whole rock (Zack et al., 2002; Luvizotto et al, 2008). The stability of rutile in metamorphic rocks is directly tied to the stability of other Ti phases, mainly ilmenite and titanite, and whole rock composition. On approximation titanite is the low temperature and low-pressure Ti phase, ilmenite is the high-temperature Ti phase and rutile is the high-pressure Ti phase (Zack et al., 2002). Rutile is stable in conditions up to 1.3-1.5 GPa in MORB within the eclogite and high-pressure granulite facies (Ernst and Liu, 1998) but it has also been identified stable under in conditions 0.6 GPa in metabasite rocks (Bohlen and Liotta, 1986). The stability of rutile is largely dependent on whole rock composition.

Rutile Thermochronometry

Because rutile is U bearing, present as a primary mineral in a wide range of lithologic and geologic settings, and resistant to weathering it offers potential as a (U-Th)/He thermochronometer. Preliminary assessments of cycled step-heating experiments and RtHe geochronology on quickly cooled volcanic samples have displayed the potential feasibility rutile as a (U-Th)/He thermochronometer. Initial laboratory diffusion experiments display ArRtHenius diffusion behavior and estimate a rutile He closure temperature based on 10°C/m.y. (T_c, Dodson, 1973) of ~210-235

ºC and E_a of 45-50 kcal/mol (Crowhurst et al, 2002; Stockli et al., 2005, 2007). Successful dating of kimberlitic rutile from Chino Valley, Arizona by RtHe thermochronometry resulted in ages of 23.1 ± 1.4 Ma, which agree well with established hornblende inverse $^{40}Ar/^{39}Ar$ eruption ages of 22.3 ± 0.6 Ma (Blackburn, 2005; Stockli et al., 2007). The presence of rutile in high pressure (HP) and high temperature (HT) metamorphic rocks provides an excellent opportunity to assess the thermal history of these often, difficult lithologies. Primarily, reconstruction of the thermal histories of these rocks has been constrained by $^{40}Ar/^{39}Ar$ method, which is an extremely powerful technique but for HP metamorphic rocks, excess ^{40}Ar has been problematic producing $^{40}Ar/^{39}Ar$ that are difficult to interpret (e.g., McDougall and Harrison, 1999; Kelley, 2002).

This study aims to further develop rutile as a (U-Th)/He thermochronometer. Down-hole (U-Th)/He analysis and He diffusion experiments on rutile from the KTB drill hole evaluates the diffusivity of He in rutile over geologic timescales and temperature ranges, particularly by comparison of thermal modeling of rutile He-diffusion kinetics to down-hole RtHe results. Trace element geochemistry and petrography on rutile from the KTB drill hole studies the effects of metamorphic breakdown and potential implications of (U-Th)/He analysis of minerals that carry portion of the whole rock's elemental budget, in the case of rutile- Ti. Application of RtHe analysis to high-grade metamorphic rocks assesses the influence of metamorphic assemblage and metamorphic grade on RtHe results.

GERMAN CONTINENTAL DEEP DRILLING PROJECT (KTB)

Regional geology of KTB drill hole

The Bohemian Massif (BM), located in eastern Germany and western Czech Republic, is composed of tectonically juxtaposed Variscan metamorphic terrains, which include the Saxothuringicum, Moldanubicum, and Bohemicum (Figure 1). Each terrain experienced a different tectonic and metamorphic history prior to amalgamation during Variscan orogeny (e.g., Hirschmann et al., 1997). The Saxothuringicum terrain defines the northern extent of the BM and contains the region of Erzgebirge, large antiformal structures with medium to high-grade Variscan basement rocks (Mingram, 1998; Rotzler et al., 1998). The Moldanubicum terrain delineates the southern border of the BM and is largely composed of three major units. The first two, Monotonous and Varied units are largely composed of amphibolite grade sequences that underlay the Gföhl unit, which is composed of granulite massifs, including the Blanskey les granulite massif (Franke, 1989; Fiala, 1995). The Bohemicum metamorphic terrain is situated in the middle of the BM and is composed of a complexly imbricated stack of alternating metamorphic slices. Along the western border of the BM, the Zone of Ebendorf-Vohenstrauss (ZEV) is situated and has been identified as a portion of the Bohemicum terrain (O'Brien et al., 1997). The ZEV is characterized by medium pressure, high temperature metamorphic rocks and granitic intrusions that postdate widespread Variscan metamorphism (Kontny et al., 1997).

Geology of the KTB drill hole

The ZEV was chosen as the site for the KTB project because of its locality near the boundary of these three major metamorphic units (Figure 1) (O'Brien et al., 1997), with the objective to study the properties and architecture of the deep continental crust (Emmerman and Lauterjung, 1997). The KTB consists of two boreholes, a pilot hole (VB- Vorbohrung) that reaches 4000 m in depth and the main hole (HB- Hauptborung) that reaches a final depth of 9100 m. The metamorphic rocks of the VB and HB are tectonically stacked and lithologically alternating sequences of gneiss, variegated, and metabasic units (Figure 2). The gneiss unit is primarily composed of monotonous paragneisses with minor intercalations of hornblende gneiss and amphibolite. Paragneiss units contain a mineral assemblage of biotite, muscovite, garnet, kayanite and/or sillimanite, Na-rich plagioclase, and quartz. Paragneiss units have pelitic greywackes and grewackes protolith signature (e.g., Hirschmann et al., 1997). Variegated units are characterized by the alternation of amphibolite, garnet-amphibolite, and paragneiss. The paragneiss layers within the variegated units are identical to those of the gneiss unit, while amphibolites have a volcano-sedimentary association of intra-plate basalts and andesites. (e.g., O'Brien et al., 1997). The metabasite units dominate the KTB drill hole and are primarily comprised of coarse- and fine-grained garnet-amphibolites, amphibolites, and metagabbros. Mineralogically garnet-amphibolites and amphibolites consist of hornblende, plagioclase ± garnet, quartz, rutile, ilmenite, titanite and biotite. Mineralogically, metagabbros contains garnet, clinopyroxene, kayanite, zoisite,

quartz and rutile (O'Brien et al., 1992). Geochemically rocks from the metabasite units are tholeiitic and have an enriched mid-ocean ridge basalt (MORB) character. In summary, the KTB drill hole penetrated through tectono-metamorphic assemblage of an ancient active continental margin (O'Brien et al., 1997).

There are three major fault zones identified in the KTB borehole the Nottersdorf Fault Zone (NFZ), SE2, and SE1. The NFZ sits between 500-1600 m. The second zone of reverse faulting is between 3200-4000 m (SE2). The third fault zone, SE1, between 6800-7300 m, was identified as the Franconian Lineament (SE1/FL). The FL is the major reverse fault zone that offsets the BM from the South German Sedimentary Basin to the west. The primary surface exposure of the FL lies approximately 5 km west of the KTB drill site, dips ~45-50º to the NW (Figure 2).

The temperature profile of the KTB is well documented by down-hole temperature logs and long-term equilibration measurements (e.g. Burkhardt et al., 1991; Clauser et al., 1997). The HB measures a bottom-hole temperature of ~260ºC at 9100 m with a mean annual surface temperature of 7°C. This corresponds to an equilibrated geothermal gradient of ~27.5ºC/km (Clauser et al., 1997).

Metamorphic Evolution of KTB

The metamorphic history of these stacked units is complex and both the paragneiss and metabasite units record multiple metamorphic events (O'Brien et al., 1992, 1997; Kontny et al., 1997). O'Brien and others (1997) suggested a two cycle

metamorphic history (Figure 3). The earliest metamorphic event is recorded in the metabasite units by rare eclogitic and granulitic lenses. These relict lenses suggest burial to depths >40 km with estimated temperatures and pressures between 600-700°C and > 1 GPa (Figure 3). This event appears to be associated with Ordovician high pressure (HP) and high temperature (HT) metamorphism recorded in the surrounding ZEV (O'Brien et al., 1992). After HP/HT metamorphism, the entire unit was exhumed back to mid-crustal levels when pegmatites intruded the paragneiss and metabasic units. The second metamorphic event occurred in the Devonian and is associated with the Variscan orogeny. Metamorphic conditions attained amphibolite facies grade at temperatures between 620-720°C and pressures <0.8 GPa (Figure 3), which largely overprinted the first HP/HT event (O'Brien et al., 1997). After peak amphibolite metamorphism at ~400 Ma, retrograde metamorphism persisted until ~360 Ma, when the entire KTB drill hole resided at temperatures below 300-350°C (Figure 4) (O'Brien et al., 1997).

Post-Variscan Thermal Evolution of KTB

Previous thermochronometric studies which assessed the tectonic history of the KTB drill hole include apatite (AFT- Wagner et al., 1997) and titanite fission track (TFT- Coyle and Wagner, 1998), $^{40}Ar/^{39}Ar$ (Warnock and Zeitler, 1998), titanite (TiHe- Stockli and Farley, 2004), and zircon (U-Th)/He analysis (Chapter 2). There are two major periods of rapid cooling recorded in thermochronometric results and depositional history of the South German Sedimentary Basin (Schroder et al., 1997),

adjacent to the ZEV (Figure 2). The earliest cooling episode is recorded in the Triassic by K-feldspar $^{40}Ar/^{39}Ar$ cooling age of ~225 Ma at 7762 m depth (Warnock and Zeitler, 1997) and invariant down-hole TFT ages from 0-4000 m of ~245 Ma (Coyle and Wagner, 1998). Although TFT annealing kinetics are not well constrained, denudation between 225-245 Ma is confirmed by coincident alluvial fan deposits in the South German Sedimentary Basin (Schroder et al., 1997). A minor cooling event between 130-95 Ma is recorded in $^{40}Ar/^{39}Ar$ samples at 0 m and 3203 m (Warnock and Zeitler, 1998) and TFT results between 5000-7000 m (Coyle and Wager, 1998). The second prominent cooling event is recorded in all thermochronometric studies except TFT. TiHe and ZrHe results record invariant down-hole ages from ~75-90 Ma in the upper four kilometers (Stockli and Farley, 2004; Chapter 2). Apatite fission track (AFT) results (Coyle et al., 1997) document rapid cooling between ~58-70 Ma from 120°C to ~45°C by ~25 Ma. $^{40}Ar/^{39}Ar$ samples record cooling between 70-60 Ma on samples from 0 m and 3203 m (Warnock and Zeitler, 1998). Surface AFT data near the KTB drill site range from 70-60 Ma (Wagner et al., 1989). TiHe data suggest the upper portion cooled rapidly in the late Cretaceous from ~210°C to >110°C (Stockli and Farley, 2004). This event is also recorded in the depositional history of the South German Sedimentary Basin with ~500 m of Cretaceous alluvial fan deposits. Down-hole muscovite and amphibole K-Ar ages exhibit invariant ages between 300-350 Ma for the entire KTB drill hole (Wemmer, 1993).

Thermo-tectonic reconstructions of the KTB drill hole divide the KTB into four metamorphic blocks A-D, which are bound by the zones of reverse faulting; NFZ, SE2, and FL/SE1 (Wagner et al., 1997) (Figure 2). All four blocks were a single ~2000 km thick crustal layer, which slowly cooled through the Permian, evidenced by the invariant K-Ar muscovite ages. Down-hole thermochronometric studies from the KTB record the subsequent faulting of the crustal layer into a ~9000 m thick antiformal stack. Movement on the SE2 fault zone (3200-4000 m) in the Triassic separated blocks A and B from C and D. The FL was active during the early Cretaceous through the Eocene separating blocks C and D, which is largely recorded in AFT, THe and ZrHe ages (Coyle et al., 1997; Stockli and Farley, 2004; Chapter 2). The NFZ became active in the Eocene, thickening blocks A and B, recorded in AFT results (Coyle et al., 1997). The South German Sedimentary Basin records these events by deposition of more than 15 km of exhumed rock since the end of the Permian (Schroder et al., 1997). Since the Eocene, the KTB region has been largely quiescent and the most recent tectonic activity produced late Tertiary Eger graben and basaltic volcanism, approximately 30 km to the northwest (Figure 1) (Schroder, 1997). Early studies attributed the rapid cooling and subsequent deposition in the Cretaceous to onset of the Alpine orogeny (Warnock and Zeitler, 1998; Coyle et al., 1997). More recent assessments attribute Late Cretaceous shortening in Central Europe to the onset of Africa-Iberia-Europe convergence and postpone the coupling of the Alps and Europe to the Cenozoic (Kley and Voight, 2008; Bosworth et al., 2008).

Previous thermochronometric studies on KTB

The KTB drill hole, having been well characterized in its thermal regime, petrologic, geochemical, and tectonic context, has provided a unique opportunity to study the *in situ* behavior of various thermochronometers over geologic time scales and temperatures. AFT results confirmed the apatite partial annealing zone (PAZ) between 60-110°C, exhibited by a systematic decrease in ages from 50-6.2 Ma from 2000 m down to 4000 m. Analysis of titanite fission track interpreted a paleo-PAZ between 265-310 ± 5-10°C, but no present day PAZ was documented in the TFT data (Coyle and Wagner, 1998). THe results record the HePRZ between ~115-195°C by a systematic decrease in ages from ~80-5 Ma beginning at 4500 m down to 7000 m (Stockli and Farley, 2004). ZrHe results display invariant ZrHe ages of 85±10Ma from 0-5000 m followed by a decrease in ages to <1 Ma at ~7200m, to document a HePRZ between ~130-210°C.

ANALYTICAL METHODOLOGY

(U-Th)/He Thermochronology

Rutile was selected primarily from amphibolite and garnet-amphibolite units, as paragneiss samples did not yield rutile. Twenty-three samples, a total of 97 aliquots from 1230-9000 m depth, were analyzed by RtHe thermochronometry. After routine mineral separation, rutile grains were selected from the zircon mineral separate. Rutile from the KTB drill hole was typically deep red to red-brown in color

and exhibited an adamantine luster on the original grain surface. Rutile from the KTB was often identified as subhedral to anhedral grains or fragments. Due to the low parent and daughter nuclide concentrations, 2-4 grains of appropriate size (~60-100 μm in width) and morphology were selected per aliquot. The sub-opaque to opaque nature of rutile can hinder identification of inclusions and fractures that are not exposed on the surface. Some fractures and inclusions were detected and avoided by utilizing 180x magnification and intense transmitted and reflected light.

Helium was extracted by a Nd:YAG laser heating the Pt packaged rutile to ~1290°C for ten minutes and reheated to ensure complete degassing of the sample (>99%). The liberated gas was spiked with ^{3}He and cryogenically purified. The $^{4}He/^{3}He$ ratio was measured by isotope dilution on a quadrapole noble gas mass spectrometer, which is calibrated against a manometerically-determined ^{4}He standard. After He extraction, rutile grains were unwrapped from Pt tubing and dissolved by pressure vessel dissolution procedures (e.g., Stockli et al., 2000). Samples were spiked with an enriched ^{230}Th, ^{235}U, ^{149}Sm and REE tracer and subsequently dissolved using an HF-HNO_3 mixture heated for 72 hours at 225°C in the dissolution vessel. This was followed by dry down and resdissolution in 6N HCl for 12 hours at 200°C to remove Th-F salts. The HCl was dried down and redissolved in ~60 μL of concentrated HNO_3 in preparation for anion exchange columns.

Before ICP-MS analysis, all rutile samples are purified by a two-step anion exchange column procedure that was developed by Blackburn (2005- Appendix C for details). Anion exchange columns separate the parent nuclides from major elements,

such as Ti^{4+}, which can decrease the accuracy of parent nuclide (U, Th, Sm) analysis by ICP-MS. Major elements with high ionization potentials can saturate the argon plasma and produce isobaric interferences and matrix effects (Baker et al., 2002; Tsuyoshi et al., 2003).

The first ion chromatography step separates Sm then purifies and collects U and Th (Table 1). Micro-columns are loaded with AGIx8 resin, which is cleaned with a sequence of water, 6N HCl, water and conditioned with 7N HNO_3. The sample is loaded into the column in ~60 μL of 7N HNO_3. The Sm is collected with a 7N HNO_3 wash. In a separate beaker Th and U are collected together by adding 6N HCl and water. The second step purifies the Sm (+REE) from Ti and other major elements by bringing the Sm through an AG50Wx8 resin. The resin is cleaned with 6N HCl, water wash and conditioned with 2.5 N HCl. The Sm is loaded in 2.5 N HCl and purified during an elution of 2.5 N HCl. Collection of the Sm occurs with additional 2.5 N HCl. After the second anion exchange column, the purified U, Th and Sm are recombined, dried down, and brought back in a solution of 100 μL of concentrated HNO_3. The enriched solution is subsequently heated at 90°C for 45 minutes, and diluted with 500 μL of water in preparation for ICP-MS.

All rutile parent nuclide concentrations were measured by isotope dilution by using a mixed ^{235}U-^{230}Th-^{149}Sm-REE spike solution calibrated against a gravimetrically determined 1ppb U-Th-Sm-REE solution. All parent analyses are performed on a VG PQII quadrapole ICP-MS at the Isotope Geochemistry Laboratory (IGL) at the University of Kansas. Estimated analytical uncertainty for (U-Th)/He

ages in IGL is ~8% based on propagated error and analytical uncertainty of replicate zircon standards, but all RtHe ages are reported as the range of age unless otherwise noted.

Rutile alpha-ejection correction

The decay energy of ^{238}U, ^{235}U, ^{232}Th, and minimally ^{147}Sm, is up to ~8 MeV, and is taken up in recoil of the parent nucleus and emission of the alpha particle (Farley et al., 1996). The total distance traveled by the alpha particle varies for each mineral, but can lead to the alpha particle being ejected from the grain, depending on the location of the parent in relation to the grain boundary. Thus (U-Th)/He ages must be corrected for alpha ejection (F_T, Farley et al., 1996). This calculation assumes a homogeneous distribution of U and Th within the crystal grain; if this assumption is violated the estimated retentivity will be miscalculated and can produce gross biases in (U-Th)/He ages (Farley, 2002; Hourigan et al., 2005; Dobson et al., 2008).

The rutile F_T correction follows after Farley and others (1996), utilizing a density of 4.25 g/cm^3 and alpha particle stopping distances in rutile (Ziegler, 2003). To determine the fraction of He atoms retained within rutile, morphometric grain dimensions (length, width and depth) were measured to calculate the surface to volume ratio (β). Assuming a grain with equal width and depth, the surface to volume ratio can be calculated by $\beta = (4L+2W)/(L*W)$, where L is the measured length and W is the measured width of the grain. For grains with varying width (W_1)

and depth (W_2), $\beta = (2LW_1+2LW_2+2W_1W_2)/(LW_1W_2)$. Therefore the alpha ejection correction can be calculated with the following equation:

$$F_T = 1 - 4.55*\beta + 5.2\beta^2 \quad (1)$$

Cycled Step-Heating Diffusion Experiment

A cycled step-heating experiment was completed on rutile from the KTB drill hole from sample RKTB1464-DE. The experiment was completed at the University of Kansas, Isotope Geochemistry Laboratory and ran on a fully automated diffusion experiment apparatus as described by Farley (1999). Multiple rutile grains (8), selected by similar grain size and morphology, were packaged in a Pt jacket and Cu-foil envelope. The packaged sample was wrapped around the thermocouple, to assure temperature measurement by the thermocouple was in direct contact with the sample. The package was suspended in a vacuum chamber and heated by a 350W light bulb through a sapphire window. The estimated accuracy of the thermocouple temperature reading was ± 5°C per step with stability of ± 1-2°C per step. The first steps of the diffusion experiment involved isothermal steps held at 400°C, which was followed by a cycle of prograde, retrograde, and prograde steps. Each temperature stepped up or down in 10°C increments and each cycle finished with a blank (0°C) measurement. The first prograde sequence increased in temperature from 420-590°C, followed by a retrograde sequence from 575-485°C. The final prograde sequence increased in temperature from 492-640°C, which is followed by a short retrograde sequence from

630-600°C (see Appendix B for complete data set). After each step, the ^{4}He liberated was measured by isotope dilution of ^{3}He on a quadrapole mass spectrometer. Calculation of bulk diffusion kinetics required complete degassing of the sample to measure the cumulative fraction of gas released in each step. Total gas values were measured with a Nd:YAG laser heating the sample to ~1285°C for 10 minutes repeatedly to completely degas the sample (>99%).

Trace Element Geochemistry

Trace element geochemistry analysis by Solution ICP-MS was performed on rutile grains from down-hole KTB samples analyzed for RtHe thermochronometry. These samples were primarily from garnet-amphibolite and amphibolite units from depths between 1230-9000 m. Two aliquots of a single grain or fragment were analyzed for each sample, except 7154, when four aliquots were analyzed. Rutile was selected based on purity and size, selecting largest available grains or fragments to maximize concentrations. Preparation for trace element geochemistry analysis by solution ICP-MS required the sample digestion and ICP-MS preparation as described above for RtHe analysis, except rutile grains did not undergo column chemistry. Samples were run on VGQ ICP-MS with a matrix-matched drift correcting solution (Chetcham et al., 1993). Drift correction and standard solutions were prepared from 10 ppm Claritas SPEX Mutli-element Solutions 2A, 3, and 4 by serial dilution in 0 ppb, 0.1 ppb, 1 ppb and 10 ppb concentrations. A 10 ppm Ti solution was added to each standard solution in order to matrix match. Drift was monitored throughout the

run by two techniques. The first method analyzed a 1 ppb standard solution every sixth sample in order to calculate a drift correction factor. The second method measured an internal standard, ^{147}Sm, which was added with the HNO_3 based ^{230}Th, ^{235}U, ^{149}Sm and REE spike.

RESULTS

KTB Rutile (U-Th)/He Results

(U-Th)/He analysis on rutile from amphibolites and garnet-amphibolites display a general decrease in ages from ~120-10 Ma between 1230-9000 m (Figure 5; Table 2). There are two large gaps in RtHe results, the first from 0-1200 m and the second from 1516-3575 m, which are due to non rutile-bearing paragneiss blocks. All RtHe age results are subsequently discussed by fault block (A-D) as distinguished by thermo-tectonic reconstructions (Wagner et al., 1998; Stockli and Farley, 2004). The majority of RtHe ages from Block A, 0-1600 m, sit within the NFZ and display irreproducible ages with standard deviations ranging from 10-55 m.y. RtHe ages between 1230-1464 m vary from RKTB1239 100 ± 40 Ma to 160 ± 40 Ma at 1464 m. In comparison, one sample RKTB1516 displays a younger RtHe age of 62 ± 27 Ma. Block B is from 1600-4300 m in depth. Sample RKTB3575 in the SE2 fault zone and resulted in a reproducible RtHe age of 136 ± 8.2 Ma. Four closely spaced samples, between 4050-4172 m, display variation in individual RtHe age from 27.3 ± 2.7 Ma (1σ) to 134 ± 13 Ma (1σ) with standard deviations of the average RtHe between 16-50 m.y. These samples sit just below the SE2 fault zone and are

significantly younger than samples above. RtHe ages from Block C, between 4300-6800 m, display a marked decrease in RtHe ages with depth and temperature. The down-hole trend of RtHe ages is not systematic and there appear to be two clusters of RtHe ages, each decreases in a similar slope. The first cluster of RtHe ages is considerably younger than the second group (e.g., RKTB4050 40 ± 30 Ma; RKTB4496 40 ± 10 Ma; RKTB5975 11 ± 6 Ma). The second cluster of RtHe ages display RKTB5608 70 ± 13 Ma; RKTB6002 61 ± 15 Ma; RKTB6750 32 ± 4.5 Ma. Generally RtHe ages in Block C are more reproducible, with smaller standard deviations compared to RtHe ages in Block A and B. Block D, 6800-9100 m, displays a continued decrease in RtHe age with increasing depth, from RKTB7153 38 ± 4.7 Ma to RKTB9000 9.9 Ma ± 4.4 Ma in the deepest sample.

In summary, RtHe results generally decrease in age with increasing depth as expected, but are characterized by intra-sample age scatter. RtHe data lack reproducibility and do not show well-behaved down-hole behavior when compared to titanite and zircon (U-Th)/He results from the KTB drill hole (Stockli and Farley, 2004; Chapter 2). In particular, a significant number of RtHe ages are substantially younger than corresponding zircon and titanite (U-Th)/He ages. RtHe ages did not behave as anticipated and therefore trace element geochemistry and petrographic investigations aimed to identify the cause(s) of inaccurate RtHe ages, such as He-implantation due to U- Th- bearing neighbors, breakdown of rutile during retrograde metamorphism, fluid mobilization caused by faulting or resetting due to intense reverse faulting seen throughout the KTB borehole.

Cycled Step-Heating Diffusion Experiment Results

One step-heating experiment on rutile from a garnet-amphibolite RKTB1464-DE yielded a well-defined Arrhenius behavior and excellent linear correlations on heating steps after 535°C (R^2 = 0.996) (Figure 4- Appendix B for complete dataset). Calculated diffusion kinetics for sample RKTB1464-DE yield E_a 203.1 kJ/mol (48.5 kcal/mol) and D_0 5.79 cm^2/s. Bulk diffusion kinetics calculations are based heating steps 535°C through 615°C (black squares). Data from the first prograde cycle (400-590°C- grey squares) initially display high diffusive behavior, which begins to roll over between 480-500°C and decreases in diffusivity. Well-behaved Arrehnius begins during the first regtrograde series at steps 535°C. This 'roll over' behavior has been documented in previous rutile diffusion experiments and its cause and affect on RtHe thermochronometry are under investigation (Stockli et al., 2007; Wolfe et al., 2008). The calculated closure temperature for RKTB1464-DE is 246°C, based on 10°C/m.y. cooling (Dodson, 1973). Diffusion kinetics agree relatively well with ranges for bulk diffusion kinetics previously measured at KU, except the Ea is slightly lower than previous analyses, which produces a closure temperature for RKTB1464-DE that is ~10-40°C higher than the average range measured at KU IGL ~210-235°C.

Rutile trace element geochemistry

Geochemical characterization of rutile by solution ICP-MS analysis was employed to investigate the potential influence of variations in rutile composition on

RtHe age in the KTB drill hole. Dissolved rutile samples were analyzed for a range of high field strength elements (HFSE) and highly charged trace elements that readily substitute in for Ti^{4+} that could distinguish if rutile is primary or seen significant recrystallization. The list also included major element constituents of possible inclusions (e.g., zircon) and major Ti-bearing minerals grow with rutile in metamorphic reactions (ilmenite and titanite). Similar elemental lists have been utilized in recent studies that assess trace element geochemistry of rutile (Luvizotto and Zack, 2008; Luvizotto et al., 2007; Zack et al., 2004; Zack et al., 2004) (Table 4).

Samples were analyzed in three separate experimental runs. Mean detection limits ranged from <5 ppm for Mn, Nb, Mo, Sn, Sb, Hf, Ta, W and U; >5-20 ppm for V, Cr, Mn, Ni, Zr and 30-1000 ppm for Al, Ca and Fe. Concentrations below the detection limits are not listed and those less than twice the detection limit are grey (Table 4). No systematic variations were identified for Al, Ca, V, Mn, Ni, Mo, Sn, Sb, W or U. Typically ^{57}Fe, Re, and Th concentrations were below detection limit for most samples. Samples are displayed in groups of metamorphic fault blocks (A-D), as subdivided in terms of their tectonic and thermal history (Wagner et al., 1997). No major correlation was seen by age behavior.

Trace element results (see Appendix C for complete results), do not exhibit a pronounced geochemical signature that evidence a possible explanation for irreproducible RtHe ages. There is a lack of consistency between particularly in Al, Ca, V, Mo and W. There is a moderate intra-sample reproducibility in Nb, Ta, Cr, Zr, and Hf concentrations (Table 4). Rutile Nb and Ta concentrations (Figure 6a) show a

moderate correlation with increasing concentration and samples from Block A and one sample in Block B, RKTB3575, have distinctly higher Ta concentrations compared to the rest of the results. There is a distinct linear correlation between Zr and Hf concentrations, which are incorporated into the lattice together (Figure 6b) (Zack et al., 2002). Paired (Zr-Hf and Nb-Ta) substitutions in rutile have been previously documented (Zack et al., 2002). Figure 7 plots Nb and Cr concentrations of rutile and rutile samples agree with the 'rutile from mafic rocks' category (Zack et al., 2002), except one or two outliers with high Nb concentrations. The geochemical signature of rutile from the KTB drill hole is consistent with a mafic protolith and the designation of the variegated units as backarc volcanic rocks and the metabasite units as oceanic crust (O'Brien et al., 1997).

Recent studies have investigated the effect of temperature (Zack et al., 2004; Treibold et al., 2007) and pressure (Tomkins et al., 2007) on the Zr incorporation into rutile and calibrated Zr in rutile as a trace element geothermometer in rutile-bearing high-grade metamorphic rocks (e.g. Treibold et al., 2007; Luvizotto et al., 2008). Metamorphic temperature conditions for rutile from the KTB were determined from Zr concentrations measured by solution ICP-MS. Assuming rutile was in equilibrium with zircon and quartz during metamorphism temperatures for each sample was calculated using the pressure dependent equation (Eq. 8 Tomkins et al., 2007).

Figure 8 displays individual temperatures for single grain rutile samples grouped by metamorphic block using estimated minimum and maximum pressures, 6 kbar and 14 kbar, of the two major metamorphic events experienced by rocks of the

KTB, eclogite-granulite phase and widespread amphibolite phase metamorphism (Box A and B in Figure 3). Average calculated temperatures of ~650°C for 6 kbar (Box B) and ~685°C for 14 kbar (Box A) are in good agreement with previously documented temperature conditions of the KTB drill hole (Kleeman and Reinhardt, 1994; O'Brien et al., 1992). Peak temperature and pressure conditions of 620-720°C and 14 kbar were determined for HP facies metamorphism preserved in relict eclogite and granulite lenses of the KTB metabasite units (O'Brien et al., 1992). Peak Variscan amphibolite facies conditions for the variegated units using petrological phase equilibrium gave temperature and pressure estimates of 700-750° C and 6-<10 kbar in (O'Brien et al., 1992). Temperatures estimates of this study appear to be in excellent agreement with previous temperature conditions of the KTB drill hole.

These data, trace element geochemistry and thermometry, suggest that rutile analyzed from the KTB drill hole is still primary and have not been altered. Results are consistent with published geochemical studies from the KTB drill hole as Cr and Nb concentrations suggest a mafic protolith signature and Zr concentrations in rutile estimate peak temperature conditions between 600-700°C. There is no geochemical signature that indicates rutile experienced hydrothermal alteration, recrystallization or fluid mobilization due to faulting, which we suspect would be problematic for RtHe analysis.

Petrography of rutile in the KTB drill hole

Because rutile can be a primary mineral or a main carrier of the Ti budget in high-grade metamorphic rocks, its stability and presence is largely controlled by temperature and pressure conditions, metamorphic assemblage, and the stability of other Ti phases, ilmenite and titanite (Ghent and Stout, 1984; Zack et al., 2002; Luvizotto et al., 2008). Unlike zircon, which is an accessory mineral and can survive multiple metamorphic cycles, rutile breakdown occurs under greenschist facies conditions (Zack et al., 2004). To assess the mineralogical and petrographic context of rutile from the KTB drill hole and any possible affects on RtHe ages, polished thick sections and grain mounts were investigated using backscattered secondary electron imaging on a LEO Field scanning electron microscope (SEM). The complex metamorphic history of the rutile-bearing metabasite units of the KTB drill hole makes this an essential investigation.

Polished thick sections were made from core samples KTB1230, 1252, 1464, 1516, 3575, and 3595. In thick section, rutile occurs intergrown with ilmenite as anhedral aggregates and as individual subhedral grains. Oxide aggregates of rutile and ilmenite are quite large (up to 500 μm in diameter) and can also contain subhedral rutile grains ~80 μm in width (Figure 11c, 13a). Individual rutile grains are typically subhedral and can vary in size from <10 μm to >80 μm in width. Rutile commonly displays breakdown textures from rutile to ilmenite in both aggregate and individual grains. Breakdown textures include growth of ilmenite lamellae or ilmenite growth at rutile grain boundaries. The presence of ilmenite as an inclusion

in rutile is rare and most often ilmenite growth occurs near grain boundaries. Besides ilmenite lamellae rutile display inclusions of zircon and less commonly pyrite, which are typically <5 μm in width. The nearly ubiquitous texture observed in every thick section on both aggregate and individual rutile grain, is a titanite rim ranging from <1-4, in some cases up to 10 μm, in width (Figure 11-14). Titanite rims commonly display undulating surfaces that vary in width around the grain, but most often surround the entire aggregate or rutile grain (Figure 11c, 13d). The sequence of Ti mineral phase growth can be distinguished by breakdown of rutile to ilmenite (formation of ilmenite lamellae), followed by growth of titanite rims (Figure 11b, 13c, 14a, 14c, 14d). In aggregates of rutile and ilmenite the titanite rim is thicker when surrounding ilmenite. Within most thick sections, rutile is identified in an amphibole, albite ± garnet, ilmenite, titanite, pyrite, zircon, ± apatite matrix or rarely as an inclusion within garnet (Figure 11a). In sample KTB1252, rutile occurs as an inclusion within titanite, indicating rutile breakdown to titanite was almost complete (Figure 12a). Notably, rutile also occurs in proximity (<20 μm) to zircon and apatite grains (Figure 9f, 11a, 11b, 13e).

Rutile grains from samples analyzed for RtHe thermochronometry were imaged in polished grain mounts. Subhedral-anhedral rutile grains or fragments were selected for the mount and vary from 50-80 μm in width. Some rutile contain micro-inclusions, <5 μm in diameter, of ilmenite and zircon (Figure 9a, 9b, 9f, 10b). Zircon inclusions can be located near the center or near the grain boundary (<20 μm). Similar to thick section a titanite rim, ranging from <1-4 μm in width, is present on

many of the imaged grains. The titanite rim never encompasses the entire rutile grain but more commonly the rim abruptly ends or is minimally preserved. Some rutile grains imaged in grain mount have matrix of plagioclase and amphibole attached, these grains preserve the titanite rim best (Figure 9, 10).

Previous petrographic studies on the KTB drill hole attribute rutile growth to different metamorphic events, depending on protolith and tectonometamorphic history (Kontny et al., 1997; O'Brien et al., 1997). (Along with an overview of the metamorphic history of the KTB drill hole, Figure 3 also estimates the timing of oxide growth). In the metabasites that preserve eclogitic and/or granulitic lenses, rutile growth is attributed to igneous Fe-Ti oxides (Box A in Figure 3) (Kontny et al., 1997; Hirschmann et al., 1997). This HP/HT event is largely overprinted by the succeeding amphibolite grade metamorphism during the Variscan orogeny. The breakdown of rutile to ilmenite and rutile growth are both noted during the Variscan event in the metabasite and variegated units (Box B Figure 3) (Kontny et al., 1997). The growth of titanite rims is associated with the breakdown of ilmenite and rutile during post-Variscan retrograde zeolite-greenschist metamorphism and fluid infiltration (Kontny et al., 1997) (Box C Figure 3).

Harlov and others (2006) investigated the presence of a titanite rim on ilmenite from various amphibolite facies localities, including the Variscan Oztal Complex. They document that the titanite-rimmed ilmenite is typically surrounded by plagioclase and occasionally in contact with amphibole. In most cases, they attributed

the presence of a titanite rim to the following hydration reaction (Eq. 4 Harlov et al., 2006):

$$7\ \text{Fe-Cpx} + 3\ \text{Ilm} + 5\ \text{Qtz} + 2\ H_2O = 2\ \text{Fe-Amph} + 3\ \text{Tnt} \quad (2)$$

In KTB samples titanite rims display phase relations that imply comparable reactions, except rutile participates in the reaction. Harlov and others (2006) observed rutile in the Oztal Complex as an inclusion within ilmenite but not in contact with the titanite rim (KTB1252 displays a similar reaction Figure 10a). In KTB samples, rutile, not associated with ilmenite aggregates, is also rimmed by titanite (Figure 11c, 12a-d). Therefore, the growth of titanite rims on rutile in KTB cannot be explained by ilmenite breakdown alone (Eq. 3) and requires coincident rutile breakdown. The following reaction replaces ilmenite with rutile as the Ti source:

$$5\ \text{Fe-Cpx} + 3\ \text{Rut} + \text{Qtz} + H_2O = \text{Fe-Amph} + 3\ \text{Tnt} \quad (3)$$

Although the growth of titanite rims directly on rutile in amphibolite grade metamorphic rocks has been identified in retrogressed mafic granulites from Saxony, Germany (Figure 3d, Romer and Rotzler, 2003) and the amphibolite unit of the Frankenberg Massif, Germany (Rotzler et al., 1999), no reaction was provided to account for its presence. It should be noted that rutile-titanite assemblages are stable again at ultrahigh- to high-pressure conditions, particularly when carbonates are present (e.g., Frank and Spear, 1985; Manning and Bohlen, 1991; Frost et al., 2000; Castelli and Rubatto, 2002; Tropper et al., 2008). Growth of titanite rims on rutile is also a common decompression reaction in high-pressure rocks (Ghent et al., 1993,

Klemd et al., 1994). Although titanite-rutile assemblages are found in high-pressure and ultrahigh-pressure assemblages, such reactions do not pertain to the amphibolite facies metamorphism experienced by samples in the KTB drill hole. Therefore, we suggest the combination of equations 2 and 3 may be the primary reactions responsible for the growth of titanite rims on rutile and ilmenite, which grew during widespread amphibolite phase metamorphism in the Devonian and subsequent retrograde metamorphism. The effect of titanite rims on RtHe analysis will be discussed in subsequent sections.

DISCUSSION

Interpretation of rutile (U-Th)/He results

Interpretation of RtHe results is conditional on comparison to modeled predictions and previous thermochronometric studies, zircon and titanite (U-Th)/He analysis (Chapter 2; Stockli and Farley, 2004). Forward modeling results are based on published thermal histories of four metamorphic fault blocks (A-D), which have been established with previous thermochronometric studies of the KTB drill hole (Wagner et al., 1997; Stockli and Farley, 2004) and a geothermal gradient of 27°C/km (Clauser et al., 1997). To assess the effects of diffusivity on down-hole RtHe results, we modeled a range of bulk diffusion parameters measured at KU-IGL that encompass diffusion kinetics with a T_c range of 220-240°C (Stockli et al., 2007) and the results from RKTB1464-DE. Forward modeling results were produced with a

MATLAB® (2008b, The MathWorks, Natick, MA) code developed at KU following equations outlined by Ketcham (2005).

Figure 15 compares the thermal history of four coherent fault blocks modeled with the range of measured diffusion kinetics, E_a 207-213 kJ/mol (49.5-51 kcal/mol) $\log(D_0/a^2)$ 6.5-7.1 s^{-1} (hatched envelope), and diffusion parameters from rutile KTB diffusion experiment (diamond RKTB1464-DE). Modeled RtHe ages are calculated employing a traditional α-ejection correction based on homogeneous U and Th distribution (Farley et al., 1996). The expected down-hole RtHe results display consistent ages between 85-95 Ma in Block A and Block B, with slight offset due to reverse faulting at the block boundaries. In Blocks C and D there is a systematic decrease in ages between a temperature range of ~160-230°C, which represents the rutile HePRZ. RtHe ages at temperatures >220°C or ~7500 m are reset and do not retain He.

Comparison of rutile (U-Th)/He results to previous studies

Due to a closure temperature for rutile between ~220-240°C, which is similar to zircon (~185°C) and titanite (~200°C), RtHe ages from the KTB drill hole were expected to be systematically older but mimic zircon and titante (U-Th)/He results. Ideally, RtHe results should also correspond to modeling results from bulk laboratory derived diffusion kinetics (Stockli et al., 2007) and a step-heating experiment on rutile from the KTB drill hole (RKTB1464-DE).

Although, RtHe results display a general decrease in ages from ~120-10 Ma between 1230-9000 m, they require a differentiated evaluation because significant portions of down-hole RtHe ages do not agree with model predictions based on laboratory-derived rutile He kinetics or corresponding rutile and zircon (U-Th)/He ages. "Poorly" behaved RtHe ages can be subdivided into three different categories: 1) inaccurate ages within a sample, resulting in large standard deviations; 2) precise ages that are either (a) younger or (b) older than expected results; 3) ages that accurately reflect expected down-hole rutile results based on previous studies and laboratory derived diffusion kinetics (Figure 15). From the 97 aliquots analyzed by RtHe analysis, ~15% yielded RtHe ages within 2σ of the predicted results, while most of the RtHe ages that were >2σ different expected results, ~40% were too old and ~60% too young.

A majority of the samples with large standard deviations occur in or near the fault zones. For example, samples in Block A sit within the NFZ and all ages are imprecise with standard deviations from 10-55 m.y. RtHe ages, except RKTB1516, are anomalously older than model predictions of ~85 ± 10 Ma. Instead, average RtHe ages vary from ~100-160 Ma, which is ~20-85% older than the expected. In contrast RKTB1516 is anomalously younger than expected with RtHe age of 62 Ma, which is ~35% younger than the expected value. In Block B, RKTB3575 is significantly older (60%) than model predictions RtHe age 136 ± 8.2 Ma. Just below the SE2 fault zone there is a cluster of four RtHe samples, RKTB4050-4172, which are significantly too young. The expected RtHe age is still 85 Ma, and average RtHe ages range from 30–

63 Ma. RKTB4050 with RtHe age of 30 ± 4 Ma is 65% younger than expected and very reproducible. The other three samples RKTB4070, 4124 and 4172 have large standard deviations of 46, 50 and 16 m.y. each. RtHe ages for these samples are slightly older, 55-64 Ma, but still ~25-30% younger than expected.

In Block C the overall trend of RtHe samples display decreasing age with increasing depth, which are younger than predicted by diffusion kinetics and previous studies, but RtHe ages are also more reproducible compared to RtHe ages in Block A and B. Best seen in Figure 15, beginning at the bottom of Block B, there are two groups that decrease in age with increasing depth at different rates. The first set yield RtHe ages that are significantly too young compared to expected results by 50-80%. The first set begin to decrease at ~120°C (4050 m) and are nearly reset by ~180°C or 6000 m. The second set of RtHe ages is in better agreement with modeled diffusion kinetics- although still younger, 10-40%, with a decrease of ages at ~160°C (5600 m) that continue to decrease with depth through Block C and sample RKTB6750 RtHe ages are 32.4 ± 4.5 Ma.

The decreasing age with increasing depth trend is continued in Block D when RtHe ages are youngest at the bottom of the borehole. In Block D, ages are again older than expected, as modeled results display completely reset RtHe ages from ~7500 – 9000 m. RtHe ages in Block D, RKTB7153, 8380, and 9000 are 38 ± 5 Ma, 20 ± 7 Ma and 12 ± 7 Ma, all significantly older than expected.

Potential causes of inaccurate rutile (U-Th)/He results

The combination of widespread RtHe ages in the upper 5000 m and two sets of decreasing RtHe ages in the lower 4 km, do not yield a data set that can be used to reliably define a rutile HePRZ, which is one of the significant goals of down-hole (U-Th)/He analysis of the KTB drill hole. As illustrated above, there are three groups of ages within the wide scatter of down-hole RtHe results: large standard deviations, RtHe ages anomalously younger and anomalously older than expected. RtHe results that are younger than expected are the most prevalent (60%) and most difficult to explain. Faulting is widespread throughout the KTB drill hole, and it is known that along with faulting fluids were present in the KTB drill hole (Zulauf et al., 1999). Initial speculation included recrystallization or resetting of RtHe ages due to fluid infiltration. Rutile trace element geochemistry results from the KTB drill hole still have primary signatures, including mafic rock protolith and peak metamorphic temperatures. As primary minerals, RtHe results do not appear to be caused by to widespread faulting and hydrothermal alteration documented in KTB drill hole. Throughout petrographic investigation the presence of zircon as inclusions in rutile and <20 μm away from rutile or the presence of a thin (<1-4 μm) titanite rim and was identified in thick section, either scenario could affect RtHe ages.

The presence of U- and Th-rich mineral, particularly zircon, as an inclusion or as a neighbor <20 μm from the rutile grain could influence RtHe ages and account for both too old and too young ages (Figure 9b, 13b). Because rutile has exceptionally low parent nuclide concentrations and zircon is highly radiogenic RtHe ages will be sensitive to micro-inclusions or even a small zircon sitting adjacent to a rutile grain.

The case of a zircon inclusion situated in the center of rutile will simulate an enriched core. RtHe ages corrected by a standard F_T correction will overestimate the amount of He ejected, resulting in ages older than expected. In contrast, a zircon inclusion situated near the edge of the grain (<20 μm) will eject He produced by the zircon while retaining the U and Th concentrations. Standard F_T corrections will underestimate the He lost and the resulting age will be too young. Another scenario, the presence of zircon or apatite (Figure 7f, 11a, 11b, 13a, 13c) situated outside the rutile grain, but within the alpha stopping distance will implant He into the rutile, producing erroneously old ages. Thus the presence of zircon, or other alpha emitting minerals, as an inclusion or as a neighbor, could potentially lead to ages that are younger or older than expected.

Zonation in grains analyzed by (U-Th)/He analysis is another documented phenomenon which can produce deviant ages. Investigations on the effects of zonation on zircon (U-Th)/He thermochronometry have noted that enriched rims 4-5 μm thick at the grain boundary can cause age bias up to ~30% with a 20% increase in U and Th concentration from the grain to the rim (Hourigan et al., 2005). The ubiquitous presence of the titanite rim on rutile throughout thick section and grain mount petrographic investigation suggests that this is a likely explanation of the consistent source of RtHe ages that are dramatically younger than expected.

Old (U-Th)/He ages are often explained by the presence of U and Th rich mineral <20 μm distance to the analyzed grain, which can be a source of He implantation due to alpha ejection (Farley, 2002). Analysis of such a grain will lead

to parentless He and anomalously old (U-Th)/He ages. Rutile will be especially prone to He implantation due to the low parent nuclide concentrations and subsequent low He concentrations. Bad neighbors, most often zircon and some apatite, which would be a mildly bad neighbor, were seen throughout thick section and even in grain mount investigations. Similarly the presence of titanite, enriched in U and Th, surrounding the rutile grain, will implant He into the rutile grain. If the titanite rim is not analyzed during (U-Th)/He analysis, the resulting age will be too old.

Although the presence of a bad neighbor or U, Th rich inclusion cannot be ruled out as part of the inconsistent RtHe ages from the KTB drill hole, we suggest that the ubiquitous presence of rutile coated by a titanite rind is a more widespread occurrence and accounts for the majority of poor RtHe results, young or old. The presence of a titanite rim also serves as the source of large standard deviations within RtHe ages, which is prevalent throughout down-hole RtHe results from the KTB drill hole.

Effect of titanite overgrowth on rutile (U-Th)/He results

It has been demonstrated that U- and Th- zonation on (U-Th)/He thermochronometry can produce significant age inaccuracies by the presence of an enriched rim (Farley et al, 1996; Farley, 2002; Tagami, 2003; Hourigan et al., 2005; Dobson et al., 2008). The main complication caused by U- and Th- zonation is application of an alpha ejection correction that assumes homogeneous U and Th distribution. For example, a rim with increased U and Th concentrations will cause

preferential loss of He by alpha ejection. If zonation is not identified, the standard F_T correction will not account for the total amount of He lost and the resulting He age will be too young.

The presence of a titanite rim surrounding rutile will have an analogous affect as a zoned grain that has a U- Th-enriched rim as described above. A titanite rim (most often <1-4 μm) was identified ubiquitously throughout thick section and on a large proportion of rutile in grain mounts. Titanite is highly enriched in U and Th, and is utilized in fission track (e.g., Coyle and Wagner, 1998) and (U-Th)/He thermochronology (e.g., Reiners and Farley, 1999; Stockli and Farley, 2004) and in U-Pb geochronology (e.g, Frost et al., 2000). The low parent nuclide concentrations of rutile and the presence of U- and Th-rich titanite encapsulating rutile produces a large uncertainty due to He implantation and rim removal.

The effective uranium concentration (eU) accounts for the total radiogenic parent that contributes to He production $eU = [^{238}U] + 0.235 \times [^{232}Th]$). The eU concentration of titanite from the KTB drill-hole analyzed for (U-Th)/He thermochronology averages ~130 ppm, ranging from 3.4 - 758 ppm (Stockli and Farley, 2004). The average eU concentration of rutile in this study is 4.53 ppm and ranges between 0.64 - 22.53 ppm. The maximum values of calculated eU concentrations for rutile (22.53 ppm), may include U and Th concentrations from a titanite rim or zircon inclusions, as ~80% of eU concentrations are ≤ 5 ppm. From the minimum and maximum values of calculated eU concentrations in titanite and rutile from the KTB drill hole, the concentration difference could span 0.2 - 1,100

increase from rutile grain to titanite rim. These values are based on end member values and instead we estimate a 5-75 fold increase in concentration difference between rutile and titanite is more probable based 90% of observed eU concentrations.

The effect of an enriched U and Th bearing rim on RtHe ages could result in two scenarios (Figure 16). The first scenario is (U-Th)/He analysis of a rutile grain with a complete or partial titanite rim preserved, resulting in a young (U-Th)/He age because of improper alpha ejection correction (Figure 16b). The second scenario is analysis of a rutile grain from which the titanite rim was completely removed. This would result in an erroneously old age due to implantation of parentless He from the titanite rim.

The first scenario, (U-Th)/He analysis with an intact titanite rim, accounts for RtHe ages that are younger than expected, which applies to ~60% of individual RtHe ages. In this scenario, an enriched rim will produce a corrected age that is younger than expected as the bulk retentivity of the grain is underestimated (Hourigan et al., 2005). This scenario assumes the rim is intact during RtHe analysis. Images of rutile in thick section always display a titanite rim surrounding the entire rutile grain, but images of rutile in grain mount typically display a partial rim. We assume the rim was removed during mechanical rock separation. This seems likely with the abrupt termination and heterogeneous widths observed in titanite rims on rutile grain mounts (Figure 10a, 11c, 13d). The low parent nuclide concentrations of rutile will make it particularly sensitive to even partial preservation of the titanite rim.

The second scenario, removal of the titanite rim, would account for RtHe ages that are older than model predictions. If the rim is removed during mechanical rock separation, the resulting rutile will have experienced He implantation over its entire surface area and produce a RtHe age older than expected. The presence of a titanite rim can also explain the inaccurate and imprecise RtHe results from the KTB, which result in larges standard deviations. For example, RKTB1230 yields an average RtHe age of 126 ± 55 Ma. Out of 6 total aliquots analyzed, 4 are older than expected and vary in RtHe age from ~157-200 Ma, we hypothesize such ages are produced by complete removal of the titanite rim. The remaining two aliquots are younger than expected and yield RtHe ages of 60-63 Ma, which we hypothesize are produced by analysis of an intact titanite rim. Therefore we conclude that the presence of a titanite rim could produce either young or old ages within a sample.

The pervasive presence of titanite rims in thick section and grain mount, irreproducible RtHe ages and extensive amphibolite grade metamorphism throughout the ZEV strongly suggest that titanite rims affect rutile utilized for this study.

Effect of titanite rims on alpha ejection correction

Application of an alpha ejection correction factor (F_T, Farley et al., 1996) for (U-Th)/He thermochronometry is common practice as it is well established that production of an alpha particle accompanies separation from the parent nuclide. The total distance traveled by the alpha particle varies from mineral to mineral, but depending on the location of the parent nuclide in relation to the grain boundary and

trajectory of the alpha particle, it can be ejected from the grain (Farley et al., 1996). The proportion of He lost is calculated based on mineral specific grain dimensions, density, and alpha ejection energy assuming a homogeneous U and Th distribution (Farley et al., 1996). Standard procedure of (U-Th)/He thermochronometry is to calculate an F_T correction for each grain based on morphometric analysis. Previous studies have investigated the effect of U and Th zonation on alpha ejection corrections and obtaining accurate and reproducible (U-Th)/He ages (Hourigan et al., 2005). The age bias (γ) calculation compares the zoned alpha ejection correction ($F_{Tzoning}$) to the standard F_T correction or the He age produced from a standard correction to the He age produced from a zoned correction ($HeAge_{zoning}$):

$$\gamma = (F_{Tzoning}/F_T) - 1 \quad = (HeAge/HeAge_{zoning}) - 1 \qquad (4)$$

In an attempt to evaluate the impact of a titanite rim on rutile and account for RtHe ages that are younger than expected, we have used an analogous approach. Figure 16 displays the percent age discrepancy possible if the standard F_T correction is applied to rutile with an enriched rim, which results in ages that are younger than expected. Modeling is based on spherical crystals of varying radii (40-60 μm) in which the concentration gradient, from grain to rim, ranges from a 5-75 fold concentration increase. Evident in Figure 16d, the greatest age bias discrepancy occurs from enriched rims ~3.5-5 μm in width with the maximum increase in U and Th concentrations from grain to rim, which is consistent with those made on enriched rims in zircon (Hourigan et al., 2005). For example, the percent age bias of a rim 2 μm wide with a 50 fold increase in U and Th concentration produces a (U-Th)/He age

that is ~50% too young. Our numerical $F_{Tzoning}$ calculation accounts for redistribution within the grain (Ketcham, 2005) and is based on grain morphology, rim width, and the concentration gradient from grain to rim (C_{rim}/C_{grain}). Our modeling, however, does not take into account the different alpha stopping distances between rutile and titanite, alpha particles travel ~3 μm (15%) less in rutile than titanite. For simplicity we assume the enriched rim is rutile and thus underestimate the total impact of the titanite rim.

In an attempt to account for RtHe ages that are older than expected, based on the hypothesis of removing the titanite rim before (U-Th)/He analysis, we modeled He diffusion and redistribution in a rutile grain with an enriched rim over an established time temperature history, but excluded the parent and daughter concentrations within the width of the enriched rim to calculate the RtHe age, in order to simulate removal of the enriched rim. To display the effect of removing an enriched rim on the He age, we produced an age bias plot similar to Figure 16. The age bias, or percent difference (γ_{RR}), of a grain that experienced rim removal, was calculated by modeling a He age for a grain with an enriched rim and comparing that to the modeled He age for the same grain but removing the enriched rim ($HeAge_{RR}$):

$$\gamma_{RR} = 1-(HeAge/He\ Age_{RR}) \quad (5)$$

Figure 17a displays the effect of removing the rim on the (U-Th)/He age with increasing grain to rim concentration for a grain with an equivalent spherical radius of 50 μm. The γ_{RR} increases the age by ~10% with removal of a 2 μm rim and the percent age bias continues to increase as the rim width increases. If the titanite rim

width is less than 99.25% of the grain's total equivalent spherical radius the age bias correction is similar to the standard F_T correction, or below it, depending on grain to rim concentration difference. For example, a rim <0.25 μm in width on a 50 μm grain would produce a He age that was 'too young', but not significantly. From Figure 17a, it is evident that the effect of removing an enriched rim can have a significant effect on (U-Th)/He age.

Corrected rutile (U-Th)/He data from KTB drill hole

One of the fundamental assumptions in (U-Th)/He thermochronometry is a homogenous distribution of U, Th, and He concentrations. These assumptions influence the amount of He lost by alpha ejection, the He concentration gradient and thus the rate of He diffusion. When U, Th and He concentrations are not homogeneously distributed and unaccounted for (U-Th)/He ages are erroneous, largely due to application of an inaccurate alpha ejection correction. Therefore, a key to obtaining correct (U-Th)/He ages, when zoning is present, is knowledge of the distribution of parent and daughter throughout the grain.

To test if 'zonation' in rutile from the KTB drill hole could account for RtHe results, we calculated $F_{Tzoning}$ corrections based on observed and approximated parameters, rim width and rim to grain concentration difference, and applied them to raw RtHe ages. $F_{Tzoning}$ corrections are applied because expected RtHe results for the KTB drill-hole are well constrained. RtHe results should mimic zircon and titanite (U-Th)/He results from the KTB drill hole, two established thermochronometers with

closure temperatures similar to rutile (Chapter 2; Stockli and Farley, 2004) and correspond to modeling predictions of down-hole RtHe behavior. $F_{Tzoning}$ corrections are based on observed parameters in rim width and the concentration gradients. Rim width estimates are well constrained by petrographic investigations of titanite rim thickness, which ranged from <1 to ~10 μm, with the majority of rims being thin, <1-4 μm in thin section and grain mount. Concentration gradients from grain to rim are based on measured U and Th concentrations from this study and titanite (U-Th)/He analysis (Stockli and Farley, 2004). We model a range from 5 to 75 times increase in U and Th concentration. Corrections are calculated on a grain with an equivalent sphere radius of 50 μm. With these parameters, $F_{Tzoning}$ corrections were calculated and applied to RtHe ages that were too young compared to modeled predictions.

The corrected RtHe ages are displayed on a scatter plot of concentration gradient vs rim width (Figure 19-21). Each point on the scatter plot represents the corrected RtHe age produced by the $F_{Tzoning}$ correction based on that point's rim width and concentration gradient. If the corrected RtHe age is within 10% of the modeled age it is plotted in a grey circle and light grey contour and within 5% it is plotted by a black circle and medium grey contour. Often times many $F_{Tzoning}$ corrections calculate RtHe ages that were within 10% and 5% of the modeled ages, i.e. a range of rim widths and concentration gradients correct to the modeled age. Based on petrographic observations, titanite rims most commonly ranged from <1-4 μm in width (dashed lines). Therefore, we assume corrected RtHe ages within 10% or 5% of the expected age that are corrected by rims between <1-4 μm in width, are the most

probable conditions which produced the too young RtHe age. The parameters that we estimate to be most likely are marked in a dark grey box.

Figure 19 displays the $F_{Tzoning}$ corrections on aliquots from sample RKTB1516. From seven aliquots the average RtHe age is 62 ± 27 Ma while modeling predicts a RtHe age of ~85 Ma. Six out of seven aliquots in RKTB1516 yield RtHe ages younger than modeled ages and are corrected by the $F_{Tzoning}$ corrections. RKTB1516-1 (Figure 19a) is corrected by many variations in rim width and concentration difference. We estimate rim widths varying from 1-5 μm in width with concentration gradients of 30-50 fold are the most suitable corrections. Aliquots 1516-5, -6, -7 (Figure 19b-d) display similar patterns and are corrected by thin enriched rims, <2 μm in width and concentration increase between 20-50 fold. Samples RKTB1516-3 and -4 could not be corrected to the modeled age by $F_{Tzoning}$ corrections with the modeled parameters as the individual aliquots were 60-67% too young (34 ± 4 Ma (1σ) and 27 ± 3 Ma (1σ) respectively). In an attempt to correct these aliquots to modeled RtHe age of ~85 Ma, extreme rim to grain concentration differences were tested, e.g., a 3 μm width rim with 5000 x greater concentration difference does not correct to a RtHe age. There appears to be a plateau, as $F_{Tzoning}$ corrections never become <0.40. RKTB1516-2 was not corrected by $F_{Tzoning}$ as the individual RtHe age based on homogeneous U and Th concentrations was 107 ± 11 Ma (1σ). Samples that were older than expected were not corrected by at $F_{Tzoning}$ that accounted for the removal of the titanite rim.

Figure 20 displays the $F_{Tzoning}$ applied to three out of four aliquots of sample RKTB4172 with an average RtHe age for 55 ± 16 Ma based on the standard F_T correction. Modeled RtHe age for rutile at 4172 m depth in the KTB drill hole is ~84 Ma, which is ~35% discrepancy between ages. All three aliquots corrected (Fig20a-c), RKTB4172-1, -2 and -3 display a similar "tornado" shape, and we assume that a thin (0.75-2 μm) rim with 20-40x increase in concentration best corrects for rutile from sample RKTB4172. Aliquot RKTB4172-4 was too young, RtHe 31 ± 3 Ma (2σ) and could not be corrected to the modeled age by the $F_{Tzoning}$ corrections tested. With similar shapes and parameters that correct to the expected RtHe age, such samples demonstrate that one process may be influencing RtHe ages.

Figure 21 displays the $F_{Tzoning}$ correction for the three aliquots of RKTB5720. RKTB5720 yields an average RtHe age of 46 ± 5.8 Ma (1σ) using a standard F_T correction, while modeled results estimate a RtHe age of ~72 Ma. The range of $F_{Tzoning}$ corrections that calculate a RtHe age of 72 ± 7.2 (10%) Ma and 72 ± 3.6 Ma (5%) for the three aliquots varies from sample to sample as seen in the difference between grey contour shapes. RKTB5720-1 (Figure 21a) can be corrected by many $F_{Tzoning}$ corrections, but the most plausible corrections are produced with a rim ranging from 1-3 μm in width with a concentration gradient between 20-40. In contrast, RKTB5720-2 is corrected with either a thin (<0.5 μm) highly enriched rim or thick poorly enriched rim. The thick rim is less probable based on petrographic observations (Figure 21b). RKTB5720-3 is corrected from a rim 1.5-4 μm enriched rim with a 50-75 fold concentration increase (Figure 22c). All aliquots from

RKTB5720 can be corrected by thin rims <1-2 μm with concentration gradients ranging from a 20-75 fold increase.

Although examples RKTB1516, RKTB4172, and RKTB5720 display a wide range of parameters in rim width and concentration difference that could affect the RtHe results, it also demonstrates that rim widths observed in petrographic investigations can account for anomalously young RtHe ages in some cases. But it should be noted that $F_{Tzoning}$ corrections are based on assumptions. One assumption is complete rim preservation but from inspection of grain mounts, no rutile grain ever preserved a complete rim. By applying a single $F_{Tzoning}$ correction, we also assume that the 2-4 rutile grains within an aliquot have the same C_{rim}/C_{grain} concentration difference and rim thickness, when each grain could vary considerably. Therefore, these assumptions do not permit this correction to tease out applicable down-hole RtHe results nor a RtHePRZ. In general, we recognize that $F_{Tzoning}$ corrections are limited in their extent and are only applied as a test. Even though we cannot rectify every aliquot to the modeled age or make corrections with specific parameters, the expected RtHe results are accurately constrained and therefore we believe these results demonstrate that the presence of a titanite rim is the most likely explanation for the inaccurate and imprecise RtHe ages seen in the KTB drill hole. Ages that cannot be corrected may be influenced by multiple processes such as a titanite rim and zircon inclusions near the grain boundary.

Regional rutile (U-Th)/He results

Rutile is a primary mineral in some metamorphic assemblages, particularly eclogites, and typically controls a large percentage of the Ti budget in high-grade metamorphic rocks. The stability of rutile depends upon mineral assemblage and metamorphic history (Luvizotto et al., 2008; Zack et al., 2002). In order to assess if RtHe results are influenced by differing metamorphic rock type, metamorphic grade, or metamorphic history, we utilized high-grade metamorphic rocks from the BM. These include two eclogite and one diamond-bearing garnet gneiss from the Erzgebirge region in the Saxothuringicum terrain (~65 km NE of KTB) and two granulite samples from the Blanksy les Granulite Massif in the Moldanubicum terrain (~85 km SE of KTB). As exposed cores of the Variscan orogen the sampled high-grade metamorphic rocks have not experienced widespread amphibolite facies metamorphism. Petrographic studies on samples from Erzgebirge (Luvizotto et al., 2008) and the Blansky les Granulite Massif (Fiala et al., 1987; O'Brien, 1996) do not record rutile with a pervasive titanite rim.

RtHe ages from Erzgebirge ranged from ~275-290 Ma. EGB R1A, the diamond-bearing garnet gneiss, yielded a RtHe age of 273 ± 31 Ma. EGB R2b and EGB R4d, the two eclogitic samples yielded RtHe ages of 292 ± 16 Ma and 248 ± 17 Ma, respectively. Granutlies from the Blanksy les Granulite Massif ranged from ~190-215 Ma. The average RtHe age for sample T5A is 189 ± 32 Ma and T8C is 216 ± 8 Ma (Table 3).

RtHe ages of ~200 Ma in the Blansky les Granulite Massif may be associated with exhumation of the Moldanubicum terrain in the Late Triassic/Early Jurassic, which is documented by concurrent alluvial fan deposits in the Bohemian sedimentary basin (Schroder et al., 1997). RtHe ages from Erzgebirge document Permian cooling between 275-290 Ma in the Saxothuringicum terrain. This is consistent with zircon fission track (ZFT) ages of 248-283 Ma from granites located approximately 30 km east of Erzgebirge (Hejl et al., 1997) and an average ZFT track age of 278 ± 19 Ma from the Ruhla Crystalline Complex, northwest of Erzgebirge (Thomas & Zeh, 2000). ZFT ages were attributed to Permian unroofing and possibly initiation of uplift of the Bohemian Massif along the Franconian Lineament.

Although RtHe ages from regional studies have large standard deviations, between 16-30 m.y., results agree with accepted thermal histories of the region and provide successful results from RtHe thermochronology on high-grade metamorphic rocks. Rutile from high-grade metamorphic rocks typically has higher U and Th concentrations in comparison to amphibolitic rutile. Regional RtHe age averaged a U concentration of 11.5 ppm compared to 5 ppm for KTB rutile, which enhances the success of RtHe analysis. When compared to rutile results from the KTB drill hole, regional results are in accordance with the existing thermal histories of each region. This is attributed to the rock type and lack of a retrograde overprint that could affect RtHe ages. Therefore, we conclude that RtHe thermochronometry can be viable when applied to high-grade metamorphic rocks, as seen in RtHe ages from Erzgebirge and the Blansky les Granulite Massif.

Implications for rutile (U-Th)/He thermochronometry

As rutile is subject to breakdown during retrograde metamorphism, it will thus be pertinent for successful RtHe analysis to have a thorough understanding of rutile in its petrographic and mineralogical context to assure it has not been subjected to extensive retrogression. The petrographic context of rutile can be easily investigated with SEM and BSEM analysis and we suggest both thick section and grain mount analysis. A second preliminary assessment of rutile should include U and Th concentrations, in order to determine the approximate mass that will yield parent and daughter concentrations above detection limits.

From this study it is evident that a thorough petrographic investigation of rutile in its metamorphic context is crucial to obtain reliable and accurate RtHe dates. Rutile from high-grade metamorphic rocks, which have not seen major retrograde metamorphism (amphibolite or greenschist facies), should be mineralogically stable and suitable for RtHe analysis, as seen in regional RtHe results. Amphibolite facies metamorphic rocks or rutile bearing rocks that have seen pervasive retrograde metamorphism should be analyzed petrographically for breakdown of rutile to ilmenite or the presence of a titanite rim, both are easily detected with BSEM analysis.

It is plausible that RtHe analysis could be performed on rutile with a titanite rim, if rim thickness, grain to rim concentration difference, and rim preservation can be measured to calculate an $F_{Tzoning}$ correction. Previous studies which have investigated U- and Th- zoning in zircon suggested application of different methods

to retrieve a (U-Th)/He age which accounted for U and Th distribution. One approach uses a quantitative grain-by-grain method, while the second method uses a qualitative population statistic (Hourigan et al., 2005; Dobson et al., 2008). The grain-by-grain method proposes to measure the U and Th distribution with a single depth profile of the grain, by laser ablation inductively coupled plasma mass spectrometry (LA-ICP-MS). This method is not yet a standard procedure in the He-thermochronometry community, but is the most explicit method to obtain zoning parameters and apply a grain-specific $F_{Tzoning}$ correction (Hourigan et al., 2005). Alternatively, Dobson and others (2008) suggest a qualitative population-based method to determine if zoning is the cause of age dispersal in zircon standard Fish Canyon Tuff. Their study utilizes cathode luminescence (CL) imaging as a proxy to map U and Th concentrations for a sample population and then applies a zonation population statistic to estimate if scatter in (U-Th)/He ages can be associated with zoning of U and Th concentrations. However, in light of the observed variations in titanite rim thickness and titanite to rutile U and Th concentration difference and the sensitivity of the ejection correction to these parameters, it seems that only an accurate determination of these parameters on same grains as analyzed for bulk U, Th, and He would ensure reproducible and reliable rutile (U-Th)/He ages. Determination of titanite and rutile concentrations and measurement of variation in rim thickness on the same rutile sample could be carried out either in 1-D (depth profile) or in 2-D (internal polish grain surface) by ion microprobe or LA-ICP-MS prior to conventional (U-Th)/He analysis. While this overgrowth and zoning

complication does not apply to all rutile, a semi-quantitative population approach, as employed in this study, or quantitative *in situ* approach on the same rutile grain in a detailed petrographic context appears to be crucial in rutile-bearing lithologies that have experienced a metamorphic overprint resulting in rutile breakdown and complex phase relationships.

CONCLUSION

In high-grade metamorphic rocks, rutile can be part of the primary mineral assemblage, as in eclogites, or a major source of the whole rock Ti budget (Zack et al., 2002). Its stability is largely dependent upon pressure, temperature and mineral assemblage conditions. This is in contrast to zircon and apatite, common accessory minerals utilized in (U-Th)/He thermochronometry, which are less influenced by pressure and temperature conditions. Although rutile is extremely resistant to weathering in sedimentary rocks, under retrograde metamorphic conditions rutile stability is volatile and breakdown to other Ti-bearing phases, such as ilmenite and titanite, is not uncommon (Zack et al., 2004). This study assesses the development of rutile as a (U-Th)/He thermochronometer and essential considerations required for successful RtHe analysis.

Investigations include down-hole RtHe analysis and a step-heating cycled diffusion experiment on rutile-bearing amphibolites from the KTB drill hole, Germany, along with RtHe analysis of high-grade metamorphic rocks from surrounding BM. The goal of down-hole RtHe analysis is to understand *in situ*

diffusion kinetics of rutile in comparison to the well constrained thermal history of the KTB drill hole and previous thermochronometric studies, zircon and titanite (Chapter 2, Stockli and Farley, 2004). From RtHe results from the KTB drill hole, it became evident that a primary consideration of RtHe analysis should be the petrologic context of rutile in the sample.

Although down-hole RtHe analysis displayed a general younging trend with increasing down-hole temperature, large standard deviations and ages that were much older and younger than expected persisted throughout the RtHe results (Figure 14b). We attributed inaccurate RtHe results to the presence of a titanite rim on rutile identified in thick section and grain mount, which acted as an enriched rim when preserved and analyzed by RtHe analysis, producing ages that were too young. And when the rim was removed acted as a 'bad family member' implanting He, producing ages that were too old. Correction of RtHe ages that were younger than modeled RtHe results by an $F_{Tzoning}$ factor suggested that the titanite rim could be responsible for some of the RtHe results. There are many factors which are poorly constrained on a sample-by-sample basis (rim thickness, partial or complete preservation, grain-rim concentration difference, etc.), which limits our ability to apply RtHe ages. Nonetheless, we believe that such a correction could be made if a titanite rim was documented and persistent in future RtHe analysis, by either depth profiling (Hourigan et al., 2005). A population approach could determine the range of the grain to rim concentration differences and rim widths of the sample population and apply a range of $F_{Tzoning}$ corrections, if the expected RtHe age is constrained. RtHe

results from KTB drill hole accentuate the need for thorough understanding of the petrographic context, particularly if the metamorphic rocks have experienced any retrograde metamorphism in which rutile breakdown could occur.

Successful RtHe results from regional high-grade metamorphic rocks in Erzgebirge and the Blansky les Granulite Massif as well as quickly cooled xenolithic rutile from Chino Valley, AZ from previous studies (Stockli et al., 2007) encourage further studies of RtHe thermochronometry. RtHe dating will provide a medium temperature thermochronometer to assess the thermal history of high-grade metamorphic terrains and as a geochronometer on rutile-bearing volcanic rocks as previously applied, while new avenues include application to ore deposits and sedimentary basins. Recent interest in rutile as a geothermometer and carrier of trace element signatures motivates further investigation of rutile as a (U-Th)/He thermochronometer as a diverse source of information of the sample's metamorphic history.

CHAPTER 3: REFERENCES

Blackburn, T., 2005, Development of new applications in volcanic (U-Th)/He geochronology, M.S. Thesis Kansas University.

Boyce, J.W., Jercinovic, M.J., Carpenter, B.D., Reiners, P.W., Hodges, K.V., Olszewski, W.J., 2006, Laser micropobe (U-Th)/He geochronology, Geochemica et Cosmochimica Acta, v. 70, p. 3031-3039.

Castelli, D.,Rubatto, D., 2002, Stability of Al- and F-rich titanite in metacarbonate: petrologic and isotopic constraints from a polymetamorphic eclogiticmarble of the internal Sesia Zone (Western Alps). Contributions to Mineralogy and Petrology, v. 142, p. 627–639.

Clauser, C., Giese, P., Huenges, E., Kohl, T., Lehmann, H., Ryback, L., Safanda, J., Wilhelm, H., Windloff, K., Zoth, G., 1997. The thermal regime of the crystalline continental crust : implications from the KTB. Journal of Geophysical Research, v. 102, p. 18417-18441.

Coyle, D.A., Wagner, G.A., Hejl, E., Brown, R., and Van den Haute, P., 1997, The Cretaceous and younger thermal history of the KTB site (Germany). apatite fission-track data from the Vorbohrung. Geol. Rundschau, v.86, p. 203-209.

Crowhurst, P., Farley, K., Ryan, C., Duddy, I., and Blacklock, K., 2002, Potential of rutile as a U-Th-He thermochronometer. Geochimica et Cosmochimica Acta, v. 66, p. A-158.

Deer, W., Howie, R., and Zussman, J., 1982, An Introduction to the Rock Forming Minerals. Longman Group Limited, London, pp. 528.

Dobson, K., Stuart, F., Dempster, T., EIMF, 2008, U and Th zonation in Fish Canyon Tuff zircons: Implications for a zircon (U-Th)/He standard. Geochemica et Cosmochemica Acta, v. 72, p. 4745-4755.

Dodson, M.H., 1973, Closure temperature in cooling geochronological and petrological systems, Contributions to Mineralogy and Petrology, v. 40, p. 259-274.

Ehlers, T.A. and Farley, K.A., 2003, Apatite (U-Th)/He thermochronometry: methods and applications to problems in tectonic and surface processes. Earth and Planetary Science Letters, v. 206, p. 1-14.

Emmerman, R., and Lauterjung, J., 1997, The German Continental Deep Drilling Program KTB: Overview and major results. JGR, v. 102, p. 18,179-18,201.

Ernst, W. and Liu, J., 1998, Experimental phase-equilibrium of Al- and Ti-contents of calcic amphibole, in MORB- A semiquantitative thermobarometer. American Mineralogist, v. 83, p. 952-969

Farley, K. A., Wolf, R., and Silver, L., 1996, The effects of long alpha-stopping distances on (U-Th)/He ages, Geochemica et Cosmochimica Acta, v. 60, p. 4223-4229.

Farley, K. A., Reiners, P. W., and Nenow, V., 1999, An apparatus for high-precision helium diffusion measurements from minerals. Analytical Chemistry, v. 71, p. 2059-2061.

Farley, K. A., 2000, Helium diffusion from apatite: General behavior as illustrated by Durango fluorapatite, Journal of Geophysical Research, v. 105, p. 2903-2914.

Farley, K.A., 2002, (U-Th)/He dating: Techniques, calibrations, and applications in: Noble Gases in Geochemistry and Cosmochemistry, Reviews in Mineralogy and Geochemistry, v. 47, p. 819-844.

Farley, K. A. and Stockli, D. F., 2002, (U-Th)/He Dating of Phosphates: Apatite, Monazite, and Xenotime. In: Kohn, M., Rakovan, J., and Hughes, J. M. (eds), Phosphates. Review of Mineralogy, v. 47, p. 559-578.

Fiala, J.,1995, General characteristics of the Moldanubian Zone. In: Dallmeyer RD, Franke W, Weber K (eds) Pre-Permian geology of Central and Eastern Europe. Springer, Berlin Heidelberg New York, p. 417–429

Franke W, 1989, Tectonostratigraphic units in the Variscan Belt of Central Europe. Geol Soc Am Spec Pap v. 230 p. 67–90

Frost, R. B., Chamberlain, K. R., and Schumacher, J. C., 2000, Sphene (titanite): phase relations and role as a geochronometer. Chemical Geology, v. 172, p. 131-148.

Ghent, E., and Stout, M., 1984, TiO2 activity in metamorphic pelitic and basic rocks: principles and applications to metamorphism in southeastern Canadian Cordillera. Contributions to Mineralogy and Petrology, v. 86, p. 248-255.

Ghent, E.D., Stout, M.Z., Erdmer, P., 1993, Pressure-temperature evolution of lawsonite-bearing eclogites, Pinchi Lake, British Columbia, Journal of Metamorphic Geology, v. 11, p. 279-290.

Harlov, D., Tropper, P., Wolfgang, S., Nijland, T., Hans-Jurgen, F., 2006. Formation of Al-rich titanite ($CaTiSiO_4O$-$CalSiO_4OH$) reaction rims on ilmenite in metamorphic rocks as a function of fH_2O and fO_2. Lithos, v. 88, p. 72-84.

Harrison, T.M., and Zeitler, P.K., 2005, Fundamentals in Noble Gas Thermochronometry, in Reiners, P.W. and Ehlers, T.A., Low Temperature Thermochronology: Techniques, Interpretations and Applications, Reviews in Mineralogy and Geochemistry, v. 58, p. 123-149.

Hejl, E., Coyle, D., Nand Lal, P., Van den Haute, P., and Wagner, G.A., 1997, Fission-track dating of the western border of the Bohemian massif: thermochronology and tectonic implications. Geol. Rundschau, v. 86, p. 210-219.

Hirschmann, G., Duyster, J., Harms, U., Kontny, A., Lapp, M., de Wall, H. & Zulauf, G., 1997, The KTB superdeep borehole: petrography and structure of a 9-km-deep crustal section. Geol. Rundsch , v. 86, p. 3-15.

Hourigan J.K., Reiners, P.W., and Brandon, M.T., 2005, U-Th zonation-dependent alpha-ejection in (U-Th)/He chronometry. Geochimica et Cosmochimica Acta., v. 69, p. 3349-3365.

House M.A., Farley K.A., and Stockli D.F., 2000, Helium chronometry of apatite and titanite using Nd-YAG laser heating. Earth and Planetary Science Letters, 183, 365-368

House, M., Farley, K., Kohn, B., 1999, An empirical test of helium diffusion in apatite: borehole deata from the Otway basin, Australia, Earth and Planetary Science Letters, v. 170, p. 463-474

Hurley, P. M., 1954, The helium age method and the distribution and migration of helium in rocks, in Faul, H., ed., Nuclear Geology. New York, John Wiley and Sons, p. 301-329.

Kelley, S., 2002, Excess argon in K-Ar and Ar-Ar geochronology. Chemical Geology, v. 188, p. 1-22.

Kleeman, U., and Reinhardt, 1994, Garnet-biotite thermometry revisted: the effect of Al^{vi} and Ti in biotite, European Journal of Mineralogy, v. 6, p. 925-941.

Klemd, R., Matthes, S., Schussler, U., 1994, Reaction textures and fluid behavior in very high-pressure calc-silicate rocks of the Munchberg gneiss complex, Bavaria, Germany. Journal of Metamorphic Geology, v. 12, p. 735–745.

Kontny, A., Fredrich, G., Behr, H.J., deWall, H., Horn, E. E., Moller, P., and Zulauf, G., 1997, Formation of ore minerals in metamorphic rocks of the German continental deep drilling site (KTB), Journal of Geophysical Research, v. 102, p. 18,323-18336.

Kroner, A., O'Brien, P.J., Nemchin, A.A., Pidgeon, R.T., 2000, Zircon ages for high pressure granulites from South Bohemia, Czech Republic, and their connection to Carboniferous high temperature processes. Contribution to Mineralogy and Petrology, v. 138, p. 127-142.

Li, Q., Li, S., ZrHeng, Y.F., Li, H., Massone, H.J., Wang, Q., 2003, A high precision U-Pb age of metamorphic rutile in coesite-bearing eclogite from the Dabie

Mountains in central China: a new constraint on the cooling history. Chemical Geology, v. 200, p. 255-265.

Lindsey, D.H., 1976, Chapter 1 – The crystal chemistry and structure of oxide minerals as exemplified by the Fe-Ti oxides, in Rumble, D., ed., Oxide Minerals. Reviews in Mineralogy, v. 3, p. L-1 – L-60.

Luvizotto, G.L., Zack, T., 2008, Nb and Zr behavior in rutile during high-grade metamorphism and retrogression: An example from the Ivrea-Verbano Zone, Chemical Geology, v. 261, p. 303-317

Luvizotto G.L., Zack, T. Triebold, S., von Eynatten, H., *in press*, Rutile occurrence and trace element behavior in low- to medium-grade metasedimentary rocks. Mineralogy and Petrology

Manning, C. and Bohlen, S., 1991, The reaction Titanite + Kyanite = Anorthite + Rutile and Titanite-Rutile barometry in Eclogites. Contributions to Mineralogy and Petrology. v. 109, p. 1-9.

MathWorks, The., 2008b. MATLAB®, Natick, MA

McDougall, I, and Harrison, M.T., 1999, Geochronology and thermochronology by the $^{40}Ar/^{39}Ar$ method, second edition. Oxford University Press, New York, 269 pp.

Mezger, K., Hanson, G.N., and Bohlen, S.R., 1989, High-precision U-Pb ages of metamorphic rutile: application to the cooling history of high-grade terrains. Earth and Planetary Science Letters, v. 96, p. 106-118.

Meinhold, G., Anders, B., Kostopoulos, D., Reischmann, T., 2008, Rutile chemistry and thermometry as provenance indicator: An example from Chios Island, Greece. Sedimentary Geology, v. 203, p. 98-111.

Mingram, B., Kroner, A., Hegner, E., Krentz, O., 2004, Zircon ages, geochemistry, and Nd isotopic systematics of pre-Variscan orthogeneisses from the Erzgebirge, Saxony (Germany) and geodynamic interpretation. Geol Rundschau, v. 93, p. 706-727.

Mingram B., 1998, The Erzgebirge, Germany, a subducted part of northern Gondwana: geochemical evidence for repetition of early Palaeozoic metasedimentary sequences in metamorphic thrust units. Geological Magazine v. 135, p. 785–801.

O'Brien, P. J., Duyster, J., Grauert, B., Chreyer, W., Stockhert, B., and Weber, K., 1997, Crustal evolution of the KTB drill site: From oldest relics to the late Hercynian granites. Journal of Geophysical Research, v. 102, p. 18203-18220.

O'Brien, P. J., and Carswell., D. A., 1993, Tectonometamorphic evolution of the Bohemian Massif: evidence from high pressure metamorphic rocks. Geol. Rundsch, v. 82, p. 531-555.

O'Brien, P.J., Rohr, C., Okrusch, M., Patzak, M., 1992, Eclogite facies relics and a multistage breakdown in metabasites of the KTB pilot hole, NE Bavaria: implications for the Variscan tectonometamorphic evolution of the NW Bohemian Massif. Contributions to Mineralogy and Petrology. v. 112, p. 261-278.

O'Brien, P.J. and Vranau, S., 1995, Eclogites with a short-lived granulite facies overprint in the Moldanubian Zone, Czech Republic: petrology, geochemistry and diffusion modeling of garnet zoning. Geol. Rundsch, v. 84, p. 473-488.

Owen J.V., Dostal J., 1996, Contrasting corona structures in mafic granulite from the Blanský Les complex, Bohemian Massif, Czech Republic. Canadian Mineral v. 34, p. 959–966

Rahl, J.M., Reiners, P.W., Campbell, I.H., Nicolescu, S., Allen, C.M., 2003, Combined single-grain (U-Th)/He and U/Pb dating of detrital zircons from the Navajo Sandstone, Utah. Geology v. 31, p. 761-764.

Reiners, P.W. and Farley, K.A., 1999, He diffusion and (U-Th)/He thermochronometry of titanite, Geochemica et Cosmochimica Acta, v. 62, p. 3845-3859.

Reiners, P.W., Farley, K.A., and Hickes, H.J., 2002, He diffusion and (U-Th)/He thermochronometry of zircon: Initial results from Fish Canyon Tuff and Gold Butte, Nevada, Tectonophysics, v. 349, p. 297-308.

Reiners, P. W., 2005, Zircon (U-Th)/He Thermochronometry, in Reiners, P. W. and Elhers, T. A., Low Temperature Thermochronology: Techniques, Interpretations and Applications, Reviews in Mineralogy and Geochemistry, v. 58, p. 151-179.

Romer, R. and Rötzler K, 2003, Effect of metamorphic reaction history on the U-Pb dating of titanite, Geological Society of London, Special Publications, v. 220, p. 147-258.

Rötzler K., Schumacher R., Maresch W.V., Willner A.P., 1998, Characterization and geodynamic implications of contrasting metamorphic evolution in juxtaposed high-pressure units of the western Erzgebirge (Saxony, Germany). European Journal of Mineralogy 10: 261–280

Rudnick, R.L., Barth, M., Horn, I., and McDonough, W.F., 2000, Rutile-bearing refractory eclogites: missing link between continents and depleted mantle. Science, v. 287, p. 278-281.

Saadoune, I., Purton, J.A., Leeuw, N.H., 2009, He incorporation and diffusion pathways in pure and defective $ZrSiO_4$: A density functional theory study. Chemical Geology, v. 258, p. 182-196.

Schroder, B., Ahrendt, H., Peterek, A., Wemmer, K., 1997, Post-Variscan sedimentary record of the SW margin of the Bohemian massif: a review. Geol Rundsch, v. 86, p. 178-184.

Stockli, D.F., Wolfe, M., Blackburn, T., Zack, T., Walker, J.D., Luvizotto, G., 2007, He diffusion and (U-Th)/He thermochronometry of rutile. Abstract. Programs AGU Fall 2007

Stockli, D.F., Farley, K.A., Walker, J.D., Blackburn, T.J., 2005, Helium diffusion and (U–Th)/He thermochronometry of monazite and rutile, Geochimica et Cosmochimica Acta, v. 69, A8.

Stockli, D.F. and Farley, K.A., 2004, Empirical constraints on the titanite (U-Th)/He partial retention zone from the KTB drill hole: Chemical Geology, v. 207, p. 223-236.

Stockli, D.F., Farley, K.A., and Dimitru, T. A., 2000, Calibration of the apatite (U-Th)/He thermochronometer on an exhumed fault block, White Mountains, California: Geology, v. 28, p. 983-986.

Tincher, C.R. and Stockli, D.F., 2008, Cenozoic volcanism and tectonics in the Queen Valley area, Esmeralda County, western Nevada, GSA Bulletin Special Paper 445, p. 225-274.

Thomson, S.N., and Zeh, A., 2000, Fission-track thermochronology of the Ruhla Crystalline Complex: new constraints on the post-Variscan thermal evolution of the NW Saxo-Bohemian Massif. Tectonophysics, v. 324, p. 17-35.

Tomkins, H.S., Powell, R., Ellis, D.J., 2007, The pressure dependence of the zirconium-in-rutile thermometer. Journal of Metamorphic Geology, v. 25, p. 703-713.

Triebold, S., von Eynatten, H., Luvizotto G. L., Zack, T., 2007, Deducing source rock lithology from detrital rutile geochemistry: An example from the Erzgebirge, Germany. Chemical Geology, v. 244, p. 421-436.

Tropper, P. and Manning, C., 2008, The current status of titanite-rutile thermobarometry in ultrahigh-pressure metamorphic rocks: The influence of titanite activity models on phase equilibrium calculations. Chemical Geology. v. 254, p. 123-132.

Vermeesch, P., Seward, D., Latkoczy, C., Wipf, M., Gunther, D., Baur, H., 2005, α-Emitting mineral inclusions in apatite, their effect on (U-Th)/He ages, and how to reduce it. Geochimica et Cosmochimica Acta, v 71, p. 1737-1746.

Wagner, C. A., Coyle, D.A., Duyster, J., Henjes-Kunst, F., Peterek, A., Schroder, B., Stockhert, B., Wemmer, K., Zulauf, G., Ahrendt, H., Bischoff, R., Hejl, E., Jacobs, J., Menzel, D., Ll, N., Van den haute, P., Vercoutere, C., Welzel, B., 1997. Post-Variscan thermal and tectonic evolution of the KTB site and its surroundings. Journal of Geophysical Research, v. 102, p. 18221-18232.

Warnock, A.C., Zeitler, P.K., Wolf, R.A., and Bergman, S.C., 1997, An evaluation of low temperature apatite U-Th/He thermochronometry. Geochimica et Cosmochimica Acta, v. 61, p. 5371-5377.

Warnock, A. and Zeitler, P., 1998, $^{40}Ar/^{39}Ar$ thermochronometry of K-feldspar from the KTB borehole, Germany. Earth and Planetary Science Letters, v. 158, p. 67-78.

Waychunas, G., 1991, Crystal Chemistry of Oxides and Oxyhydroxides. In: Oxide Minerals: Petrologic and magnetic significance, Ed. Lindsley, D., Reviews in Mineralogy v. 25, p. 12-68.

Wemmer, K., 1991, K/Ar-Altersdatienrungsmoglickkeiten fur retrograde Deformationsprozesse im sproden und duktilen Bereich- Beispiele aus der KTB VB (Oberfalz) und dem Bereich der Insubrischen Linie. Gottinger Arb. Geol. Palantol, v. 51, p. 1-61.

Wolf, R.A., Farley, K.A. and Silver, L.T., 1996, Helium diffusion and low-temperature thermochronometry of apatite, Geochimica et Cosmochimica Acta, v. 60, p. 4231-4240.

Wolf, R.A., Farley, K.A., and Kass, F.M., 1998, Modeling of the temperature sensitivity of the apatite (U-Th)/He thermochronometer. Chemical Geology, v. 148, p. 105-114.

Zack, T., Kronz, A., Foley, S., Rivers, T., 2002, Trace element abundances in rutiles from eclogites and associated garnet mica schists. v. 184, p. 97-122

Zack, T., Moraes, R., Kronz, A., 2004a, Temperature dependence of Zr in rutile: empirical calibration of a rutile thermometer, Contribution to Mineralogy and Petrology, v. 148, p. 471-488.

Zack, T., Eynatten, H. von., Kronz, A., 2004b, Rutile geochemistry and its potential use in quantitative provenance studies. Sedimentary Geology, v. 171, p. 37-58.

Zeitler, P.K., Herczeg, A.L., McDougall, I. and Honda, M., 1987, U-Th-He dating of apatite: A potential thermochronometer: Geochimica et Cosmochimica Acta, v. 51, p. 2865-2868.

Zulauf, G., Palm, S., Petschick, R., Spies, O., 1999, Element mobility and volumetric strain in brittle and brittle-viscous shear zones of the superdeep well KTB (Germany). Chemical Geology, v. 156, p. 135-149.

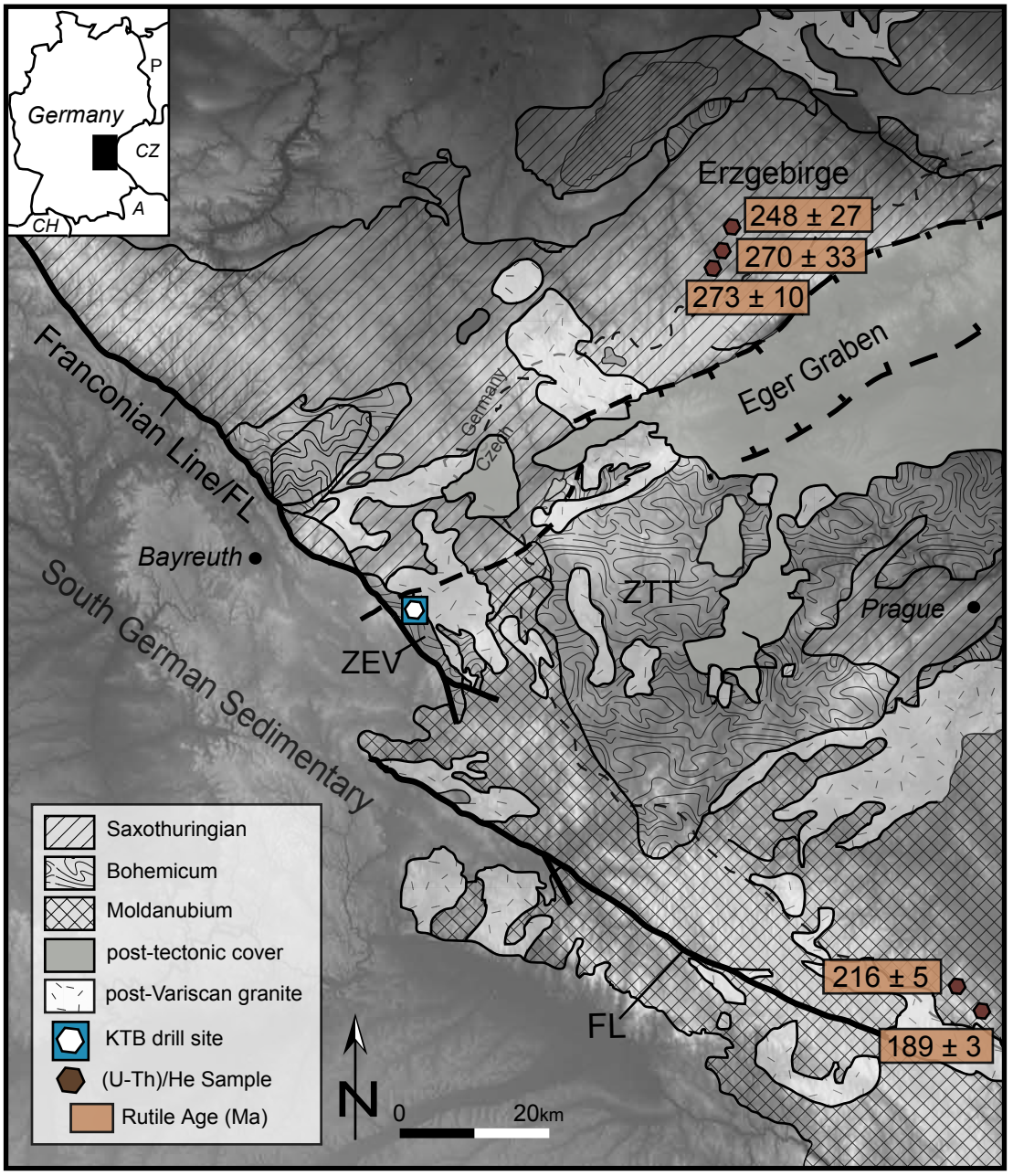
Germany
P
CZ
A
CH
Erzgebirge
248 ± 27
270 ± 33
273 ± 10
Eger Graben
Franconian Line/FL
Germany
Czech
Bayreuth
South German Sedimentary
ZTT
Prague
ZEV
FL
216 ± 5
189 ± 3
Saxothuringian
Bohemicum
Moldanubium
post-tectonic cover
post-Variscan granite
KTB drill site
(U-Th)/He Sample
Rutile Age (Ma)
N
0
20km

Figure 1. Regional geologic map of KTB region and surrounding western extent of the Bohemian Massif (modified from Franke, 1989). Sample localities of rutile bearing high-grade metamorphic rocks from the Blanksy les Granulite Massif in southern Bohemia and Erzgebirge in Saxony utilized for regional RtHe analysis.

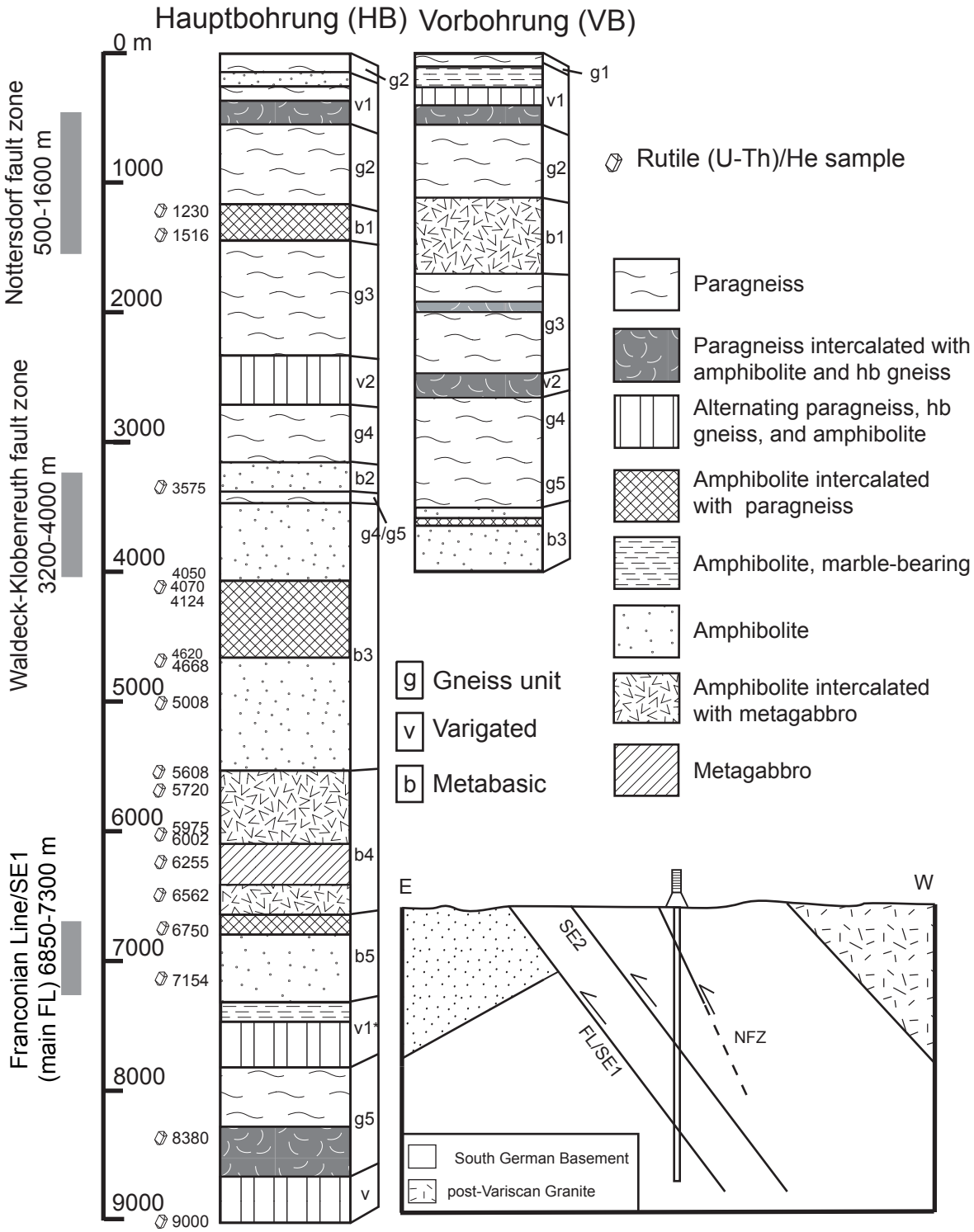
Hauptbohrung (HB)
Vorbohrung (VB)
0 m
1000
2000
3000
4000
5000
6000
7000
8000
9000
1230
1516
3575
4050
4070
4124
4620
4668
5008
5608
5720
5975
6002
6255
6562
6750
7154
8380
9000
g2
v1
g2
b1
g3
v2
g4
b2
g4/g5
b3
b4
b5
v1*
g5
v
g1
v1
g2
b1
g3
v2
g4
g5
b3
Nottersdorf fault zone
500-1600 m
Waldeck-Klobenreuth fault zone
3200-4000 m
Franconian Line/SE1
(main FL) 6850-7300 m
Rutile (U-Th)/He sample
Paragneiss
Paragneiss intercalated with amphibolite and hb gneiss
Alternating paragneiss, hb gneiss, and amphibolite
Amphibolite intercalated with paragneiss
Amphibolite, marble-bearing
Amphibolite
Amphibolite intercalated with metagabbro
Metagabbro
g Gneiss unit
v Varigated
b Metabasic
E
W
SE2
FL/SE1
NFZ
South German Basement
post-Variscan Granite

Figure 2. Down-hole profile of the KTB drill hole, including both the pilot hole (VB) and main drill hole (HB). The simplified lithologic columns (after Hirschmann et al., 1997) display repetition of gneissic (g), variegated (v) and metabasic (b) units. Major fault zones are noted on the far left and identify boundaries between stacked metamorphic units. Numbers next to HB column represent rutile samples analyzed for (U-Th)/He analysis for this study.

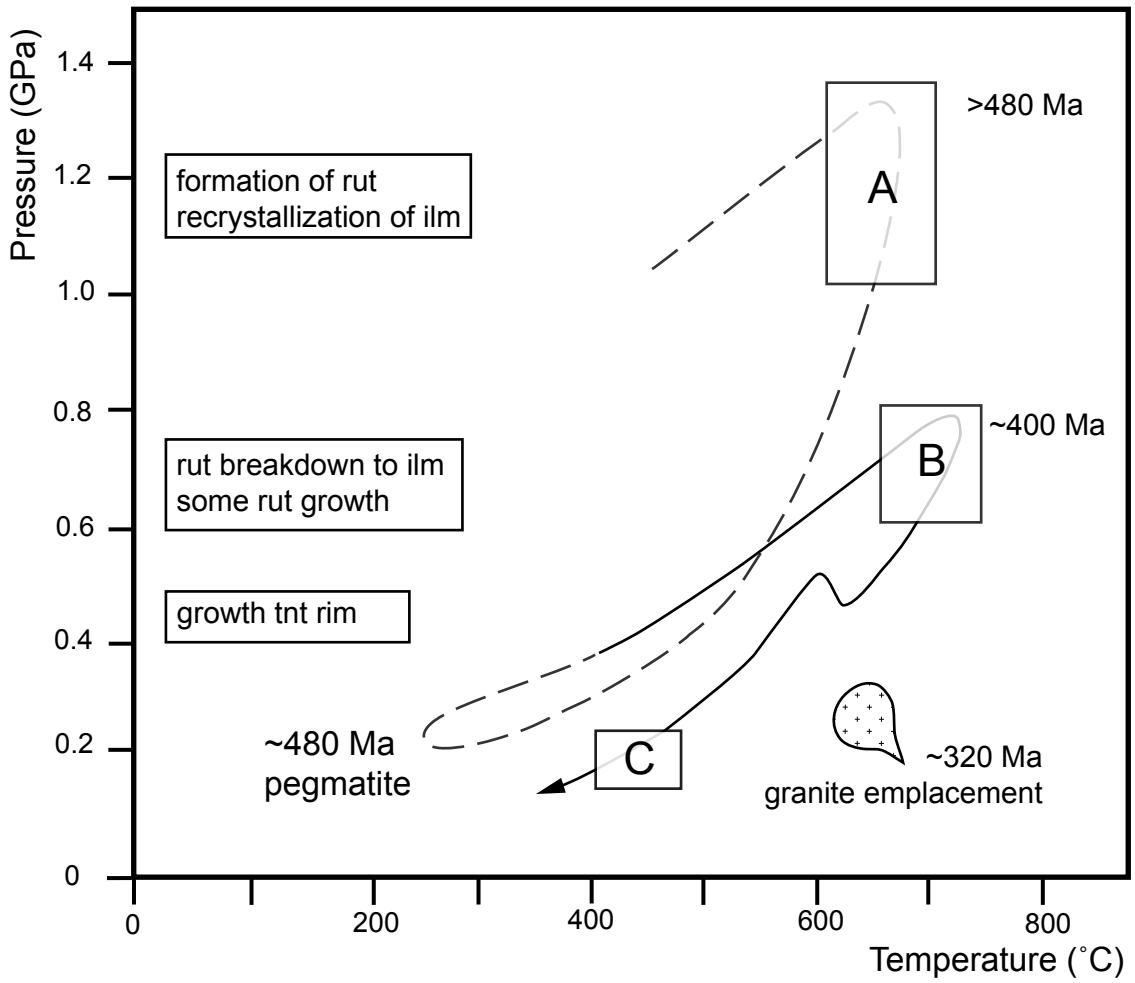
Pressure (GPa)
1.4
1.2
1.0
0.8
0.6
0.4
0.2
0
0
200
400
600
800
Temperature (˚C)
formation of rut
recrystallization of ilm
rut breakdown to ilm
some rut growth
growth tnt rim
A
>480 Ma
B
~400 Ma
C
~480 Ma
pegmatite
~320 Ma
granite emplacement

Figure 3. Estimated double-loop pressure-temperature path and ore mineral growth throughout metamorphic history of ZEV, modified and combined from (O'Brien et al., 1997 and Kontny et al., 1997). Box A- Peak HP conditions from eclogitic lenses preserved in metabasic rocks calculate 1.3-1.4 GPa and 650-700°C (O'Brien et al., 1992). Rutile growth from Fe-Ti oxides (Kontny et al., 1997). Box B- Widespread amphibolite facies metamorphism record PT conditions 0.6-0.8 GPa 660-720 °C (Reinhardt et al., 1989). Rutile breakdown to ilmenite and some rutile growth. Box C- Low-amphibolite to greenschist facies retrograde conditions along with fluid emplacement caused growth of pyrite and other sulfide assemblages and breakdown of ilmenite and rutile to titanite in thin rims.

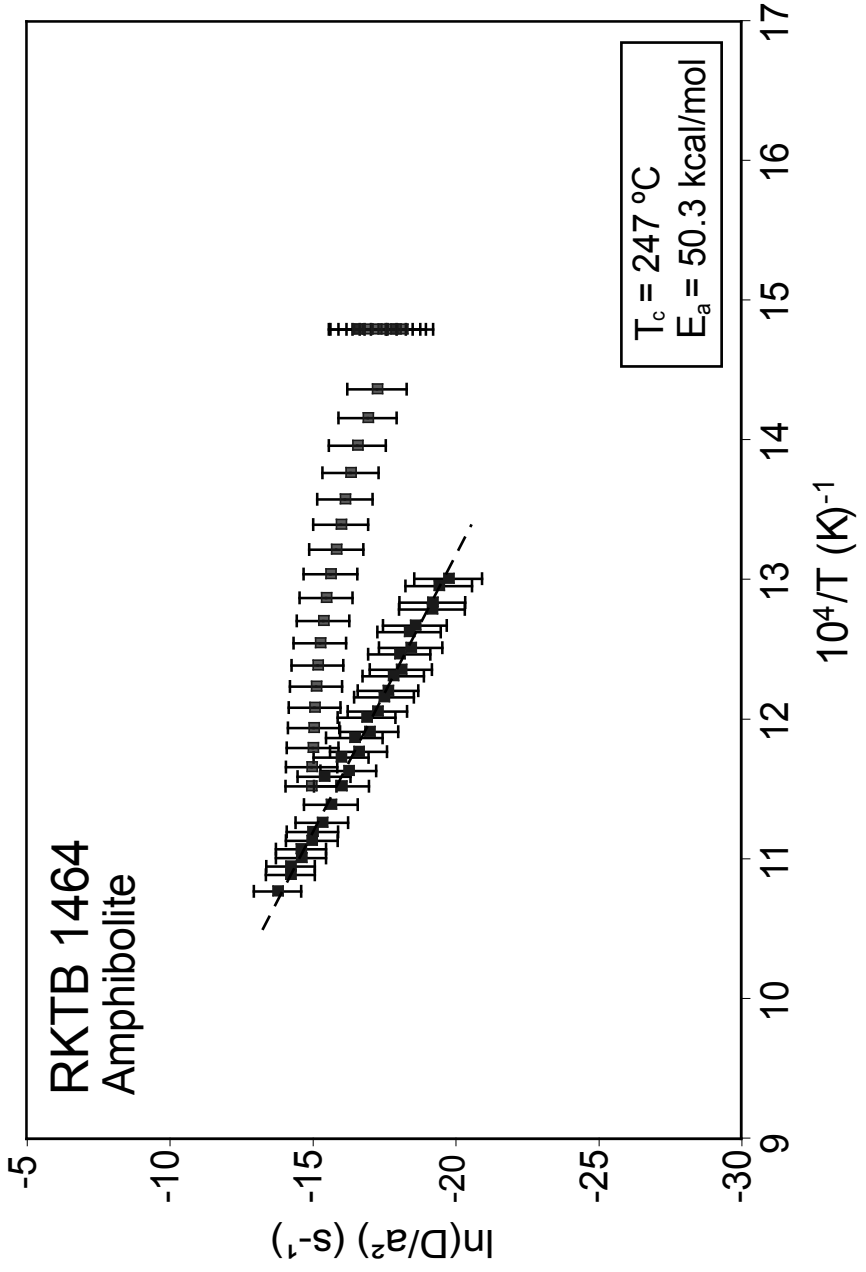
RKTB 1464
Amphibolite
T_c = 247 °C
E_a = 50.3 kcal/mol
ln(D/a²) (s⁻¹)
10^4/T (K)$^{-1}$
-5
-10
-15
-20
-25
-30
9
10
11
12
13
14
15
16
17

Figure 4. Arrhenius plot of complete cycled step-heating diffusion experiment from RKTB1464 in the KTB drill hole. First prograde heating steps display the typical behavior of He diffusivity in rutile, a lower diffusivity up to ~500°C when a rollover occurs. The proceeding retrograde and prograde steps are well-behaved and display simple Arrhenius behavior. Diffusion kinetics calculated from the dashed line yield an activation energy of 50.3 kcal/mol (210 kJ/mol) and $\ln(D/a^2) = 13.8\ s^{-1}$. A closure temperature of 247°C, based on dt/dT 10°C/m.y. (Dodson, 1973) is higher than previous unpublished rutile diffusion experiments, which vary from ~210-235°C.

U-Th micro column chemistry	Reagent	Vol (µl)
Resin	AG1x8 resin	100
Clean	H_2O	200
Clean	6N HCl	200
Clean	H_2O	100
Condition	7N HNO_3	150
Load Sample	7N HNO_3	60
Collect Sm	7N HNO_3	350
Collect U-Th	6N HCl	250
Collect U-Th	H_2O	250

Sm Column Chemistry	Reagent	Vol (ml)
Resin	AG 50Wx8 resin	2
Clean	6N HCl	6
Clean	H_2O	5
Condition	2.5N HCl	2
Load Sample	2.5N HCl	1
Wash (Elute Ti, major elements)	2.5N HCl	12
Collect Sm	2.5N HCl	10

Table 1. Column chemistry procedure utilized to purify parent U, Th, and Sm concentrations from major elements, which can impede ionization during ICP-MS analysis.

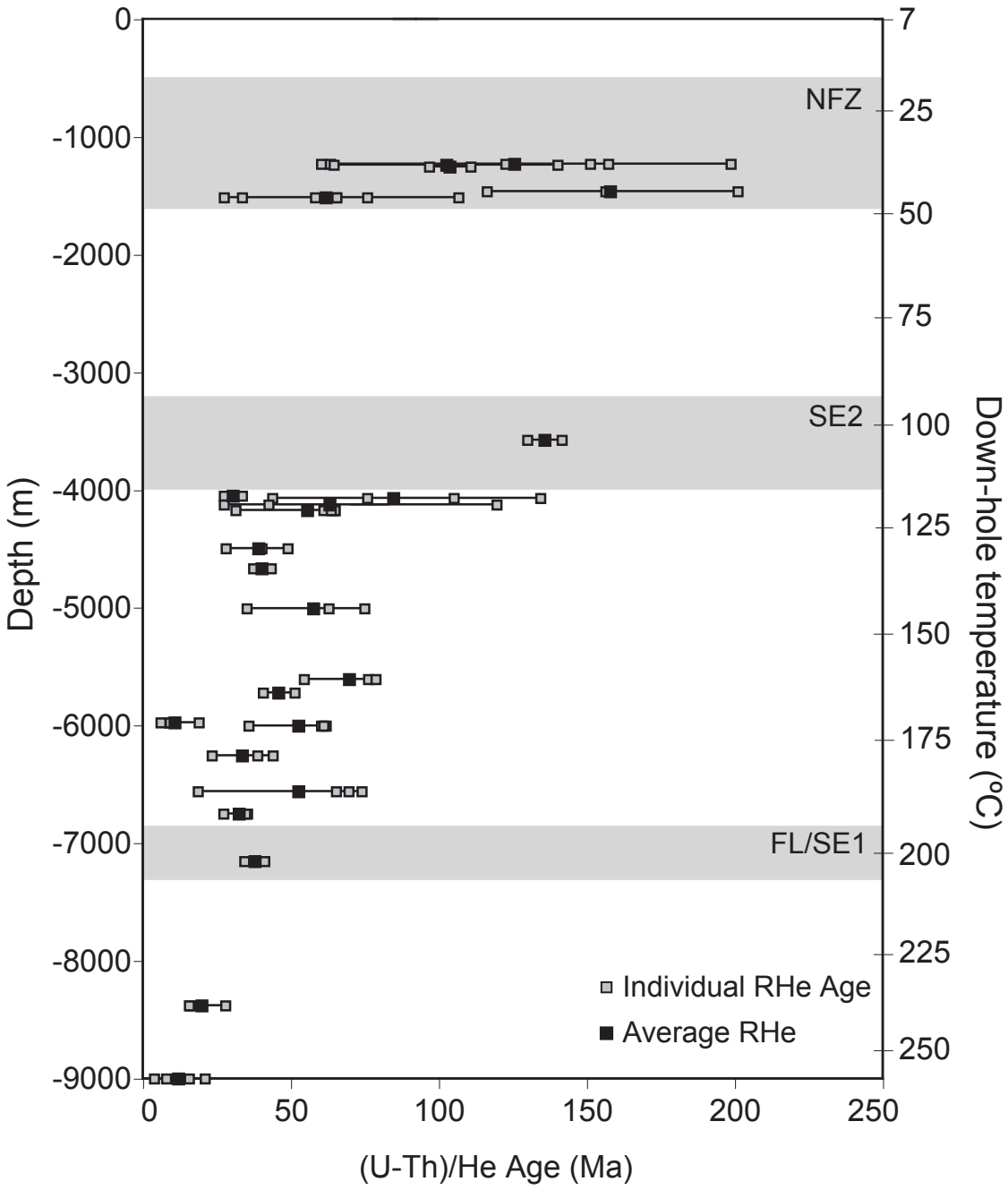
0
-1000
-2000
-3000
-4000
-5000
-6000
-7000
-8000
-9000
Depth (m)
7
25
50
75
100
125
150
175
200
225
250
Down-hole temperature (°C)
NFZ
SE2
FL/SE1
Individual RHe Age
Average RHe
0
50
100
150
200
250
(U-Th)/He Age (Ma)

Figure 5. Rutile (U-Th)/He (RtHe) ages from the KTB drill hole corrected by alpha-ejection correction factor based on homogeneous distribution of U and Th. Error on RtHe age spans from oldest to youngest individual RHe age in each sample. Gaps (0-1200m and 1516-3575 m) between rutile (U-Th)/He ages can be attributed to the presence of paragneiss blocks, which did not yield rutile. Large standard deviations can be seen in samples within the NFZ and samples just below SE2 fault zone (4050-4172 m). Marked decrease in RtHe age can be seen below ~4000 m depth with youngest samples at 9000 m.

Sample	Age [Ma]	± (stdev) [Ma]	U [ppm]	Th [ppm]	Sm [ppm]	e[U] (ppm)	Th/U	He [nmol/g]	mass [mg]	F_T*	Depth	Raw Age [Ma]	n
RKTB 1230	125.5	55.0	3.7	0.3	12.6	3.7	0.1	11.2	12.2	0.77	-1230	96.3	6
RKTB 1239	102.5	37.8	4.1	0.2	7.3	4.1	0.0	1.8	22.5	0.77	-1239	79.0	3
RKTB 1252	103.7	9.9	15.8	0.5	10.0	15.9	0.0	6.9	17.9	0.75	-1252	77.9	2
RKTB 1464	157.8	42.4	1.6	1.3	4.6	1.9	0.9	1.2	15.8	0.77	-1464	120.7	3
RKTB 1516	61.7	26.5	4.8	1.4	4.2	5.2	0.3	0.8	7.1	0.71	-1516	46.0	7
RKTB 3575	135.7	8.2	1.2	0.7	1.4	1.4	0.5	0.8	15.4	0.82	-3575	108.3	2
RKTB 4050	30.4	4.4	2.8	2.2	1.6	2.8	0.8	0.52	6.2	0.70	-4050	19.6	4
RKTB 4070	84.6	45.9	5.1	0.8	0.9	5.3	0.1	1.45	7.1	0.72	-4050	30.2	3
RKTB 4124	63.1	49.4	1.7	1.1	1.4	1.9	0.9	0.38	4.6	0.72	-4070	29.5	3
RKTB 4172	55.4	16.2	4.0	-0.6	1.7	3.9	-0.2	0.79	6.1	0.70	-4172	20.9	4
RKTB 4496	39.0	10.6	12.6	0.6	4.8	12.7	0.1	2.2	11.0	0.82	-4496	31.5	3
RKTB 4668	40.1	3.0	5.0	0.6	1.1	5.2	0.1	0.82	8.6	0.73	-4668	26.2	3
RKTB 5008	57.6	20.5	2.8	0.3	1.7	2.9	0.2	0.7	22.0	0.80	-5008	28.2	3
RKTB 5608	69.7	13.3	1.2	0.3	1.5	1.3	0.3	0.4	23.8	0.79	-5608	60.2	3
RKTB 5720	45.8	5.3	1.5	0.1	1.4	1.5	0.1	0.3	23.0	0.78	-5720	30.8	3
RKTB 5975	10.7	5.6	2.3	0.6	2.0	2.4	0.3	0.0	11.9	0.78	-5975	7.0	4
RKTB 6002	52.6	14.7	1.4	0.9	1.1	1.5	0.8	0.4	14.1	0.80	-6002	49.6	3
RKTB 6005	22.3	9.6	2.1	0.4	1.5	2.2	0.3	0.23	32.9	0.80	-6005	17.5	3
RKTB 6255	33.5	10.3	2.9	0.5	9.1	3.0	0.2	0.4	11.0	0.78	-6255	16.8	3
RKTB 6562	52.5	29.7	2.0	0.6	2.4	2.1	0.3	0.5	7.2	0.75	-6562	53.8	3
RKTB 6750	32.4	4.5	3.0	1.1	5.1	3.3	0.5	0.4	5.1	0.67	-6750	23.8	3
RKTB 7153	37.7	4.7	4.9	0.4	0.9	5.0	0.1	0.8	17.3	0.76	-7153	30.6	2
RKTB 8380	19.8	7.0	3.0	1.2	5.2	3.3	0.6	0.2	10.6	0.71	-8380	14.1	3
RKTB 9084	11.9	6.6	16.0	0.4	0.8	16.1	0.0	0.3	11.3	0.80	-9000	9.5	6

* Assumes homogeneous U and Th distribution (Farley, 1996)

Table 2. Average rutile (U-Th)/He ages from KTB drill hole, corrected based on traditional alpha ejection correction, assuming a homogeneous distribution of U and Th. All rutile are from amphibolite and garnet-amphibolite metabasite units.

Sample	mass (μg)	Fault Block	Ca (ppm)	Cr (ppm)	Zr (ppm)	Nb (ppm)	Hf (ppm)	Ta (ppm)	U (ppm)	$^{+}$T (°C) P = 14 kbar	$^{+}$T (°C) P = 6 kbar
1230-1*	7.8	A	1750	18.3	238	371	0.7	15.6	-	648	615
1230-2*	4.6	A	1600	630	226	308	2.1	47.1	-	644	611
1252-1*	2.4	A	20300	220	207	405	-	-	-	637	604
1252-2*	3.4	A	2780	34.0	88.3	169	-	40.6	-	576	545
1464-1*	13.7	A	-	149	165	204	1.9	-	-	620	588
1464-2*	14.8	A	14600	374	1750	543	39.5	52.5	-	837	797
1516-1*	7.2	A	-	25.5	379	96.9	4.9	-	-	686	651
1516-2*	4.3	A	13800	47.9	122	262	-	41.6	-	599	567
3575-1**	11.08	B	-	637	176	234	-	-	-	625	592
3575-2**	8.6	B	4620	879	2710	272	58.8	49.6	-	890	847
4050-1**	16.7	B	1030	1140	220	230	9.0	9.1	1.5	642	609
4050-2**	11.4	B	2330	265	255	251	9.6	11.8	4.3	654	620
4070-1**	11	B	1810	2150	437	289	13.4	12.5	2.9	699	663
4070-2**	9.3	B	3780	539	465	860	18	32.4	8.5	704	667
4172-1	4.7	B	2520	178	310	152	7.8	4.4	6.7	670	635
4172-2	4.6	B	6880	115	367	249	9.5	7.4	6.7	684	649
4668-1	4.9	C	12400	541	338	246	9.0	15.5	7.9	677	642
4668-2	5.5	C	10900	79.5	243	1470	8.3	335	5.6	650	616
5008-1	3.4	C	5060	2260	215	161	-	5.5	7.4	640	607
5008-2	4.5	C	5170	2780	202	109	-	2.5	2.4	636	602
5608-1	8.8	C	1690	347	483	529	13.2	19.4	1.5	708	672
5608-2	8.7	C	1890	313	373	324	10.2	12.7	1.8	685	650
5975-1	15.6	C	2590	913	407	319	10.4	21.7	1.5	692	657
5975-2	14.8	C	2080	499	218	318	7.01	7.0	1.9	64	608

Sample	mass (μg)	Fault Block	Ca (ppm)	Cr (ppm)	Zr (ppm)	Nb (ppm)	Hf (ppm)	Ta (ppm)	U (ppm)	+T (°C) *P* = 14 kbar	+T (°C) *P* = 6 kbar
6002-1	11.8	C	1850	1090	377	246	9.2	14.3	2.7	686	651
6002-2	4.3	C	7030	969	426	202	9.2	8.8	3.6	697	661
6255-1	7.2	C	5520	210	199	92.4	3.7	1.9	1.7	635	601
6255-2	2.6	C	6320	743	388	398	5.3	12.4	7.6	688	653
6750-1	6.5	C	2820	68.5	584	92.5	14.2	3.6	2.2	725	688
6750-2	3	C	12600	95.4	353	126	9.8	5.2	4.1	680	646
7153-1* **	15.2	D	797	867	881	218	23	4.1	1.9	764	726
7153-2* **	18.3	D	2430	199	248	393	9.1	11.3	5.5	651	618
7153-3* **	5.9	D	13500	1000	592	1120	19.7	32.1	6.3	726	690
7153-4* **	7.4	D	3770	332	299	410	7.7	11.4	2.5	667	632
8380-1	6.3	D	2760	881	866	457	21.1	15.1	2.9	763	725
8380-2	1.9	D	7140	235	500	5040	16.1	313.5	10.4	711	675
9000-1	6.4	D	10100	309	547	420	19.6	20.5	20.7	719	683
9000-2	9.9	D	2090	714	187	732	9.6	31.9	13.9	623	596
9000-3	1.9	D	30700	5323	504	374	12.6	11.8	38.1	711	675

Concentrations below the detection limit are not listed, while values less than twice the detection limit are in +grey.
* Within Nottersdorf Fault Zone (NFZ)
** Within SE2 Fault zone
*** Within Franconian Lineament (FL)
+ Peak metamorphic temperature estimates calculated based on Zr concentration (Tomkins et al., 2007) and pressure estimates of the maximum (14 kbar) and minimum (6 kbar) conditions of the peak metamorphic events experienced by samples in the KTB drill hole (O'Brien et al., 1992). See text for further explanation

Table 3. Selected trace element geochemistry results, for complete elemental list and results see Appendix D.

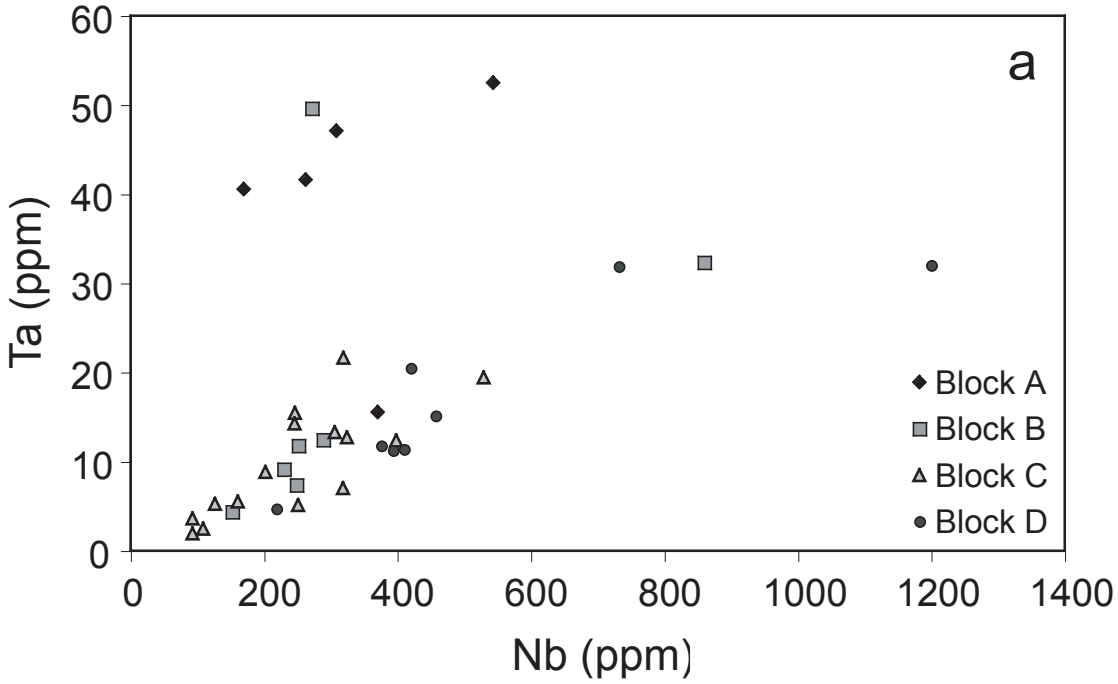
a
Ta (ppm)
Nb (ppm)
0
10
20
30
40
50
60
0
200
400
600
800
1000
1200
1400
Block A
Block B
Block C
Block D

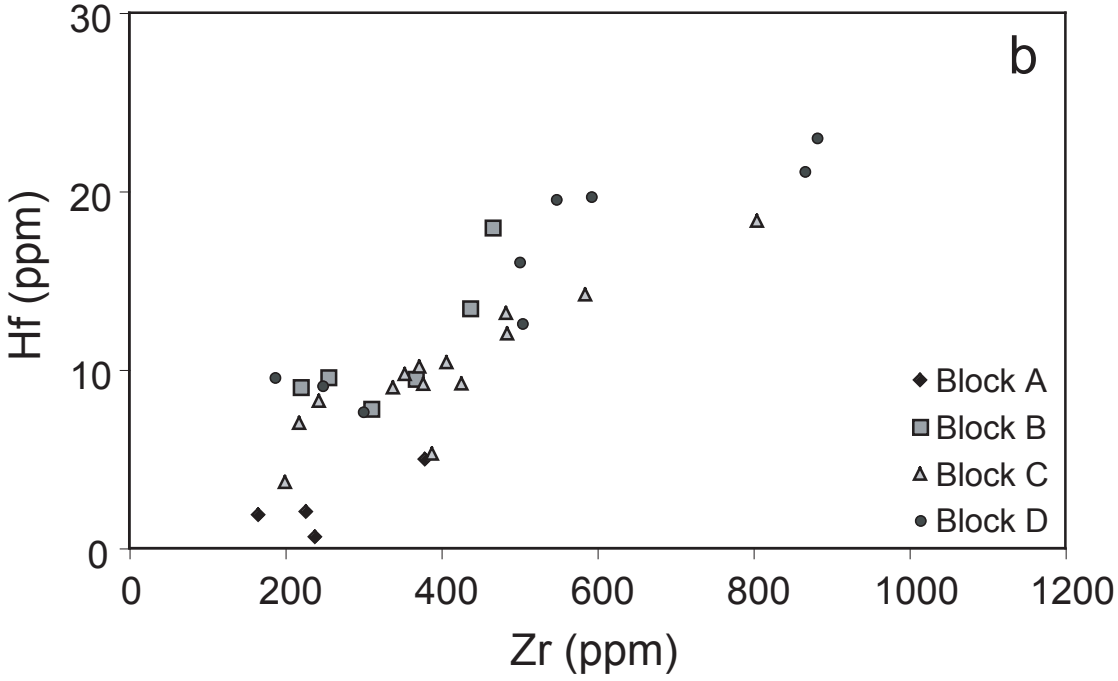
b
Hf (ppm)
Zr (ppm)
0
10
20
30
0
200
400
600
800
1000
1200
Block A
Block B
Block C
Block D

Figure 6. Trace element geochemistry plots of Nb, Ta, Zr, Hf concentrations in rutile from the KTB drill hole, measured by solution ICP-MS on single grains. Samples are grouped into metamorphic fault blocks delineated by Wagner and others (1997). (a) Nb vs. Ta concentrations display a modest compatibility. Samples from Block A and one from Block B have increased Nb and Ta concentrations. (b) Zr vs. Hf concentrations display a strong correlation as they are incorporated into the crystal lattice together (Zack et al., 2002).

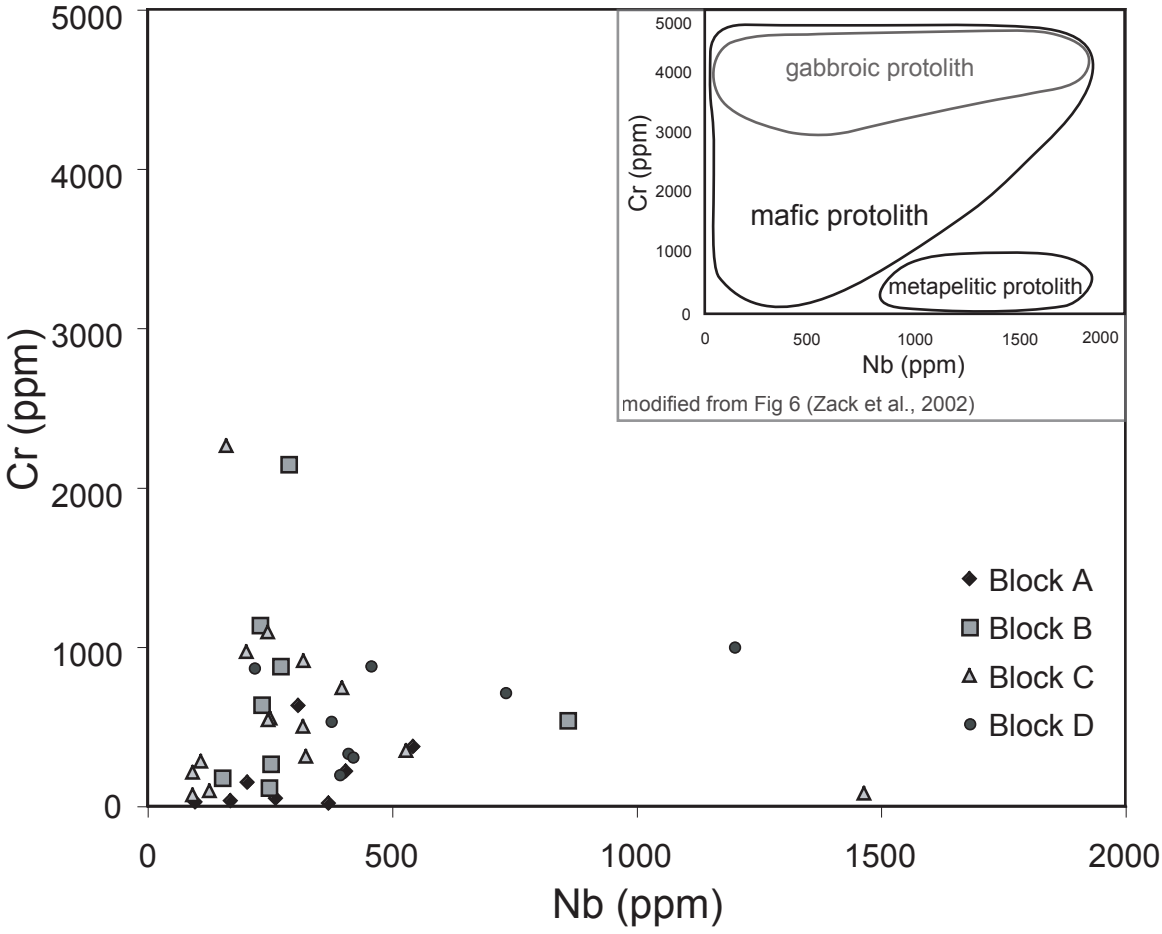
5000
4000
3000
2000
1000
0
Cr (ppm)
0
500
1000
1500
2000
Nb (ppm)
Block A
Block B
Block C
Block D
gabbroic protolith
mafic protolith
metapelitic protolith
modified from Fig 6 (Zack et al., 2002)

Figure 7. Nb vs. Cr concentrations can be utilized to determine protolith of the rutile bearing host rock (see inset for modified Fig 6. Zack et al., 2002). In general, rutile from the KTB drill hole, utilized for this study have a mafic signature, except for an outlier from Block C, which has Nb concentrations ~1500 ppm, and two samples which have high Cr concentrations from Block B and C. Results are in good agreement with previous geochemical studies that assign metabsic units to oceanic crust and variegated units to back arc volcano-sedimentary units (O'Brien et al., 1997). Rutile have retained parent trace element concentrations and do not indicate recyrstallization or rutile growth from a different source (Luvizotto et al., 2008).

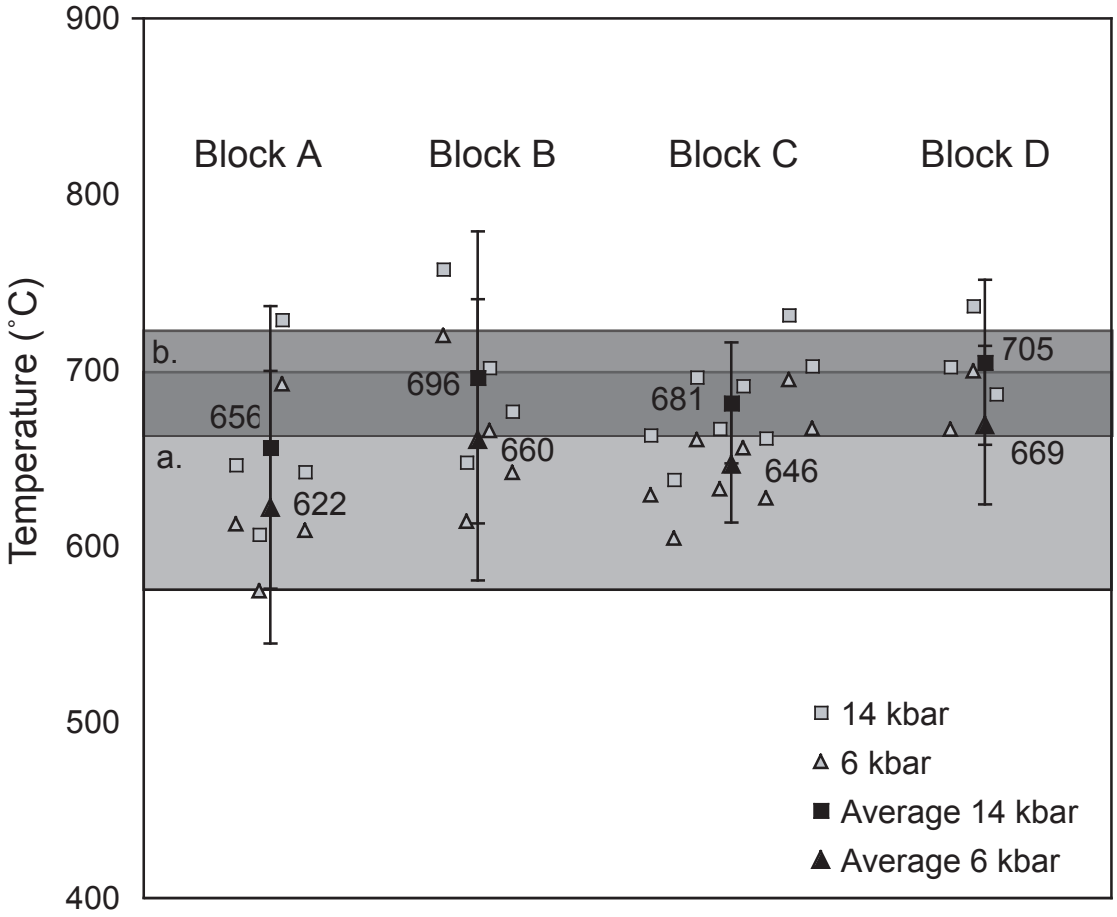
900
800
700
600
500
400
Temperature (˚C)
Block A
Block B
Block C
Block D
b.
a.
656
622
696
660
681
646
705
669
14 kbar
6 kbar
Average 14 kbar
Average 6 kbar

Figure 8. Calculated peak metamorphic temperatures are based on Zr concentrations (ppm) measured by solution ICP-MS (Table 3). Zr concentrations (ϕ) were put into Eq. 2 (Tomkins et al., 2007). Maximum (14 kbar) and minimum (6 kbar) pressure (*P*) parameters utilized in calculations were taken from published pressure conditions for the two major metamorphic events experienced by the KTB drill hole. Temperatures for the HP/HT event (14 kbar) and amphibolite facies metamorphism (6 kbar) events were calculated for each sample, with the average temperature for each metamorphic block displayed near the black symbol. Error on average is the standard deviation from average temperature. Temperatures calculations are in surprisingly good agreement with published data (O'Brien et al., 1992) in consideration of technique and number of grains analyzed. Temperatures estimates for the HP eclogite/granulite facies (a. dark grey box) event range from ~575-700°C and at least 14 kbar. For the amphibolite facies (b. light grey box) event, temperature estimates range from 620-720°C and 6-8 kbar pressure conditions (O'Brien et al., 1992).

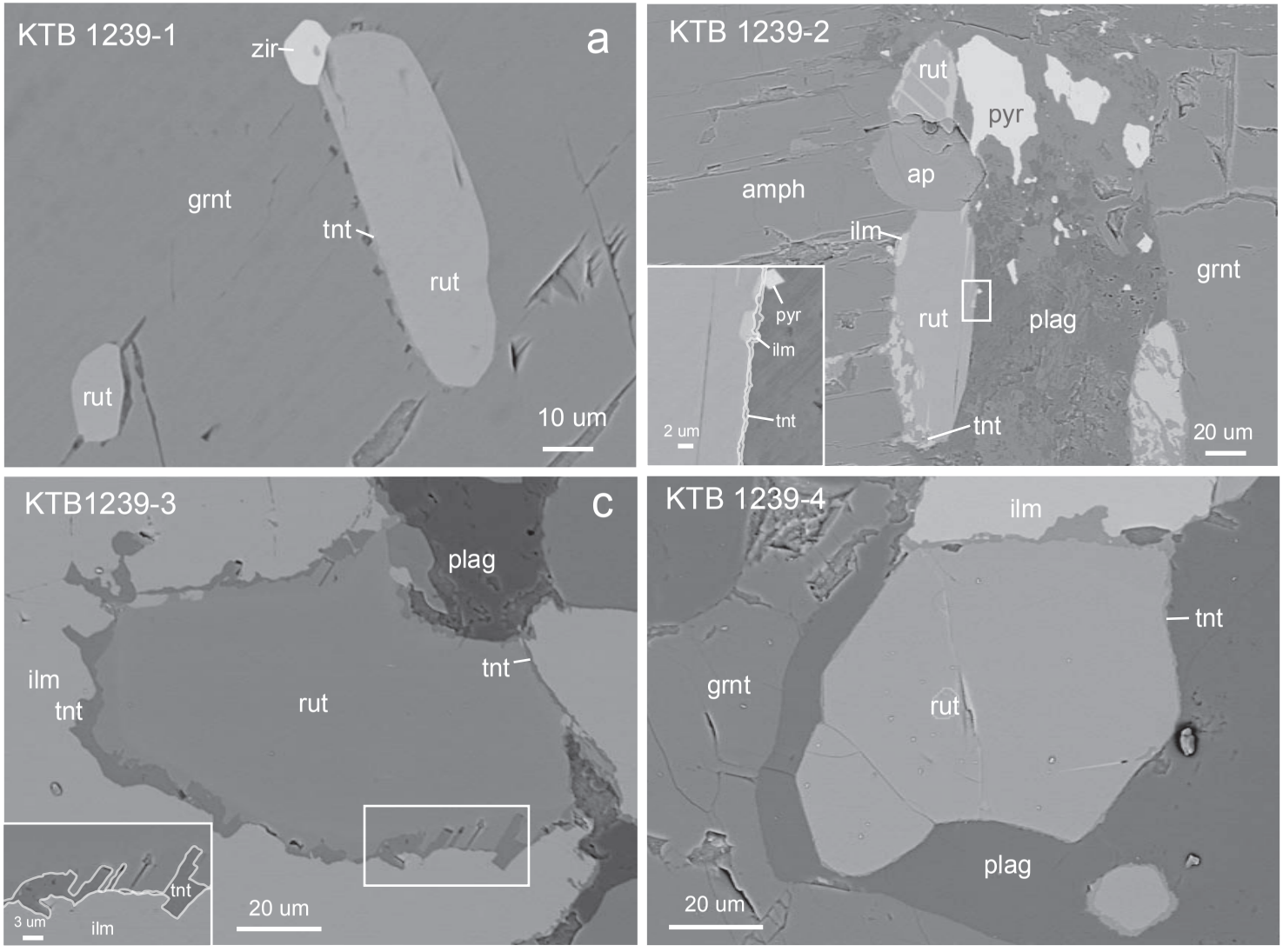
KTB 1239-1
a
zir
grnt
tnt
rut
rut
10 um
KTB 1239-2
rut
pyr
amph
ap
ilm
grnt
pyr
ilm
rut
plag
2 um
tnt
tnt
20 um
KTB1239-3
c
plag
tnt
ilm
tnt
rut
tnt
3 um
ilm
20 um
KTB 1239-4
ilm
tnt
grnt
rut
plag
20 um

Figure 9. Backscatter secondary electron microscope images from thin sections of KTB1239 analyzed by (U-Th)/He analysis, which yielded an average RtHe age of 100 ± 40 Ma (std dev). (a) Rutile is found as an inclusion within garnet, (b) as grains in an amphibole, plagioclase, garnet matrix and (c, d) growing with ilmenite as an aggregate of oxides. All rutile seen in thin section was surrounded with a thin titanite rim. (c) Displays intergrowth between titanite and rutile, which suggests recrystallization and not only a breakdown reaction. 9b displays primary breakdown of rutile to ilmenite and later growth of a thin titanite rim as a breakdown reaction. Rutile was also situated near zircon (a) and apatite (b).

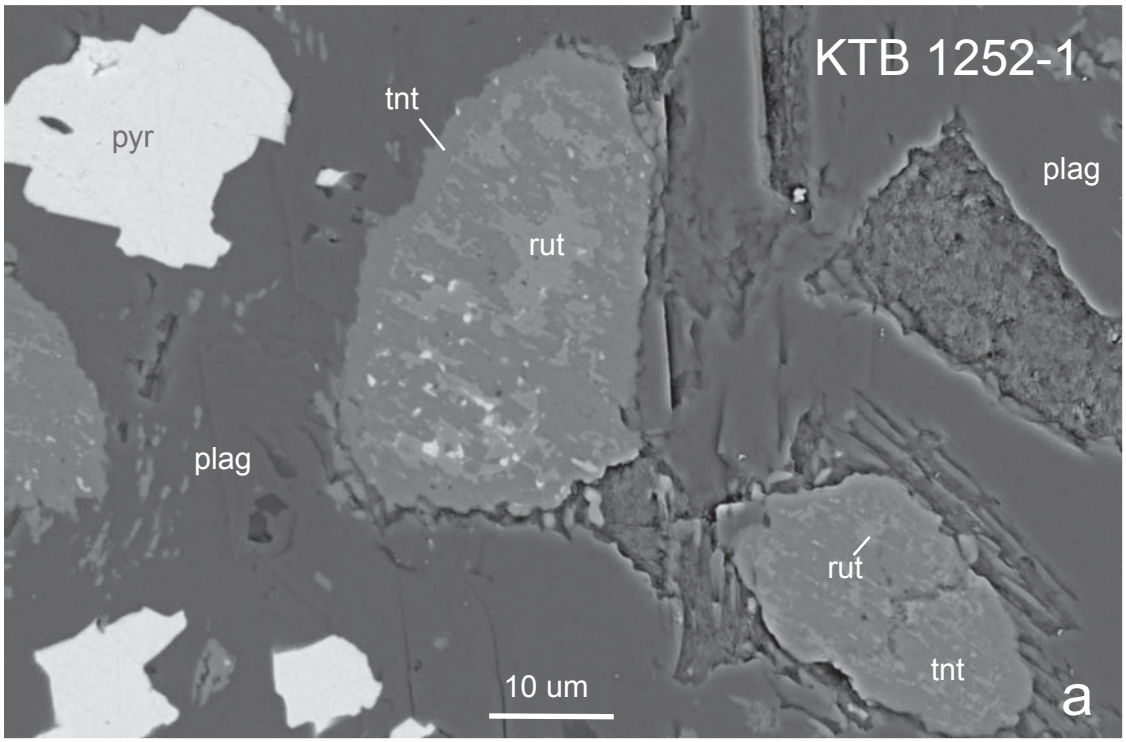
KTB 1252-1
pyr
tnt
rut
plag
plag
rut
tnt
10 um
a

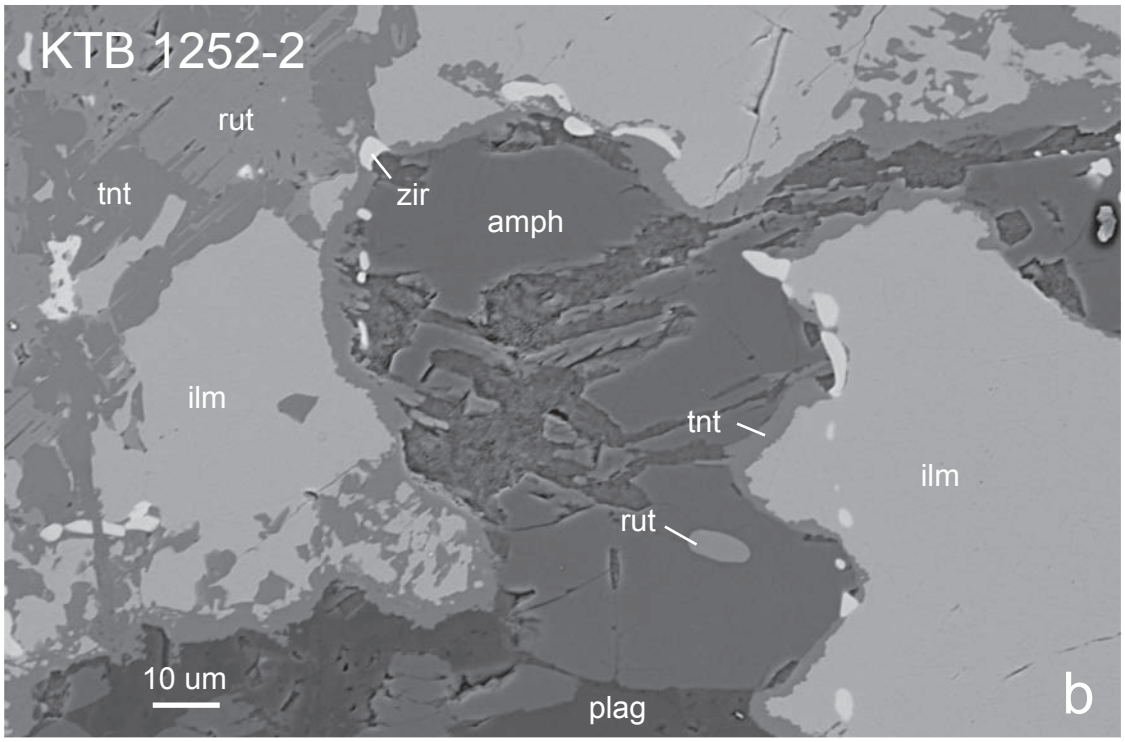
KTB 1252-2
rut
tnt
zir
amph
ilm
tnt
ilm
rut
10 um
plag
b

Figure 10. Backscatter secondary electron microscope images from thin sections of KTB1252 analyzed by (U-Th)/He analysis, which yielded an average RtHe age of 104 ± 10 Ma (std dev). Rutile was not identified as a free grain in thin section, but only as a former grain, which is broken down to titanite (a). Figure 10b, displays a ring of zircon, which appear to be exsolved from a previous grain(?).

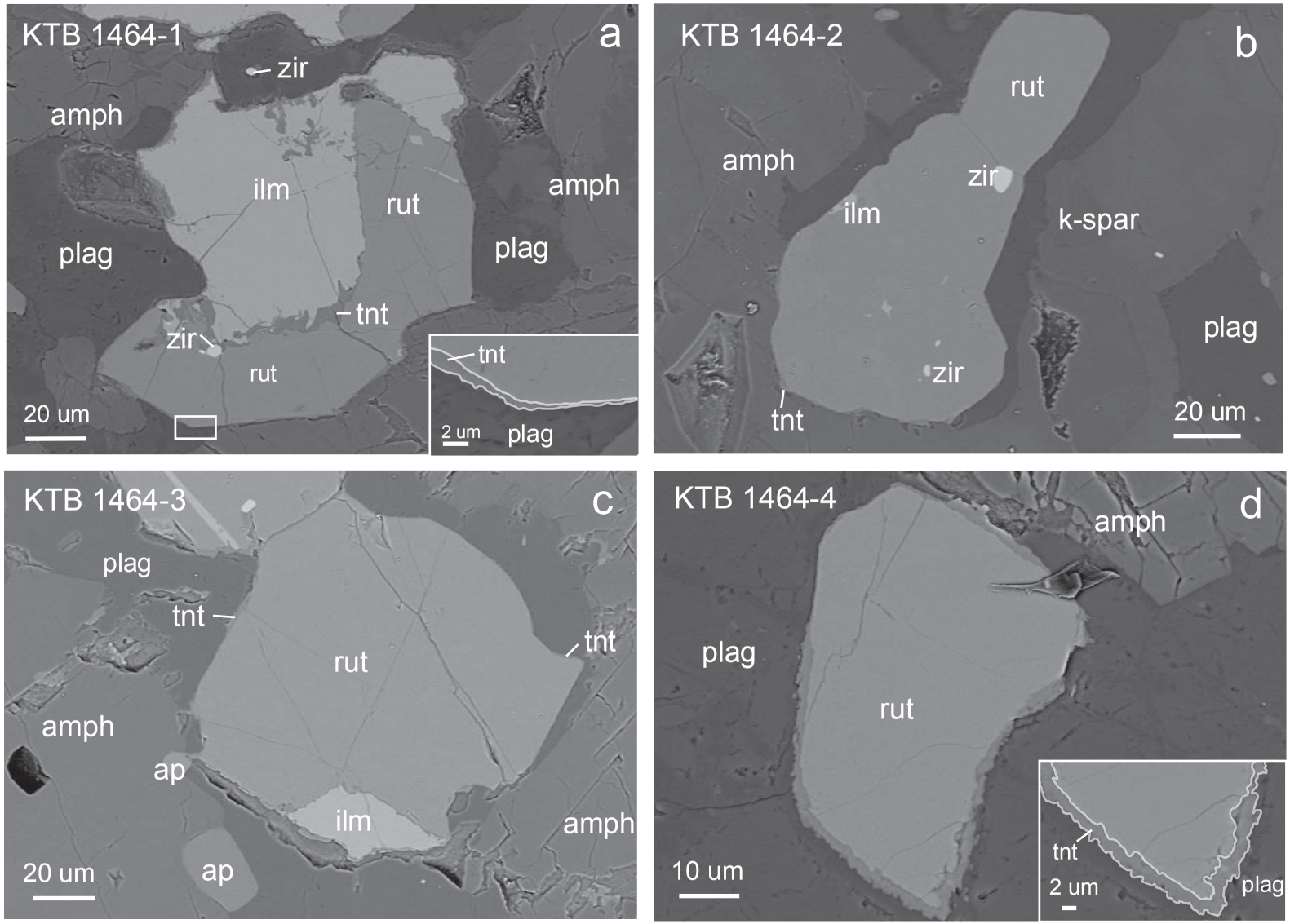
KTB 1464-1
a
zir
amph
ilm
rut
amph
plag
plag
tnt
zir
rut
20 um
tnt
2 um
plag
KTB 1464-2
b
rut
amph
zir
ilm
k-spar
plag
zir
tnt
20 um
KTB 1464-3
c
plag
tnt
tnt
rut
amph
ap
ilm
amph
20 um
ap
KTB 1464-4
d
amph
plag
rut
tnt
2 um
plag
10 um

Figure 11. Backscatter secondary electron microscope images from thin sections of KTB1464 analyzed by (U-Th)/He analysis, which yielded an average RtHe age of 160 ± 40 Ma. As seen in previous thin sections, rutile occurs as an aggregate with ilmenite (a) and individual grains (b-d) and a similar thin titanite rim is persistent throughout the thin section. Inclusions of zircon and ilmenite are found as inclusions (b,c). Bad neighbors of zircon and apatite (a, c) could provide a source of excess He along with implantation from titanite rim.

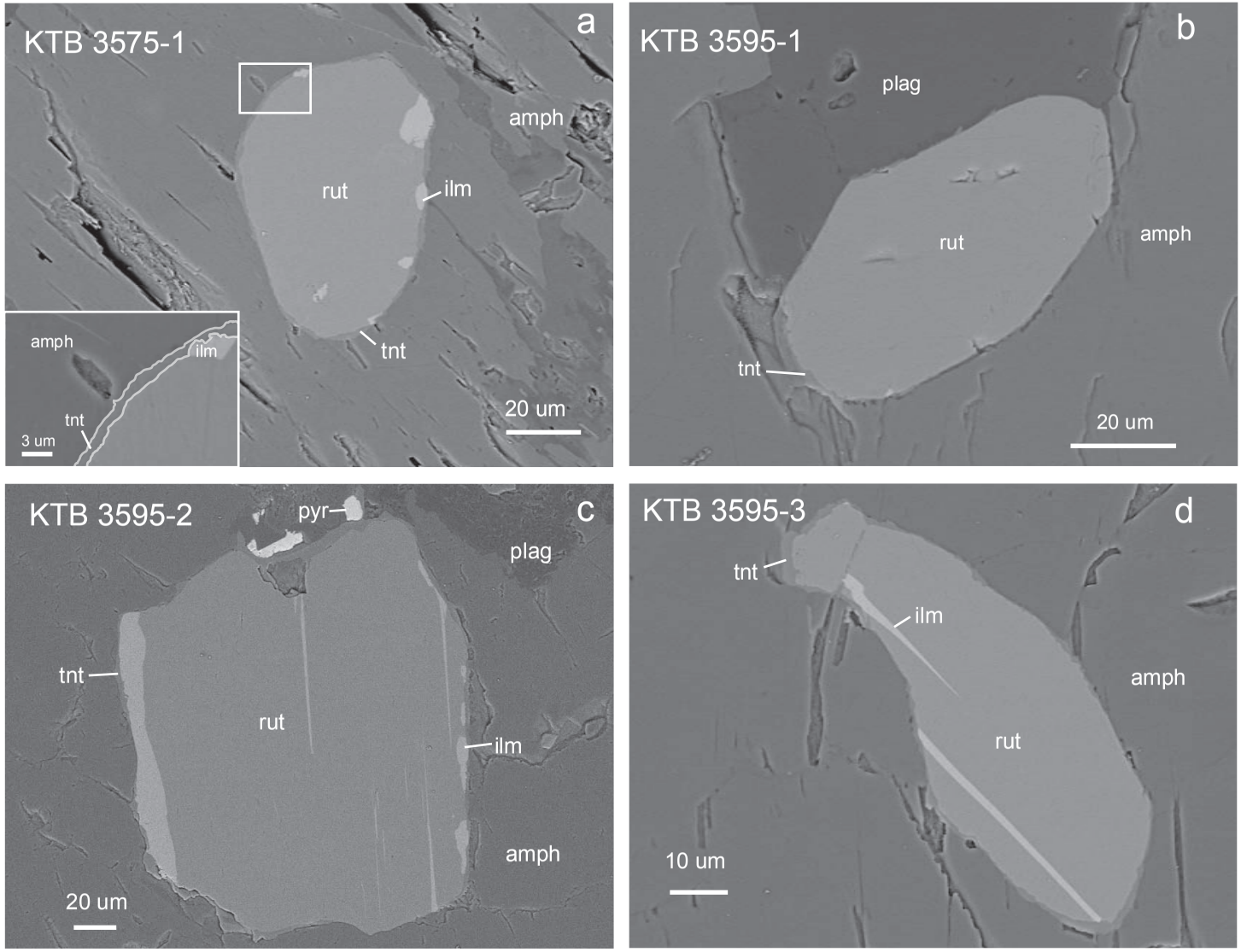
KTB 3575-1
a
amph
rut
ilm
tnt
20 um
amph
ilm
tnt
3 um
KTB 3595-1
b
plag
rut
amph
tnt
20 um
KTB 3595-2
c
pyr
plag
tnt
rut
ilm
amph
20 um
KTB 3595-3
d
tnt
ilm
amph
rut
10 um

Figure 12. Backscatter secondary electron microscope images from thin sections of 3575 and 3595 m (3595 was not analyzed for (U-Th)/He), but sample 3575 yielded an average RHe age of 135 ± 9. Ilmenite lamellae and a thin titanite rim is persistent throughout the thin section, as well as being situated near bad neighbors. The growth of ilmenite lamellae surrounded by a titanite rim suggests that rutile breakdown occurred first, followed by further breakdown when rutile reacted to produce titanite.

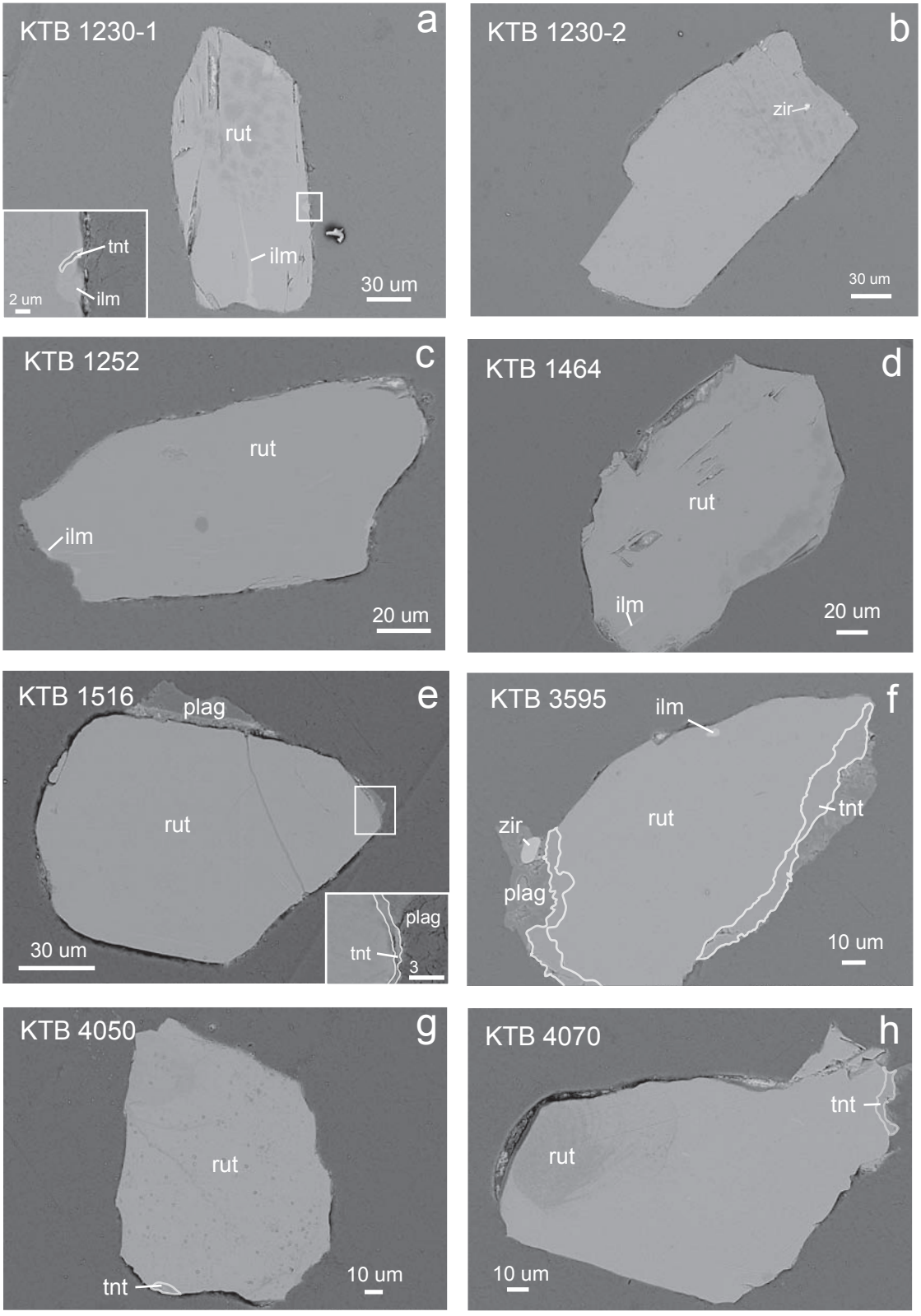
KTB 1230-1
a
rut
tnt
ilm
2 um
ilm
30 um
KTB 1230-2
b
zir
30 um
KTB 1252
c
rut
ilm
20 um
KTB 1464
d
rut
ilm
20 um
KTB 1516
plag
e
rut
30 um
plag
tnt
3
KTB 3595
ilm
f
zir
rut
tnt
plag
10 um
KTB 4050
g
rut
tnt
10 um
KTB 4070
h
tnt
rut
10 um

Figure 13. Secondary backscatter images of grain mounts from depths 1230-4070 m analyzed by (U-Th)/He analysis. Throughout grain mounts thin titanite rim is partially preserved. Zircon inclusions are seen in 13b, while a zircon grain is situated closely to a rutile in matrix, which would be a source of implanted He and produce an erroneously old age.

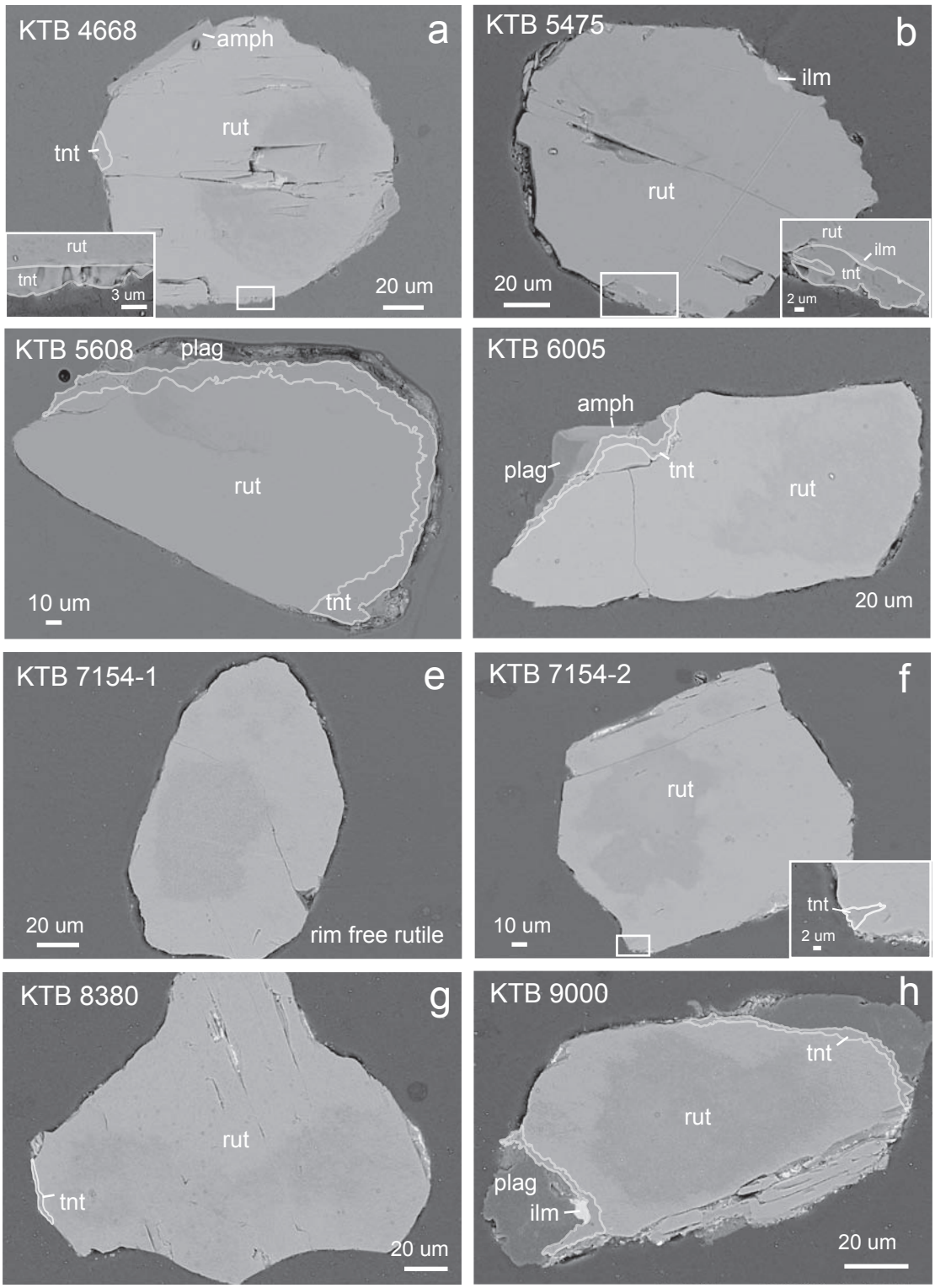
KTB 4668
a
amph
rut
tnt
rut
tnt
3 um
20 um
KTB 5475
b
ilm
rut
rut
ilm
tnt
20 um
2 um
KTB 5608
plag
rut
tnt
10 um
KTB 6005
amph
plag
tnt
rut
20 um
KTB 7154-1
e
20 um
rim free rutile
KTB 7154-2
f
rut
tnt
10 um
2 um
KTB 8380
g
rut
tnt
20 um
KTB 9000
h
tnt
rut
plag
ilm
20 um

Figure 14. Secondary backscatter images of grain mounts from depths 4668-9000 m analyzed by (U-Th)/He analysis. Throughout grain mounts thin titanite rim is partially preserved, except for KTB7154 (e).

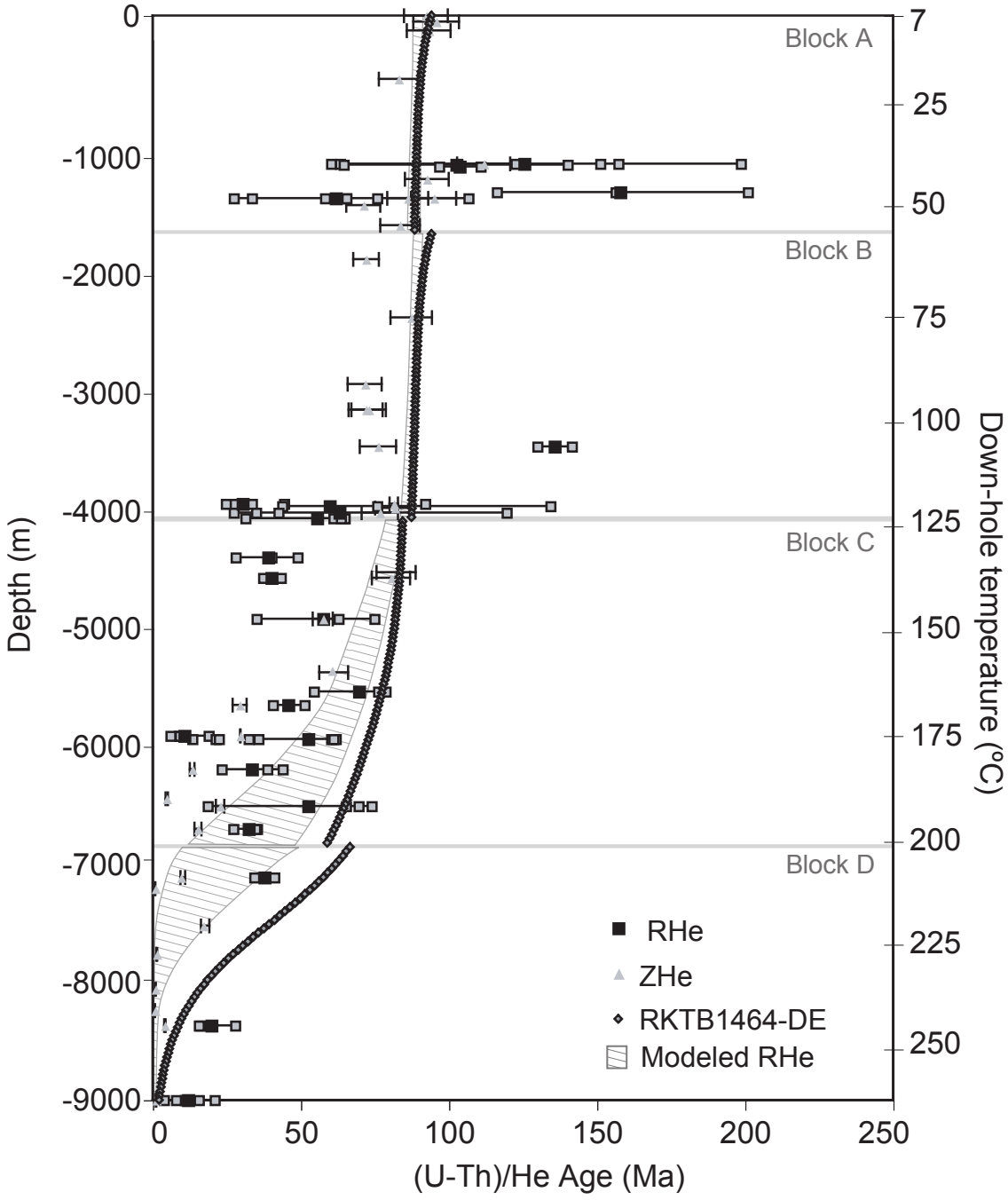
Block A
Block B
Block C
Block D
RHe
ZHe
RKTB1464-DE
Modeled RHe
Depth (m)
Down-hole temperature (°C)
(U-Th)/He Age (Ma)
0
-1000
-2000
-3000
-4000
-5000
-6000
-7000
-8000
-9000
7
25
50
75
100
125
150
175
200
225
250
0
50
100
150
200
250

Figure 15. Plot of average down hole RtHe and zircon (U-Th)/He results (Chapter 2) from the KTB drill hole. Error on RtHe age reaches to the maximum and minimum RtHe age (small grey boxes). Error on zircon data is the largest error measured, either standard analytical error (± 8%) or standard deviation of sample. Zircon (U-Th)/He results are well behaved displaying a defined zircon HePRZ between ~140-210 °C. RtHe results are compared to modeled down hole RHe results (lined envelope) based on tT History proposed by Wagner and others (1998) and refined by Stockli and Farley (2004) with varying diffusion kinetics based on laboratory cycled step-heating experiments on rutile from the KTB drill hole Ea 207-213 kJ/mol (49.5-51 kcal/mol) $\log(D_0/a^2)$ 6.5-7.1 s^{-1} for a grain with a r_{eq} = 60 μm. Modeled results display older ages in the upper most samples of Block A and Block B and not the invariant ~85 Ma from surface to ~4000 m depth seen in modeling results for zircon (Chapter 2). This is due to the higher closure temperature of rutile (220-240 °C), which allows it to retain He before movement along the FL at 85 Ma.

a CORRECT AGE

No rim, homogeneous U and Th distribution

b YOUNG AGE

Enriched titanite rim preserved and [U] & [Th] measured during RHe. Titanite rim preferentially-looses He by alpha ejection producing young age

c OLD AGE

Enriched titanite rim is removed during mineral separation. Parentless He is implanted from titanite rim producing old age

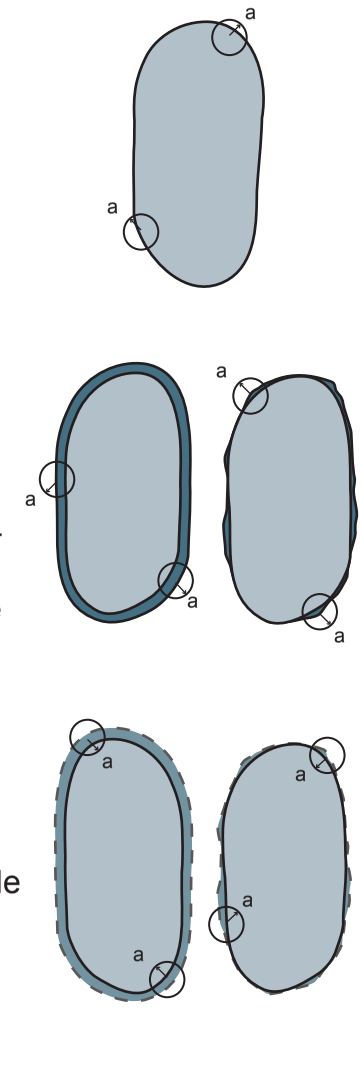

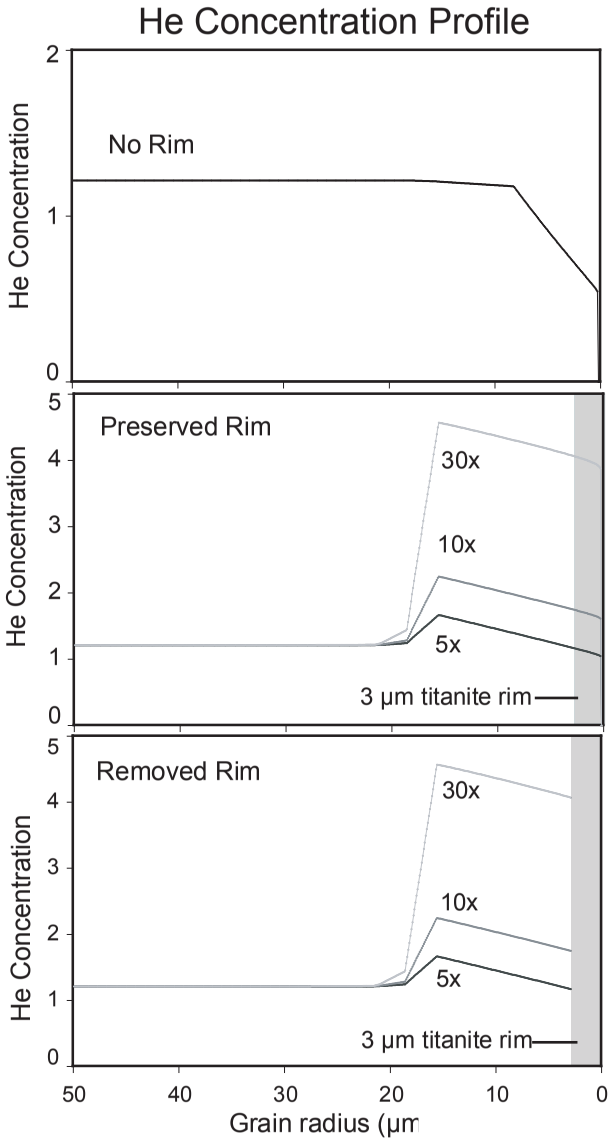

Figure 16. Depicts the possible scenario of rutile analyzed by (U-Th)/He analysis for this study from the KTB drill hole. Diffusion profile of rutile affected by the titanite rim displays various rim to grain concentration differences (5x, 10x, and 30x). (a) The incorrect scenario assumed throughout initial RHe analysis of rutile with no rim and homogeneous U and Th distribution, application of the standard alpha ejection correction. (b) Rutile grain analyzed by the standard (U-Th)/He process with an intact titanite rim. Resulting (U-Th)/He age is too young, as He is preferentially lost from the U- and Th-enriched rim by alpha ejection, while analyzing the parent concentrations. A young age would result if only a fraction of the rim was preserved, due to the drastic concentration difference between rutile and titanite. (c) Rutile grain that lost enriched titanite rim during mechanical mineral separation. Due to parentless He implanted from the enriched rim, (U-Th)/He analysis would result in an erroneously old age.

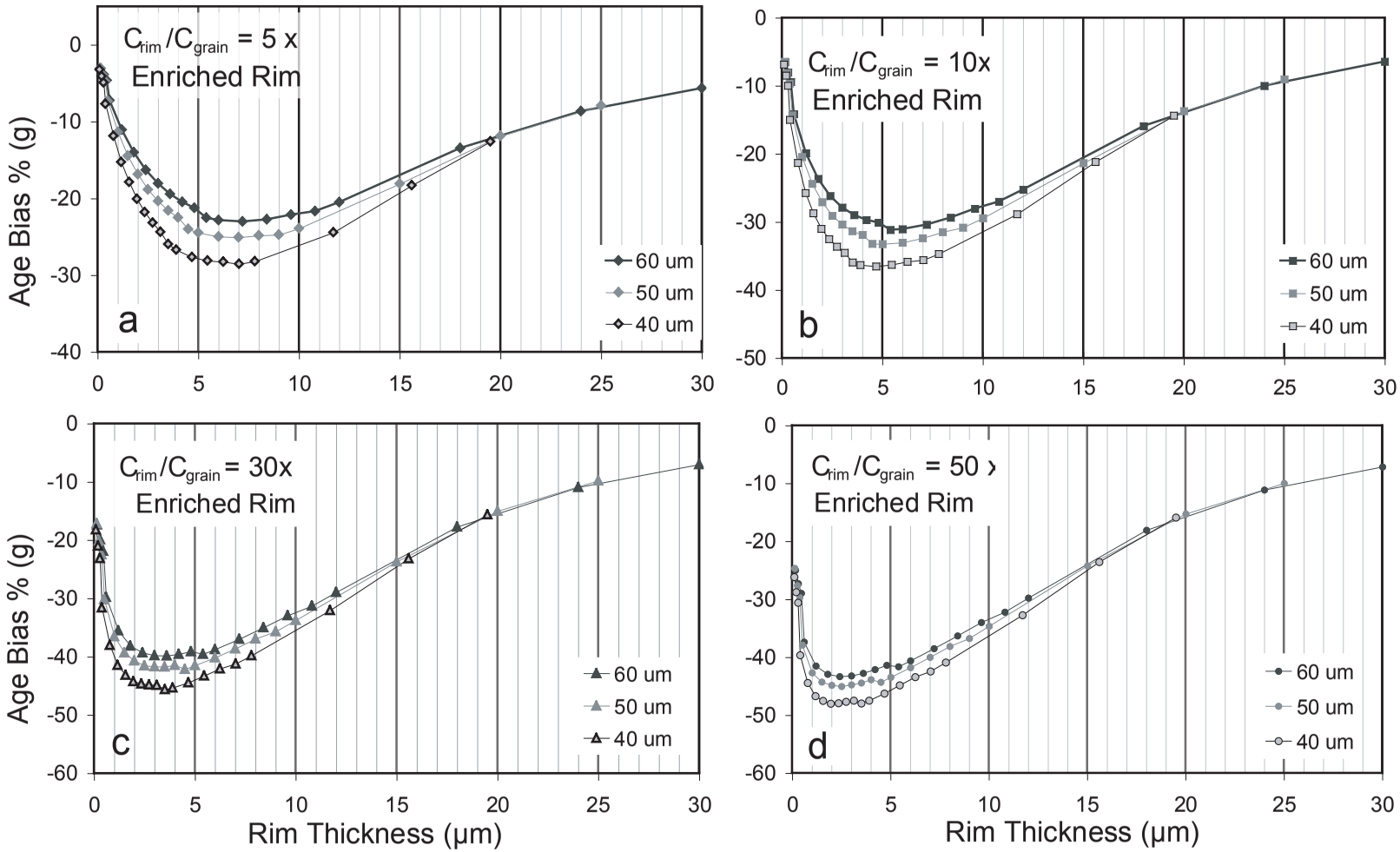
C_{rim}/C_{grain} = 5 x
Enriched Rim
a
60 um
50 um
40 um
C_{rim}/C_{grain} = 10x
Enriched Rim
b
C_{rim}/C_{grain} = 30x
Enriched Rim
c
C_{rim}/C_{grain} = 50 x
Enriched Rim
d
Age Bias % (g)
Rim Thickness (µm)

Figure 17. Age bias plots for spherical rutile grains display the percent age difference produced from an enriched rim with varying rim thickness and concentration gradient 5x (a), 10 (b), 30x (c), 50x (d). Enriched rims yield corrected ages that are erroneously young as $F_{Tstandard}$ correction underestimates grain retentivity. Maximum age bias for a rim to grain concentration difference of 5x is ~5-7 μm in width, where maximum age bias for a 75x concentration difference is ~1-3 μm in width. Age bias also scales with grain size as the greatest age bias is seen in the r_{eq} 40 μm grain.

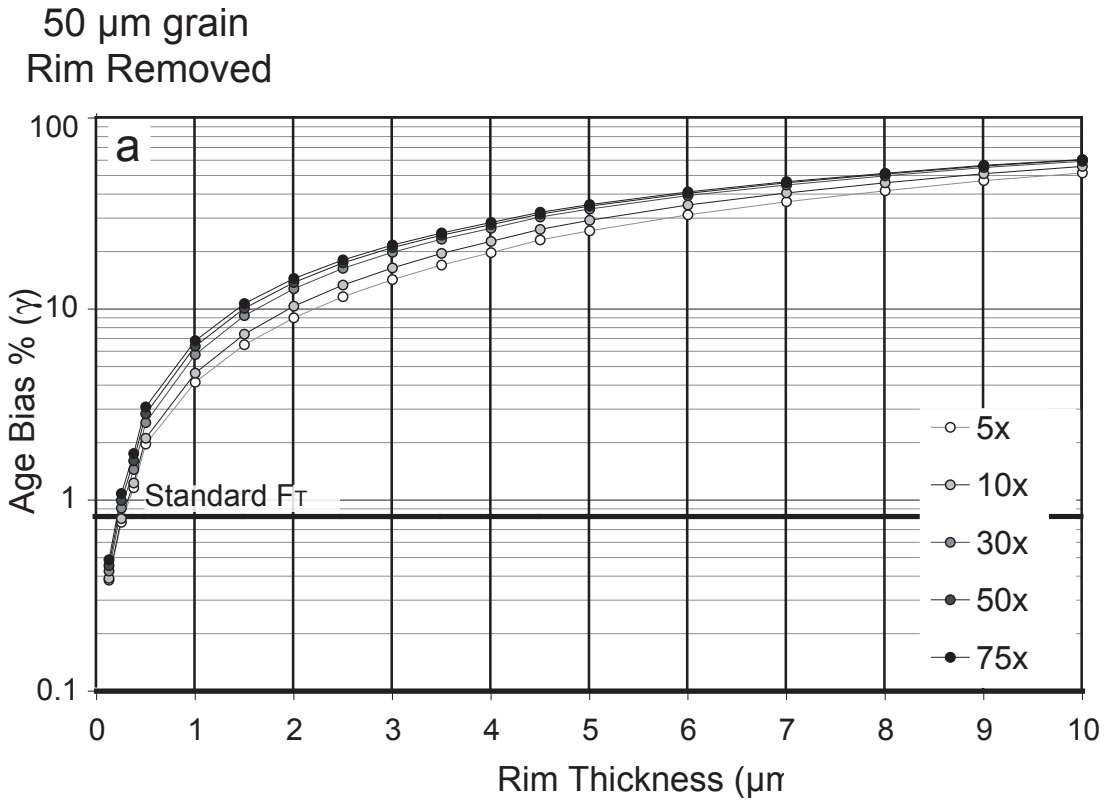
50 µm grain
Rim Removed
a
100
10
1
0.1
Age Bias % (γ)
Standard FT
5x
10x
30x
50x
75x
0
1
2
3
4
5
6
7
8
9
10
Rim Thickness (µm

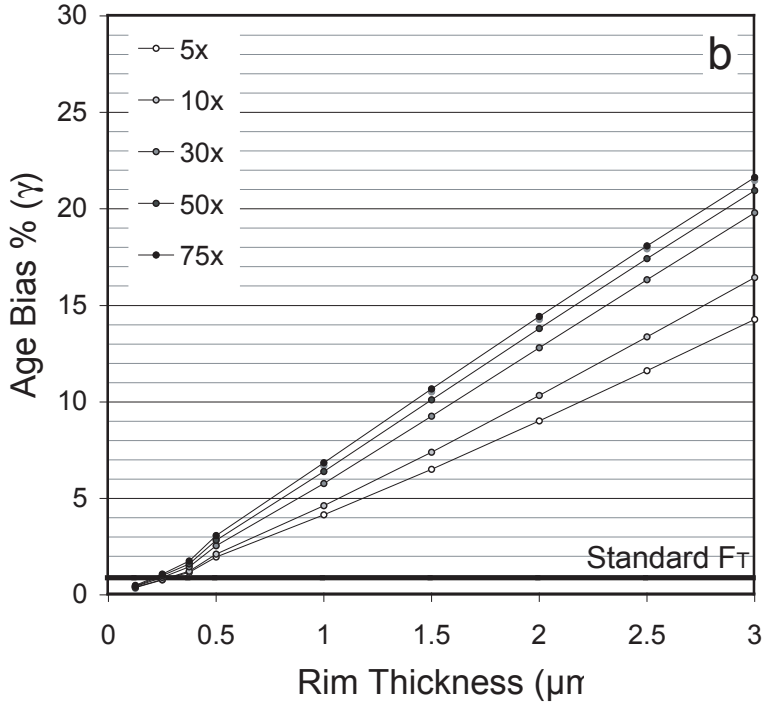
b
30
25
20
15
10
5
0
Age Bias % (γ)
5x
10x
30x
50x
75x
Standard FT
0
0.5
1
1.5
2
2.5
3
Rim Thickness (µm

Figure 18. Age bias plot for spherical rutile (r_{eq} 50 μm) grain based on scenario if enriched rim is removed before (U-Th)/He analysis (Figure 16c). Removal of enriched rims produces erroneously old ages because of implantation of parentless He. (a) Log plot of age bias % highlights the rapid age increase for rim width <1 μm, removal of a 1μm rim grain produces an age bias of 4-7%. (b) Zooms into the same scenario without the log scale to display the effect of concentration difference between rim to grain.

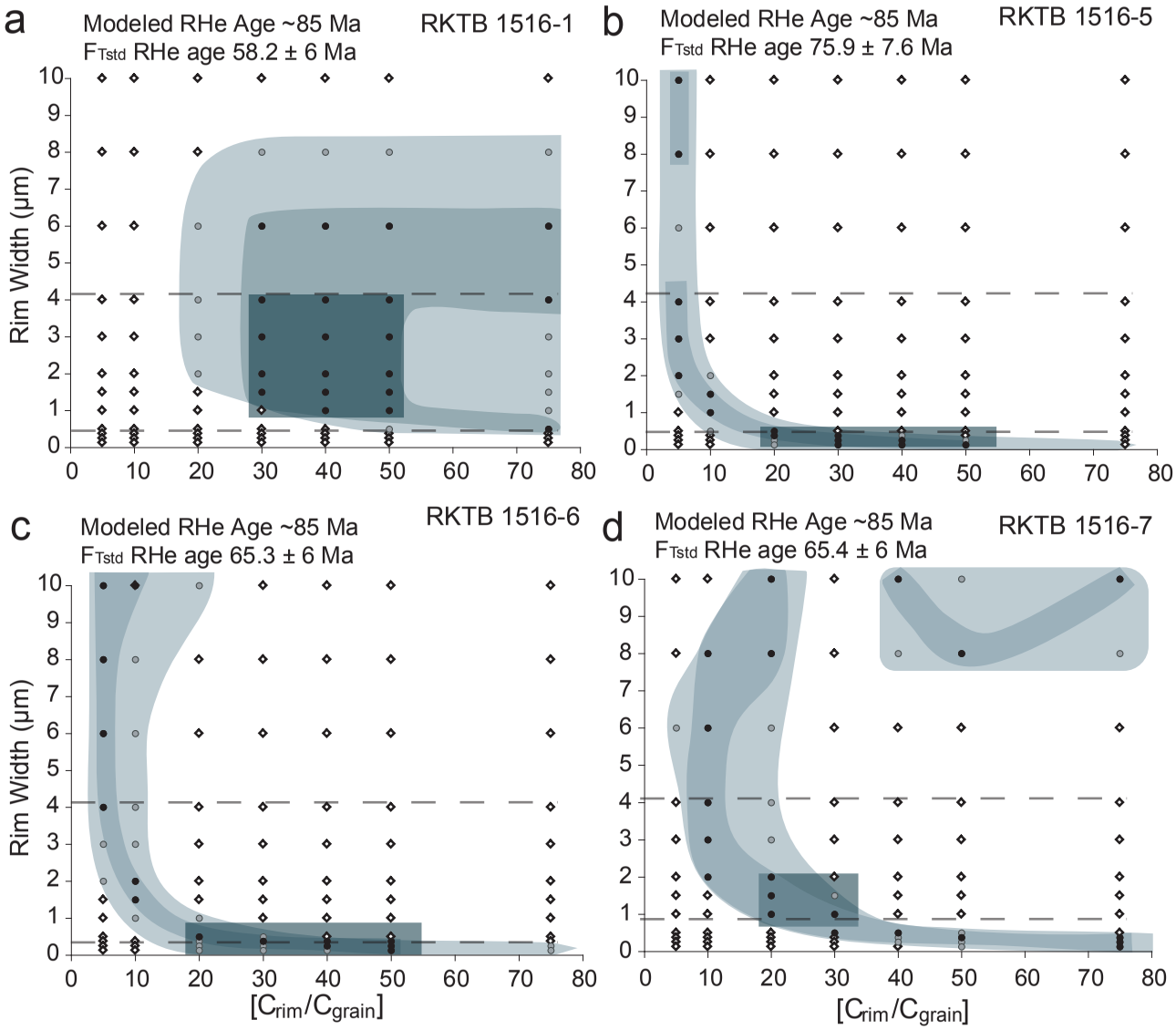
a
Modeled RHe Age ~85 Ma
FTstd RHe age 58.2 ± 6 Ma
RKTB 1516-1
b
Modeled RHe Age ~85 Ma
FTstd RHe age 75.9 ± 7.6 Ma
RKTB 1516-5
c
Modeled RHe Age ~85 Ma
FTstd RHe age 65.3 ± 6 Ma
RKTB 1516-6
d
Modeled RHe Age ~85 Ma
FTstd RHe age 65.4 ± 6 Ma
RKTB 1516-7
Rim Width (μm)
[Crim/Cgrain]

Figure 19. The following contour plots (Figure 19-21) display the $F_{Tzoning}$ corrections of single RtHe ages, which correct the raw RtHe age within 10% (grey circles, light grey) and 5% (black circles, grey) of the modeled RtHe age. Darkest grey box is the estimated correction that best fits observed rim width (<1-4 μm- dashed lines), which is typically produced by high (20-50) rim-to-grain concentration differences. Modeled RtHe is based on results from Figure 5. $F_{Tzoning}$ applied to four out of seven aliquots of sample RKTB1516, average RtHe age for 62 ± 26 Ma (std dev) based on a F_T correction. Modeled RtHe age for rutile at 1516 m depth in the KTB drill hole is 85 Ma. (a) Aliquot RKTB1516-1 displays the largest variety of $F_{Tzoning}$ corrections that will produce the modeled age. (b-d) Aliquots RKTB1516-5, -6, -7 have similar patterns and most likely were effected by a thin concentrated rim. RKTB1516-2 was erroneously old (RtHe age 107 ± 11 Ma), while aliquots RKTB1516-3 and -4 were too young and could not be corrected to the modeled RtHe age by the $F_{Tzoning}$ corrections calculated (RtHe age 33.5 ± 3.4 Ma and 27.3 ± 2.7 Ma respectively).

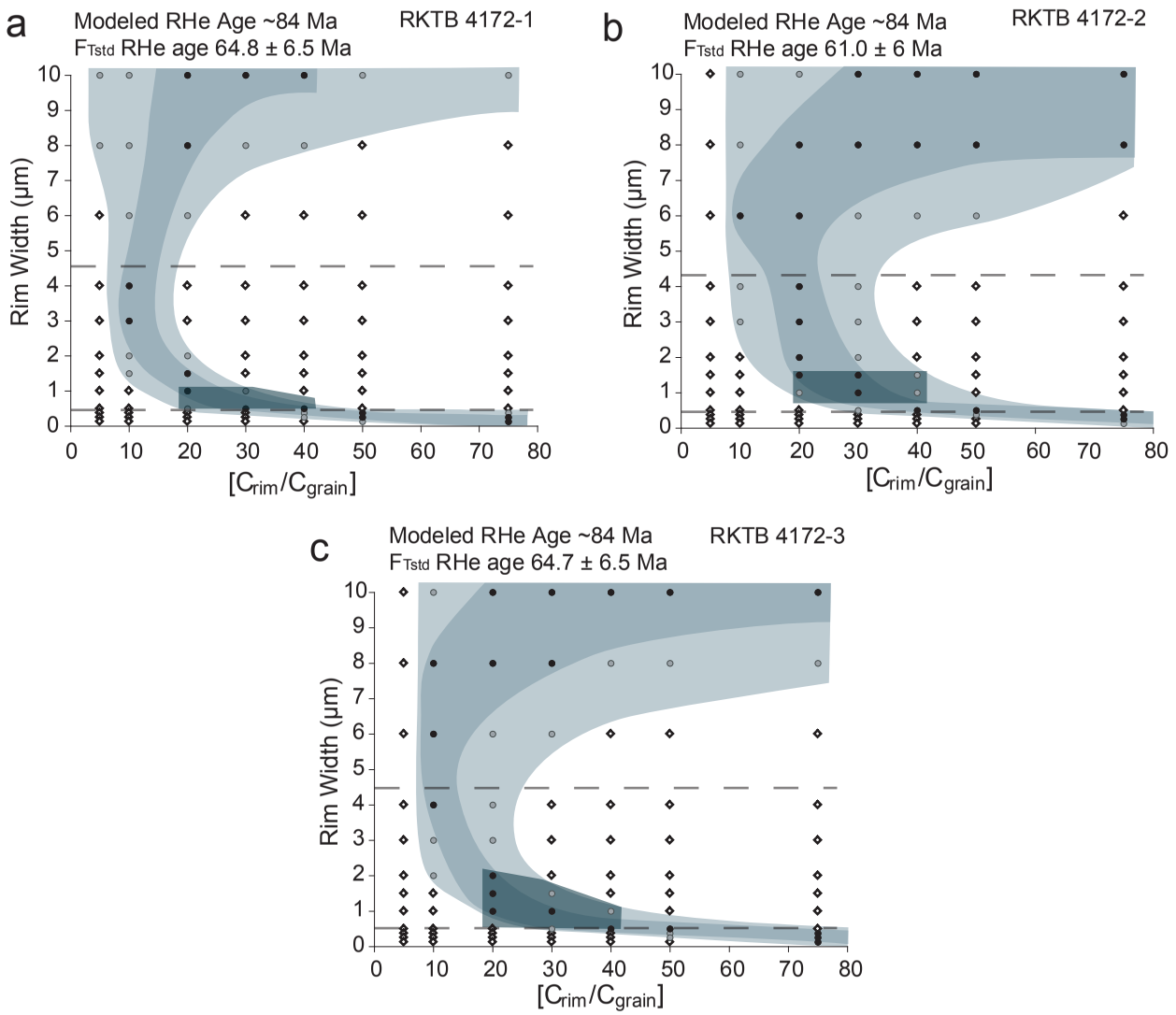
a
Modeled RHe Age ~84 Ma
FTstd RHe age 64.8 ± 6.5 Ma
RKTB 4172-1
Rim Width (µm)
[Crim/Cgrain]
b
Modeled RHe Age ~84 Ma
FTstd RHe age 61.0 ± 6 Ma
RKTB 4172-2
Rim Width (µm)
[Crim/Cgrain]
c
Modeled RHe Age ~84 Ma
FTstd RHe age 64.7 ± 6.5 Ma
RKTB 4172-3
Rim Width (µm)
[Crim/Cgrain]

Figure 20. $F_{Tzoning}$ applied to three out of four aliquots of sample RKTB4172, average RtHe age for 55 ± 16 Ma (std dev) based on F_T correction. Modeled RtHe age for rutile at 4172 m depth in the KTB drill hole is ~84 Ma. (a-c) Aliquots RKTB4172-1, -2 and -3 all display a corresponding "tornado or boomerang" shape, and we assume that a thin (0.75-2 μ m) rim with 20-40x increase in concentration affected rutile from sample RKTB4172. Aliquot RKTB4172-4 was too young and could not be corrected to the modeled age by the $F_{Tzoning}$ corrections tested (RtHe 31 ± 3 Ma based on homogeneous U and Th distribution).

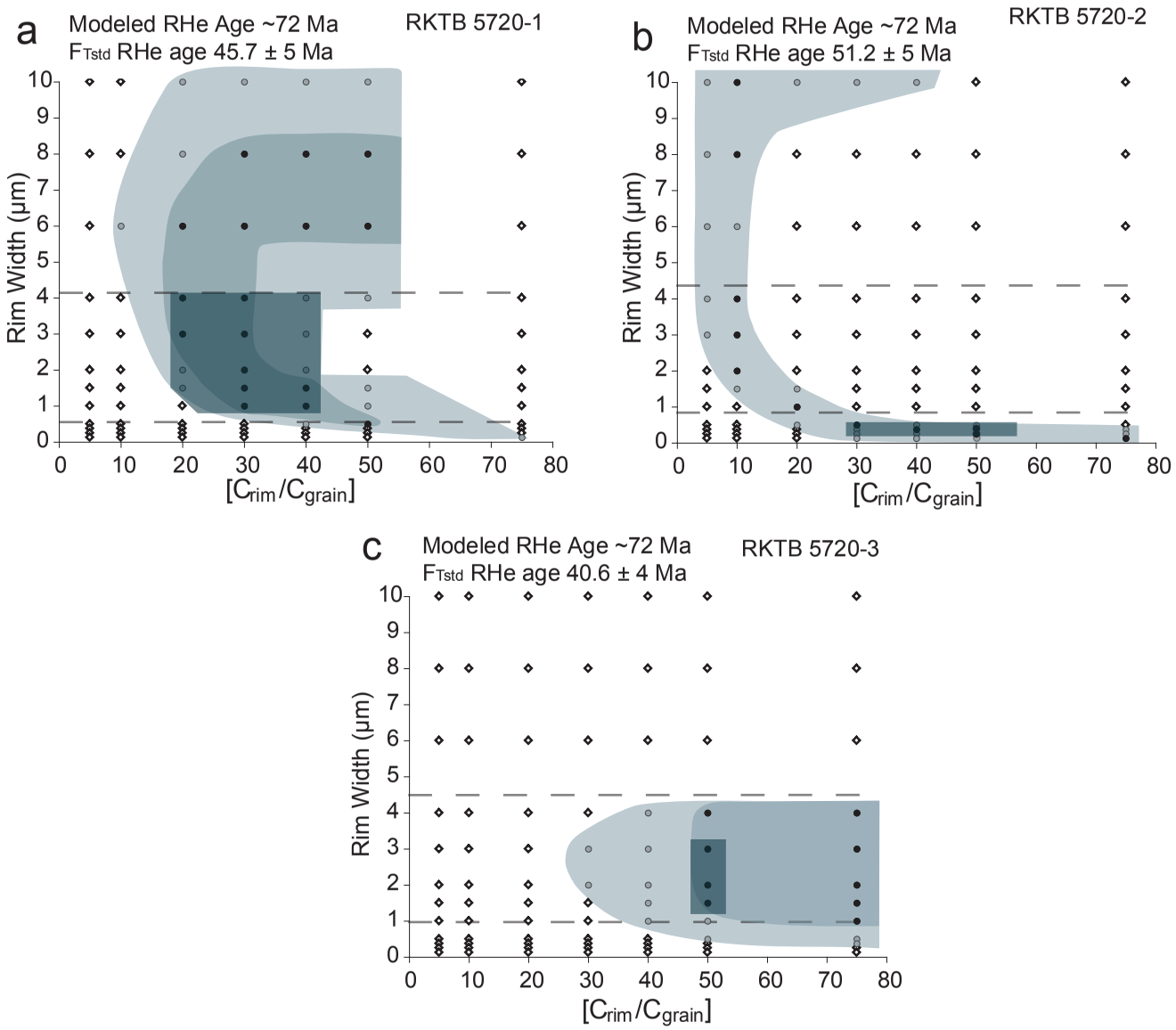
a
Modeled RHe Age ~72 Ma
FTstd RHe age 45.7 ± 5 Ma
RKTB 5720-1
b
Modeled RHe Age ~72 Ma
FTstd RHe age 51.2 ± 5 Ma
RKTB 5720-2
c
Modeled RHe Age ~72 Ma
FTstd RHe age 40.6 ± 4 Ma
RKTB 5720-3
Rim Width (µm)
[Crim/Cgrain]
0
10
20
30
40
50
60
70
80
1
2
3
4
5
6
7
8
9

Figure 21. $F_{Tzoning}$ corrections applied to all three aliquots from sample RKTB5720, average RtHe age for 45.8 ± 5.3 Ma (std dev) based on homogeneous U and Th distribution. Modeled RHe age for rutile at 5720 m depth in the KTB drill hole is ~72 Ma. (a) Aliquot RKTB5720-1 displays a range of $F_{Tzoning}$ corrections that can correct back to the modeled age. (b) RKTB5720-2 displays the "tornado or boomerang" shape indicating it may have been affected by a thin (0.5-0.75 μm) rim with 30-50 fold increase in concentration. (c) Aliquot RKTB5720-3 requires an $F_{Tzoning}$ correction produced by a 1-4 μm rim with a 50-75 increase in concentration from grain to rim to produce the modeled age.

Sample	Rock Type	Age [Ma]	± [Ma]	U [ppm]	Th [ppm]	Sm [ppm]	Th/U	He [ncc/mg]	mass [mg]	F_T*	stddev
Blansky les Granulite Massif, Czech Republic											
RT5A-1		186.4	2.49	18.1	-0.2	18.6	0.0	307.4	4.5	0.74	
RT5A-3		221.2	3.25	15.4	-0.1	17.7	0.0	312.6	4.5	0.73	
RT5A-4		158.5	3.15	26.9	0.0	4.9	0.0	421.7	11.3	0.80	
RT5A	***Granulite***	***188.7***	***3.0***	***20.1***	***-0.1***	***13.7***	***0.0***	***347.2***	***6.8***	***0.8***	***31.4***
RT8C-1		217.6	3.45	15.5	1.0	21.1	0.1	312.2	4.1	0.73	
RT8C-2**		313.8	4.27	18.7	0.7	10.1	0.0	565.7	4.1	0.76	
RT8C-3		223.4	5.52	25.4	0.9	11.3	0.0	579.6	10.3	0.81	
RT8C-4		207.5	5.73	11.3	0.9	1.8	0.1	257.7	26.3	0.87	
RT8C	***Granulite***	***216.2***	***4.7***	***17.7***	***0.9***	***11.1***	***0.1***	***428.8***	***11.2***	***0.8***	***8.0***
Erzgebirge, Germany											
EGB R1A-1		263.4	5.97	2.8	0.0	1.6	0.0	82.7	64.4	0.89	
EGB R1A-2		306.3	6.25	3.6	0.0	1.0	0.0	119.8	40.1	0.87	
EGB R1A-3		276.9	4.84	3.4	0.0	4.9	0.0	101.9	22.8	0.86	
EGB R1A-4		246.3	23.38	5.1	0.7	5.9	0.1	135.5	15.6	0.83	
EGB R1A	***Dia-Grnt Gneiss***	***273.2***	***10.1***	***3.7***	***0.2***	***3.3***	***0.0***	***110.0***	***35.7***	***0.9***	***25.4***
EGB04 R2b-1		303.9	28.71	13.7	1.6	7.7	0.1	429.4	8.4	0.80	
EGB04 R2b-2		299.7	28.37	14.1	1.8	8.5	0.1	419.3	5.2	0.77	
EGB04 R2b-3		203.7	47.99	9.1	3.0	321.7	0.3	232.8	3.6	0.75	
EGB04 R2b-4		273.9	25.89	9.6	1.0	2.1	0.1	269.0	8.2	0.80	
EGB04 R2b	***Eclogite***	***292.5***	***27.7***	***12.4***	***1.5***	***6.1***	***0.1***	***372.6***	***7.2***	***0.8***	***16.2***
EGB04 R4d-3		236.7	22.37	5.4	0.8	1.3	0.1	138.6	14.4	0.84	
EGB04 R4d-4		260.2	30.78	2.0	0.2	18.6	0.1	60.9	16.6	0.84	
EGB04 R4d	***Eclogite***	***248.4***	***26.6***	***3.7***	***0.5***	***9.9***	***0.1***	***99.8***	***15.5***	***0.8***	***16.6***

* alpha ejection correction based on homogenous distribution of U and Th
** not included in average or standard deviation

Table 4. Regional RtHe ages from southern Bohemian Massif in the Blansky les Granulite Massif and northern Bohemian Massif in Erzgebirge.